Trabajo Fin de Grado
Grado en Ingeniería Aeroespacial

Dynamic analysis of the ITER Fast-Ion Loss Detector

Autor: Juan Manuel Núñez Portillo
Tutor: Juan Manuel Ayllón Guerola
Tutor ponente: Carlos Navarro Pintado

Dep. de Ingeniería Mecánica y Fabricación
Escuela Técnica Superior de Ingeniería
Universidad de Sevilla

Sevilla, 2018

Trabajo Fin de Grado
Grado en Ingeniería Aeroespacial
Intensificación Vehículos Aeroespaciales

Dynamic analysis of the ITER Fast-Ion Loss Detector

Autor:
Juan Manuel Núñez Portillo

Tutor:
Juan Manuel Ayllón Guerola
Profesor Invitado

Tutor ponente:
Carlos Navarro Pintado
Profesor Titular

Dpto. de Ingeniería Mecánica y Fabricación
Escuela Técnica Superior de Ingeniería
Universidad de Sevilla

Sevilla, 2018

Trabajo Fin de Grado: Dynamic analysis of the ITER Fast-Ion Loss Detector

Autor: Juan Manuel Núñez Portillo

Tutor: Juan Manuel Ayllón Guerola

Tutor ponente: Carlos Navarro Pintado

El tribunal nombrado para juzgar el Proyecto arriba indicado, compuesto por los siguientes miembros:

Presidente:

Vocales:

Secretario:

Acuerdan otorgarle la calificación de:

Sevilla, 2018

El Secretario del Tribunal

A mis abuelos

A mis padres

A mis hermanas

A mis sobrinos

Resumen

La sociedad se enfrenta en nuestros días a la búsqueda de una fuente de energía limpia y fiable con la que superar la actual dependencia de los combustibles fósiles. En este sentido, la energía producida por el Sol ha despertado el interés de la comunidad científica. Desde mediados del siglo pasado, muchos han sido los avances en el campo de la fusión nuclear. No obstante, para demostrar su viabilidad técnica y económica es necesaria una apuesta sin precedentes.

La Unión Europea, China, India, Japón, Corea del Sur, Rusia y los Estados Unidos cooperan en la construcción del reactor de fusión nuclear ITER, que va a suponer un auténtico hito en la historia de la humanidad. Desde un punto de vista ingenieril, una organización suficientemente robusta entre los distintos miembros es clave para garantizar un alto nivel de seguridad, siendo indispensable estructurar el trabajo y seguir un proceso de diseño estandarizado.

Dentro de la estructura del proyecto se encuentra el sistema de diagnósticos. Estos diagnósticos juegan un papel esencial en la investigación de la fusión nuclear. En particular, uno de esos diagnósticos es el Detector de Pérdidas de Iones Rápidos (FILD), que proporciona información relevante acerca de la eficiencia de la reacción nuclear y del posible daño que se produce en las paredes del interior del reactor.

A día de hoy, el diseño del FILD de ITER se encuentra aún en una fase conceptual, si bien encara la preparación para la revisión antes de pasar a la siguiente fase de diseño. Durante esa revisión, un equipo multidisciplinar de ITER evaluará el cumplimiento de los requerimientos del diseño conceptual propuesto. Para ello, es necesaria la entrega, en plazo y formas adecuados, de la documentación que lo justifica.

El presente trabajo fin de grado ha tenido por objeto investigar y reunir todas las herramientas requeridas para realizar el análisis dinámico del FILD de ITER, cuyos resultados habrá que recoger debidamente en un informe entregable junto con el resto de la documentación exigida antes de la revisión del diseño. Puesto que el estado exigido para la revisión conceptual de ese informe es preliminar, no se ha buscado obtener unos resultados definitivos. Más bien, se ha pretendido entender a fondo las particularidades de este tipo de análisis, siguiendo las directrices propuestas por la Organización de ITER.

En particular, el estudio dinámico del FILD de ITER se ha llevado a cabo mediante un análisis de espectro de respuesta, un método ampliamente utilizado en la industria nuclear por su sencillez y rapidez a la hora de obtener resultados conservadores.

Aunque el análisis de espectro de respuesta se ha realizado con la ayuda del paquete ANSYS, ha sido crucial entender desde un punto de vista teórico el problema; en concreto, entender bien los sistemas de un grado de libertad, puesto que el estudio de los sitemas de N grados de libertad puede reducirse al estudio de N sistemas de un grado de libertad por medio de la técnica de superposición modal.

Finalmente, se han obtenido unos resultados interesantes para un modelo de FILD ligeramente distinto, con un punto de apoyo que no estaría en la realidad, pero que ha sido necesario usarlo teniendo en cuenta la linealidad del análisis usado y el estado prematuro del diseño mecánico empleado.

Abstract

Nowadays, the society faces the search for a reliable environmentally-friendly energy source in order to overcome the current dependency on the fossil fuels. In this way, the energy released by the Sun has awakened interest in the scientific community. Since the middle of the 20th century, there have been a lot of breakthroughs in the field of nuclear fusion. However, an unprecedented investment is necessary to prove the technical and economic feasibility of fusion power.

The EU, China, India, Japan, South Korea, the Russian Federation and the USA are collaborating in the construction of the ITER nuclear fusion reactor, which will mark a milestone in the history of humanity. From the point of view of engineering, a sufficiently robust organization among the different members is key to ensure a high safety level, being indispensable to structure the work and to follow a standardized design process.

Inside the project structure, the diagnostics system is found. These diagnostics play an essential part in the nuclear fusion research. In particular, one of those diagnostics is the Fast-Ion Loss Detector (FILD), which provides important information about the nuclear reaction efficiency and the possible damage to the inner walls of the reactor.

As of today, the ITER FILD design is still at a conceptual stage, but it faces the preparation for the previous review to go ahead until the next design phase. During this review, a multidisciplinary team from ITER will assess the compliance of the conceptual design proposed with the requirements. For that reason, it will be required to properly deliver the documentation that justifies it.

The aim of the present final project has been to study and collect all the tools needed to perform a dynamic analysis of the ITER FILD, whose results will have to be appropiately included in a deliverable together with the rest of documentation demanded before the design review. Since the state that is required for the conceptual review is preliminar, the goal has not been to obtain definite results. On the contrary, the scope of this work has been limited by the well understanding of this type of analysis, following the guidelines proposed by ITER Organization.

In particular, the dynamic study of ITER FILD has been carried out by means of a response spectrum analysis, a method widely used by the nuclear industry because of its simplicity and rapidity in obtaining conservative results.

Even though the response spectrum analysis has been performed with the help of the ANSYS package, it has been crutial to understand the problem from a theoretical point of view; specifically, to well understand the single degree-of-freedom systems, since the study of the N degree-of-freedom systems can be reduced to the study of N single degree-of-freedom systems by using the modal superposition technique.

Finally, some interesting results have been obtained for a slightly different FILD model, with a support point that would not exist in reality, but that has been necessary taking into consideration that the analysis used is linear by nature and because of the premature state of the mechanical design used.

Contents

Index of Figures

Index of Tables

Acronyms

CD	Conceptual Design phase
CDR	Conceptual Design Review
CQC	Complete Quadratic Combination
CPPE	Common Port Plug Engineering Sub-Section
D	Deuterium
DA	Domistic Agency
DAF	Dynamic Amplification Factor
DBS	Document Breakdown Structure
DFW	Diagnostic First Wall
DSM	Design Shielding Module
FD	Final Design phase
FDR	Final Design Review
FE	Finite Element
FILD	Fast-Ion Loss Detector
FRF	Frequency Response Function
IO	ITER Organization
MDOF	Multi Degree-of-Freedom
NBI	Neutral Beam Injection
ODE	Ordinary Differential Equation
PBS	Plant Breakdown Structure
PD	Preliminary Design phase
PDR	Preliminary Design Review
RF	Radiofrequency
RO	Responsible Officer
RS	Response Spectrum/Spectra
RSA	Response Spectrum Analysis
SDOF	Single Degree-of-Freedom
SDP	System Design Process
SDR	System Design Review

SIR	Structural Integrity Report
SISO	Single Input Single Output
SLS	System Load Specification
SMHV	Séismes Maximaux Historiquement Vrasemblables (= Maximum Historically Probable Earthquakes)
SRSS	Square Root of Sum of Squares
T	Tritium
ULSS	Upper Level Support Structure
VDE	Vertical Displacement Event
VV	Vacuum Vessel
WBS	Work Breakdown Structure
ZPA	Zero Period Acceleration

1 Introduction

1.1 Introduction to Nuclear Fusion

1.1.1 Nuclear Fusion as an Energy Source

The enormous amounts of energy released by the Sun and other stars come from the nuclear fusion reactions which take place in their cores. Faced with the challenge to overcome the current dependence on fossil fuels, it is not strange that these amounts of energy have awakened interest in the scientific community. In fact, nuclear fusion is considered to be one of the most promising energy sources, which will permit humanity to satisfy their increasing energy demand in an environmentally-friendly way.

Persuing the goal above-mentioned, an extensive research has been conducted since the middle of the 20th century. In order to directly harness the nuclear fusion energy, i.e. building a fusion reactor on Earth, the conditions to achieve fusion have been studied [1]. There are three requirements that must be fulfilled; it is required to confine

- the sufficient fuel ions,
- at a temperature level higher than 100 million Kelvin
- and for the sufficient time.

In relation to the former conditions, the fusion reaction that appears to be the most interesting on Earth is the reaction between two hydrogen isotopes, deuterium (*D*) and tritium (*T*). Whilst the Earth's oceans is full of deuterium, the tritium can be readily produced. This reaction can be achieved at lower temperatures than the others (e.g. deuterium-deuterium or deuterium-helium-3), producing the highest energy gain. As it is shown in Eq. (1.1), the products of this fusion reaction are a helium-4 atom and a neutron (which has almost the 80% of the energy released) [2 p. 39].

$$D + T \rightarrow^{4} He + n + 17.6\text{MeV}\ ^{1} \tag{1.1}$$

Among different methods to achieve the former reaction, thermonuclear fusion is one of the most promising. In a controlled manner, matter is suffciently heated until deuterium and tritium particles gain enough kinetic energy to overcome the repulsive Coulomb forces that hinder them from fusing when they are brought close enough (Coulomb barrier) [2 p. 40]. Since, under these conditions, matter becomes extremely hot plasma, it is essential to confine it in order to avoid any direct contact with any solid material inside the reactor, which immediately would lead to eroded walls and polluted plasma [3]. That is why achieving the proper confinement is key to go ahead with fusion.

Current researches point out two ways to confine plasma successfully: magnetic confinement and inertial confinement. This workwill be focused on the magnetic confinement approach, which uses a strong magnetic field to keep the plasma away from the walls of its container.

The way to keep the plasma magnetically confined for enough time is by using a toroidal system where, additionally, the magnetic field lines are twisted intentionally to avoid an unstable configuration. There are two

[1] 1eV (electronvolt) = 1.602 177 10^{-19} J

main devices to magnetically confine plasma that are being investigated worldwide: the stellarator and the tokamak. Once again, this work is focused on the tokamak approach[2].

Regarding the way to magnetically confine the plasma in a tokamak, the magnetic field lines follow a helical trajectory around the torus. The toroidal component of this magnetic field is produced by toroidal field coils, whereas the poloidal component is generated by an electric current inside the plasma, which travels around the torus. This current is induced in the plasma by a central solenoid, in an identical way to the induced current in the secondary coil of a transformer, during a finite time interval [4 pp. 33-34]. Additionally, poloidal field coils are used for plasma positioning and shaping. See Figure 1.1 to obtain more details about the tokamak configuration.

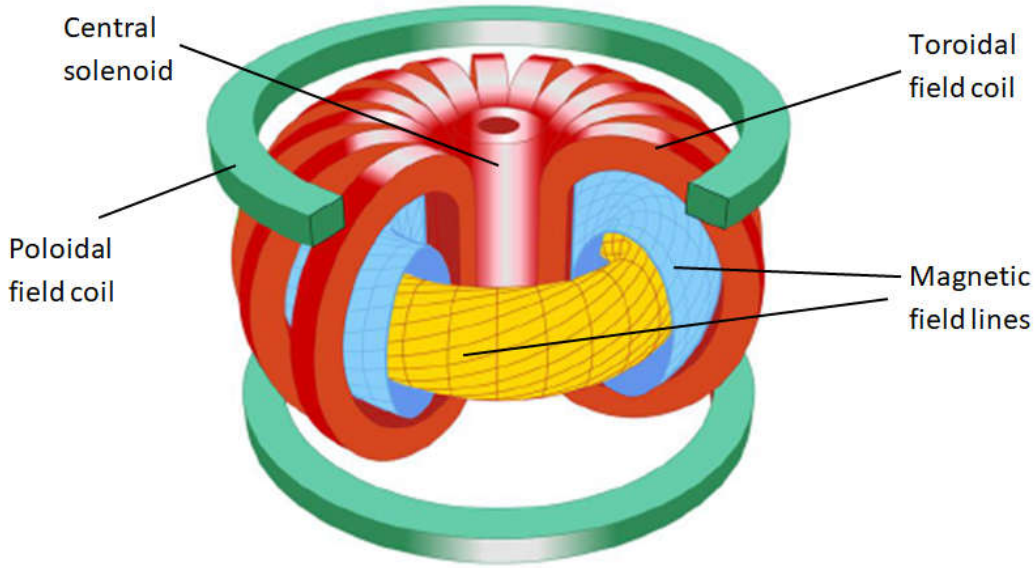

Figure 1.1 Colour scheme of the tokamak concept [2 p. 46]. In blue and yellow, the magnetic field surfaces. In red, the toroidal field coils and the central solenoid. In green, the poloidal field coils.

So far, the tokamak is the most widely adopted option to achieve fusion. Several examples of tokamaks which are currently in operation are JET (Culham Centre for Fusion Energy, UK) [5], ASDEX Upgrade (Max Planck Institute of Plasma Physics, Germany) [6] or DIII-D (DIII-D National Fusion Facility, USA) [7]. Others, such as JT-60SA (Naka Research Centre of QST, Japan) [8] and ITER (Cadarache, France) [9], are being constructed and are planned to operate in the future. The latter will become the world's largest tokamak (with a plasma volume of 830 cubic metres[3]), attempting to prove the technical and economic feasibility of fusion power, as well as its high safety level.

At the end, the fusion energy will be harnessed by absorbing heat in the walls of the doughnut-shaped vacuum chamber that contains the confined plasma. Similarly to a conventional power plant, a fusion power plant will eventually generate electricity by means of the produced steam, which will move through the blades of certain turbines whose shafts are coupled to generators.

1.1.2 The Fast-Ion Loss Detector (FILD)

In the frame of nuclear fusión research, the so-called diagnostics are developed to investigate hot magnetized plasma. A variety of fields of physics are involved. There are two types of diagnostics, depending on how they extract information from the confined plasma: passive, if the observation depends on the spontaneous behaviour of the plasma (such as bolometry, spectroscopy, electron cyclotron emission, etc.); or active, if it is required the injection of light beams, particles or probes to observe the induced effect (such as polarimetry, reflectometry, etc.). However, there is one common aspect among all of them: plasma probing has to be

[2] Further information about magnetic confinement can be found in [2 pp. 45-47].
[3] Some facts and figures of ITER can be found in [9].

conducted without any material contact between the measuring instrument and the plasma, due to the extreme plasma conditions [2 p. 137].

One of the existing diagnostic systems is the Fast-Ion Loss Detector (FILD). It is the most widely used diagnostics for measuring fast-ions escaping from the plasma. The term fast-ion refers to those ions which, forming part of the plasma in magnetic confinement devices (as well as thermal electrons or ions and neutral particles), have a higher energy than the thermal particles[4] [10 p. 43]. Monitoring these fast-ions losses permits to have certain evidence of the fusion reaction efficiency and the damage of the first wall due to the impact of these fast-ions, and to know the different mechanisims that cause them. In order to better understand the relation between fast-ions and the reduction of the fusion reaction efficiency, it has to be noted how the required high plasma temperature is accomplished.

As it was explained in the subsection 1.1.1, due to kinetic reasons, a high temperature is needed to aim to a higher reactivity. In order to produce a self-sustaining reaction (ignition), the helium resulting in the reaction (1.1), which has around the 20% of the total energy realeased, can be harnessed to keep the plasma warm. Nevertheless, additional heating techniques are necessary at the beginning of the process [2 p. 105]. Some of them are neutral beam injection heating (NBI) and radiofrequency heating (RF). The former consists in injecting a beam of neutral fuel atoms at high energy into the plasma, transferring its energy to the confined plasma particles through collisions. The latter consists in launching high power electromagnetic waves into the plasma, which will eventually heat a part of the plasma depending on the choice of frequency.

All the mechanisms to heat the plasma mentioned in the previous paragraph generate fast-ions, such as the non-confined α-particles, i.e. ${}^{4}He$, or the neutral particles injected by NBI which are prematurely ionized and unintentionally deflected by certain field lines that intersect material components. Since they will leave the plasma before thermalizing, the larger the number of fast-ions losses is, the lower the energy transmission is, and, therefore, the colder the plasma become.

Attempting to measure the losses above-said, a FILD is located at a certain position on the diagnostic first wall[5] (DFW), where a fraction of the incident fast-ions will encounter a scintillator material (that emits light when it is hit by the escaping ions). Its interaction will eventually provide measurement of their energy (related to the gyroradius of the particle around the magnetic field line) and their pitch angle[6] (to calculate the orbits followed by the ions) depending on the point of the scintillator where the flash is produced, as well as their frequency (to know the detailed time evolution). The information is extracted by means of an optical system. Additionally, it should be noted that the whole velocity-space will not be measured, just those fast-ions with velocities limited by a collimator (improving the resolution in energy and pitch angle). A detailed scheme of FILD is shown in Figure 1.2.

A detailed explanation about FILD is accrued in [10], whereas in [11], it is possible to find a detailed knowledge about the implementation of FILD. This diagnostic is present worldwide in tokamaks such as ASDEX [12-14], JET [15] and DIII-D [16]. Moreover, a new FILD concept is being developed for ITER [17]. With goals such as producing 500 MW of fusion power for 50 MW of injected heating power, achieving a self-maintained deuterium-tritium plasma and remaining stable for longer periods of time (around 500 s)[9], ITER places a large number of requirements on the FILD design. Among these requirements [18], it can be noted: the compatibility with thermal plasma and fast-ion heat loads [19], which make indispensable a reciprocating concept [20]; a fast retraction if necessary from a measuring position to a parking position; and the capacity to operate in ultra-high vacuum, which makes even more complex a mechanical design that must be extremely reliable, because mechanical and electrical faults of the components have to tolerate long time intervals without maintenance.

The mechanical design of the ITER FILD is precisely related to the objective of this work.

[4] Thermal particles are those particles inside the plasma which are in thermal equilibrium.

[5] It corresponds to the first physical barrier which faces the plasma, specifically to the area customized by diagnostics.

[6] The pitch angle is the angle between the velocity vector of the particle and the magnetic field line around which that particle gyrates.

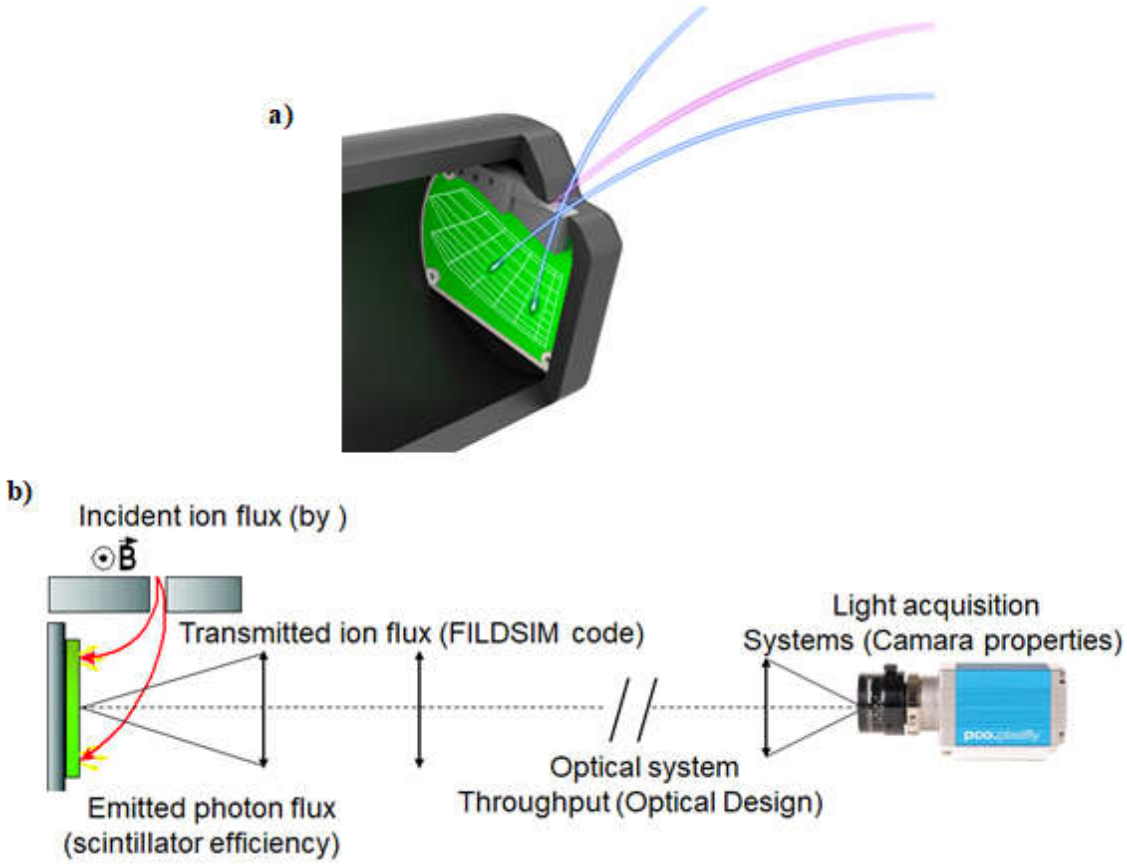

Figure 1.2 a) Schematic of some fast-ions hitting the scintillator material, where it is drawn the so-called strike map in a explainatory way, to better understand the process of extracting the discrete information of energy and pitch angle. **b)** Schematic of the data acquisition by means of the optical system. Both images are courtesy of the Plasma Science and Fusion Technology group (PSFT, University of Seville).

1.2 Motivation

The ITER Project is one of the most ambitious projects in the history of humanity. It is an international collaborative venture in which the EU, China, India, Japan, South Korea, the Russian Federation and the USA are taking part. The overall Project comprises several millions of parts arranged in 36 systems and 50[7] susbsystems along the Plant Breakdown Structure[8] (PBS), whose development is established according to a Work Breakdown Structure (WBS) [21 p. 12].

Given the highly integrated design of ITER, the nuclear safety requirements and the complexity of the procurement scheme, it is mandatory to establish a standardized design process [21 p. 8]. The so-called ITER System Design Process (SDP) defines all those steps to be followed by the ITER Organization (IO), the Domestic Agencies[9] (DAs) and their suppliers, for the successful design of the ITER systems products. Specifically, the role of the SDP includes creating a design that fulfils all the requirements and justifying it [22 p. 2].

The SDP is divided into three phases depending on the system maturity: Conceptual Design phase (CD), Preliminary Design phase (PD) and Final Design phase (FD), as it is shown in Figure 1.3. The ITER FILD is in the conceptual design phase presently.

[7] As of 2009. Today, it is likely to be larger.
[8] The ITER FILD belongs to the diagnostics system (PBS55), specifically it is the subsystem PBS55.B9. The term "system" is used to refer to ITER FILD hereunder.
[9] The Domestic Agencies are involved in the ITER Project through the Procurement Arrangements and Tasks Agreements. In the case of the ITER FILD, the DA is the University of Seville by way of the CNA.

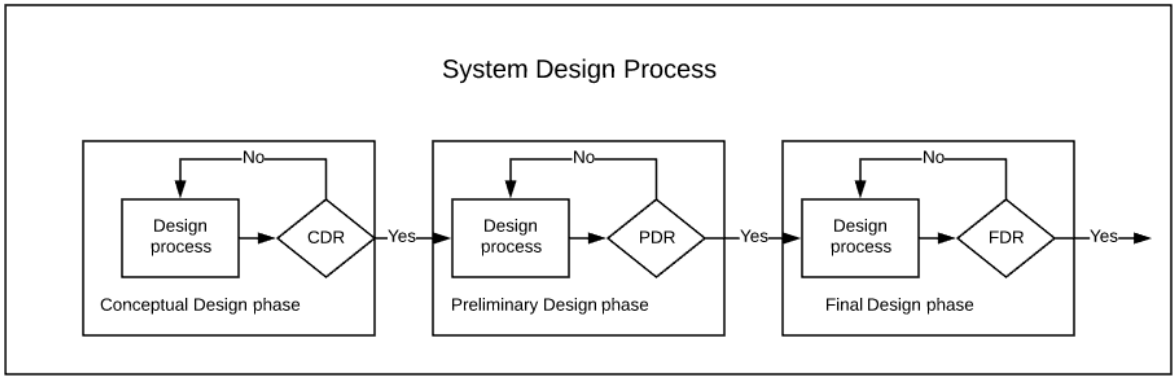

Figure 1.3 Schematic view of the design process divided into its three phases.

In the schematic above-mentioned, it is shown that the results of the design process throughout each phase have to be assessed before going to the next phase. These assessments are performed by the IO and are called System Design Reviews (SDRs). The general aims of SDRs are to ensure the suitability, adecuacy and effectiveness of the system design to achieve the requirements [23 p. 14]. Generally, there are three SDRs[10]: Conceptual Design Review (CDR), Preliminary Design Review (PDR) and Final Design Review (FDR).

Throughout the different phases of the design process, a set of engineering data (2D-3D data, calculation notes, schematics, etc.) has to be produced by the pertinent Design Developer (in this case a DA, external to IO) taking into consideration the design work plan defined by the so-called Responsible Officer[11] (RO). These documents will be provided for IO before each SDR by means of a list of deliverables called Input Data Package according to [23 pp. 16-17].

The design documentation is organized according to the Document Breakdown Structure (DBS) [24], which comprises the following folders: Requirements, Description, Operation, Justification, Test & Comissioning and Design Management. Each folder is headed by a leading document, which refers to lower level design documents such as drawings, schematics, etc. according to [25 p. 6]. The leading documents for the current state of ITER FILD are summarised in the Table 1.1. A detailed explanation about the different documents to deliver can be found in [25 pp. 8-40].

Table 1.1 List of leading documents to deliver before the CDR.

DBS	Leading documents	State at conceptual level
Requirements	System Requirements Document (SRD)	Complete
Requirements	Interface Control Documents (ICD)	Complete
Description	System Design Description (DD)	Preliminary
Justification	Design Compliance Matrix (DCM)	Preliminary

1.3 Purpose and Scope

The aim of this work is to carry out the dynamic analyses related to the vibration of the ITER FILD. The results extracted from these analyses will eventually form part of the set of reports grouped in a top level report called Structural Integrity Report (SIR) [26 p. 9]. In this way, it will be provided a justification for the reaction of the system to both the seismic loads and the inertial excitation from the Vacuum Vessel (VV), considered in the System Load Specification (SLS) [27 pp. 8-9], which is under construction presently. This justification will be linked in the DCM to support the structural integrity assesment.

[10] So far, just a pre-conceptual status review has taken place for ITER FILD.
[11] The RO designates the person in charge of the development of a product, e.g. ITER FILD, within IO.

On the other hand, the main scope of this work is to initiate a plan for the progressive refinement of the different vibrational studies, which will permit to update the reports quickly and efficiently in the future. Since the current state of the design of ITER FILD is not frozen, it is not a goal to obtain final results, but representative results that show the dynamic behaviour of the system at this stage.

The procedures used to obtain the solution follow [28; 29].

1.4 Structure of the work

In order to detail how the desired goals have been achieved, this document is structured in chapters.

In chapter 2, the description of the system is addressed to know the main components and details of interest. Additionally, the load combinations that are inside the scope of this work are included here.

In chapter 3, all those key theoretical aspects to understand the dynamic study of the ITER FILD are logically presented. At the end of this chapter, the type of analysis that will be carried out is mentioned and justified.

In chapter 4, all the theoretical content previously presented is treated from a practical point of view. The modelling of ITER FILD, as well as the numerical tools used to resolve the problem, is presented here.

Next, in chapter 5 the results obtained are exposed. This chapter is divided into four sections. Each section presents some progress with respect to the former. At the end, the dynamic study of ITER FILD is addressed with a sufficiently complete final model.

Finally, in chapter 6, the part of discussion is addressed. First, in section 6.1, the main conclusions after performing the dynamic analisys are brought into focus. Secondly, in section 6.2, the work that will be necessary to do in the future is collected.

2 ITER FILD Design Description

2.1 System Description

The assembled ITER FILD, shown in Figure 2.1, briefly consists of the following parts:

- **The linear manipulator** is divided into four parts:
    - ***Redundant linear actuators:*** create motion in a straight line to bring the probe head closer to the plasma for measuring and to move back to the parking position.
    - ***Fixed part:*** comprises the fixed support, the outer pipe (to limit the deformation of the movable part during EM transient events and/or seismic events) and the outer neutron shielding cylinder.
    - ***Movable part:*** comprises the probe head (equally, heat shielding, scintillator plate and collimator), the probe head support, the guide assembly (rolling guide and rollers), the inner neutron shielding cylinder and the first mirror. Particles escaping from the plasma are "filtered" by the collimator and eventually hit the scintillator plate. The position of the strike points on this plate is tracked by an optical system allowing the characterization of the velocity space of the escaping particles.
    - ***The edge welded metallic bellow***, needed to provide a private gas chamber inside the fixed support avoiding gas leakage into the Vacuum Vessel. The bellow accommodates the reciprocating displacement of the probe avoiding in vacuum contacts between moving parts (rollers and fixed support).
- **The optical system**, consisting of several mirrors (including the optical hinge) responsible of transmitting the detector optical signal out of the port plug, back to the optical acquisition systems (camera and photomultipliers).
- **Other FILD common services** such as gas feedthrough, cabling and electric isolating, etc.

However, in accordance with [27 pp. 4-5], just the linear manipulator is considered at this CD stage, with the exception of the elements inside the probe head heat shielding and the bellow (exclusively for the present work).

The design of ITER FILD is the result of the consideration of multiple aspects as it was revealed in 1.1.2. In particular, two factors are considered to be key in the current design configuration. On the one hand, the *cantilever* configuration comes of attempting to set the parking position back as much as possible, due to the difficulty to incorporate cooling. In this way, a longer life of the probe head is expected. On the other hand, it is a requirement to take up the minimum space inside the DSM, where it is inserted, in order to maximize the neutron shielding that protects against the neutron flux effects.

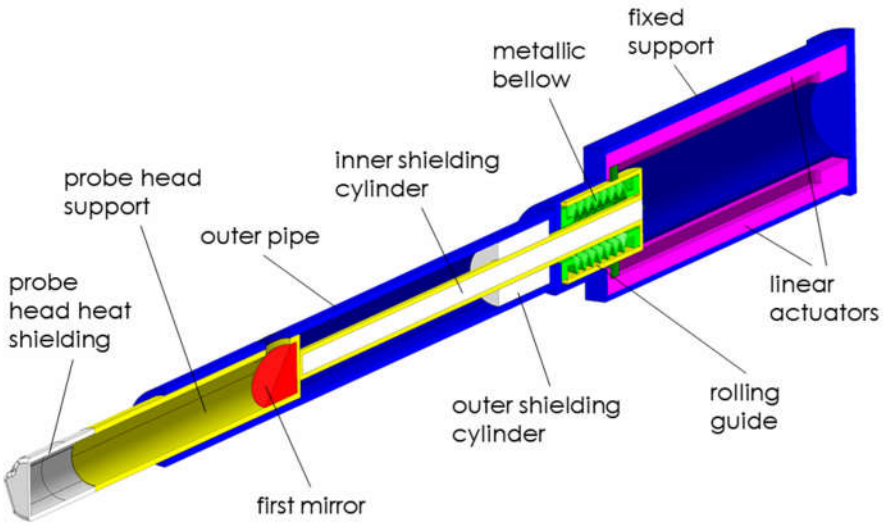

Figure 2.1 Different elements integrating the ITER FILD. The assembly formed by rolling guide-probe head support-probe head heat shielding has a length of around 2 m. The diameter of the probe head support is 108 mm. The radial gap between the probe head support and the outer pipe is 1 mm.

The ITER FILD is located at one of the three Design Shielding Modules (in particular, DSM 2), within the Equatorial Port Plug #8. Specifically, as shown in Figure 2.2, it is attached to the last vertical blade of the DSM 2 by the fixed part. This fixed part serves as a support and guide for the movable part, which holds the probe head and pushes it close to the plasma for measuring. A comparison between the parking and measuring positions of ITER FILD can be seen in Figure 2.2.

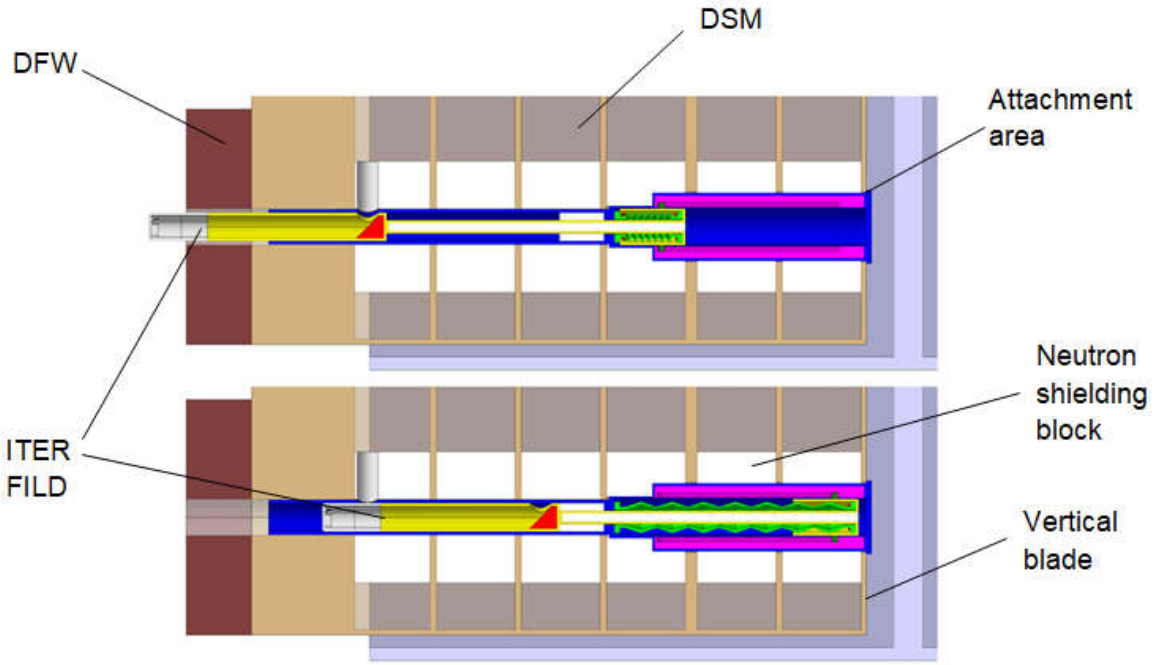

Figure 2.2 ITER FILD in measuring (up) and parking (down) positions.

To get a global view of the position of ITER FILD with respect to the tokamak and its main components, see Figure 2.3. Note that during the operation of ITER FILD, the probe head is inside the VV. Thus, it is

considered to be an in-vessel diagnostic system.

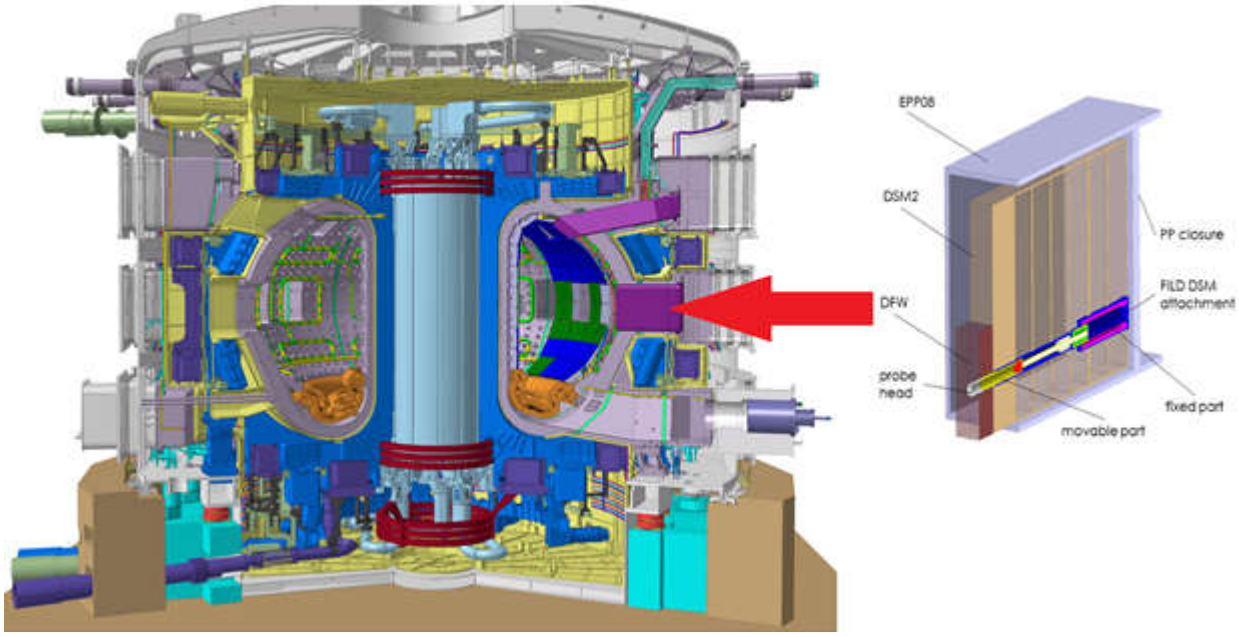

Figure 2.3 Location of the ITER FILD inside the ITER tokamak. During operation, the ITER FILD is expected to be inserted into the Vacuum Vessel, which is the doughnut-shaped chamber where the ports are supported. The image of the tokamak is courtesy of the ITER Organization [9].

The good knowledge of the location of the ITER FILD will be essential to understand the types of loads that have a possible impact on it. In particular, it is key to know how the ITER FILD interacts with its surroundings and the path that the different loads follow from their sources to the ITER FILD, as well as the path followed by the reactions originated. A deeper explanation of all of these aspects is presented in the corresponding Load Specification [27], which is under construction now.

The definition of the loads that are considered to be analysed will be presented in section 2.2. There, a brief description of the nature of the loads will be done.

2.2 Load combinations

In this section, the load combinations to which the ITER FILD is subject will be specified. The load combinations that are inside the scope of this work are included in Table 2.1:

Table 2.1 Load combinations of interest extracted from [27].

#	Operating conditions		Initiating event	Concatenated event	Category	Number of events
1	Gravity effect	Measuring position	VDE III	-	III	-
2	Gravity effect	Measuring position	SMHV	-	III	-

There are two load combinations that will be taken into consideration in the dynamic analysis of the ITER FILD. In this case, just an initiating event exists, which makes it easier to obtain the solution. Each solution will be calculated separately. In relation to the ITER FILD operating conditions, it is important to see that both

load cases are subjected to the self-weight, and those loads associated with the measuring position, e.g. thermal loads. Nevertheless, the latter will not be considered here.

VDE stands for Vertical Displacement Event, and it consists of the loss of the vertical position control of the plasma as a consequence of a failure of the feedback control system. A plasma VDE is characterised by three phases: start of plasma vertical movement, thermal quench and current quench. This work is focused on the intertial excitation from VV, which involves the effect of the movement of the VV (an extremely massive body) due to the transient event on the system under study, that is, ITER FILD. In particular, a VDE III represents the worst case expected to occur.

SMHV (Séismes Maximaux Historiquement Vraisemblables = Maximum Historically Probable Earthquakes) is the most penalising earthquake liable to occur over a period of about 1000 years.

All the inputs which are necessary to perform the analyses are included in part 4.7.1.2.

3 Theoretical Background

The history shows how important it is to perform vibration analyses in order to avoid undesirable oscillations from a position of equilibrium, which increase stresses and induce fatigue, eventually leading to the collapse of the structure.

The 19th century is full of examples of bridges that collapsed due to external factors such as the wind or the march in unison of the soldiers across the structure. More recently, the first Tacoma Narrows Bridge collapsed brutally in 1940 due to the wind excitation, whereas the Millennium Bridge began to vibrate strongly in 2000 because of the steps of the large influx of pedestrians on the bridge.

The previous examples, as well as lots of different cases in a wide range of engineering applications, justify a deep study in terms of dynamics for the ITER FILD.

3.1 Introduction to Single Degree-of-Freedom (SDOF) Systems

In general, a SDOF system is modelled as illustrated in Figure 3.1, comprising a rigid mass (capable of storing kinetic energy), a spring (capable of storing potential energy) and a damper (capable of absorbing energy gradually). In this way, if the vibrating system is displaced from its position of stable equilibrium, a linear motion is created by means of the elastic potential energy stored in the spring, which gives kinetic energy to the mass, and vice versa, according to the conservation of mechanical energy. Nevertheless, due to the dissipation of energy in the damper, the motion eventually vanishes to satisfy the law of conservation of energy.

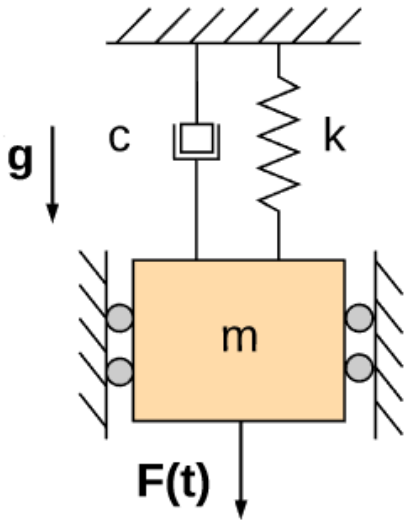

Figure 3.1 General schematic of a SDOF system.

In Figure 3.1, the letters *m*, *k* and *c* denote the mass of the body, the stiffness of the spring and the damping coefficient of the damper, respectively.

As a result of the dissipation of energy, an external force ($F(t)$) is required, to maintain the system in motion. In order to generalize even more, the system was drawn in a vertical position to include the effect of gravity as well. Additionally, a couple of roller bearings were added to represent the linear motion. From this point forward, they will not be added for simplicity.

The derivation of the equation of motion is addressed now. Since it is a SDOF system, just a single coordinate is needed to describe the motion. In this case, the downward sense, with the origin where the spring is at its natural length, is taken without loss of generality. See Figure 3.2.

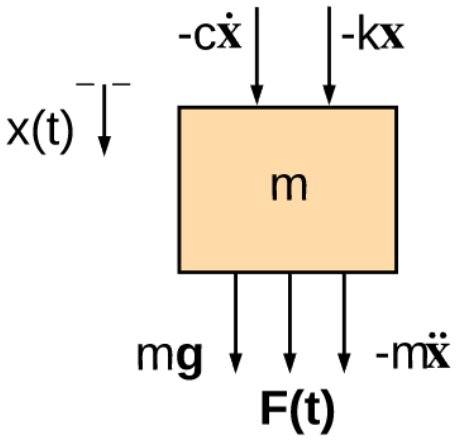

Figure 3.2 Free-body diagram of the mass m.

Applying the d'Alembert's principle in Figure 3.2, the following force balance is obtained:

$$m\ddot{x} + c\dot{x} + kx = mg + F(t) \tag{3.1}$$

This is a non-homogeneous second-order linear ordinary differential equation (ODE) with constant coefficients. In order to simplify a bit the ODE, a change of variable is made. The new variable x_1 refers to the static equilibrium position:

$$x = \delta_{st} + x_1 \Rightarrow m\ddot{x}_1 + c\dot{x}_1 + kx_1 = F(t) \tag{3.2}$$

Although the gravity cannot generally be removed from the ODE (e.g. in the typical case of an oscillating pendulum), in this particular case, it can be done by considering the reference with respect to the static equilibrium position. In this way, the so-called initial value problem looks like this:

$$\begin{cases} m\ddot{x}_1 + c\dot{x}_1 + kx_1 = F(t) \\ x_1 = x_{10}, \dot{x}_1 = \dot{x}_{10} \end{cases} \tag{3.3}$$

where x_{10} and $\dot{x}_{10}$ denote the initial position and velocity, respectively. To find the solution of the non-homogeneous ODE, it is required to obtain the general solution of the homogeneous ODE ($x_{1h}(t)$) and a particular solution of the non-homogeneous ODE ($x_{1p}(t)$), according to the theory of differential equations. The sum of both solutions constitute the general solution of the non-homogeneous second-order linear ODE.

First, it is known that the general solution of the homogeneous ODE seems: $x_1(t) = Ae^{pt}$. Plugging it into the homogeneous ODE, and handling the resulting expression a bit (eliminating the case $A = 0$), it turns out the following characteristic (or auxiliary) equation

$$mp^2 + cp + k = 0 \tag{3.4}$$

whose roots are

$$p = \frac{-c \pm \sqrt{c^2 - 4mk}}{2m} \tag{3.5}$$

Now, it is interesting to manipulate the former expression by introducing the following definitions:

- Undamped natural frequency: $\omega_n = \sqrt{k/m}$
- Critical damping coefficient: $c_{cr} = 2m\omega_n$
- Damping ratio: $\zeta = c/c_{cr}$
- Damped natural frequency: $\omega_d = \omega_n\sqrt{1-\zeta^2}$

After introducing them into (3.5) and recasting the resulting expression, it is obtained

$$p = -\zeta\omega_n \pm \omega_n\sqrt{\zeta^2 - 1} \tag{3.6}$$

The form of the solution $x_{1h}(t)$ can be different depending on the sign of the discriminant:

- If it is positive ($\zeta > 1$): $x_{1h}(t) = A_1 e^{\left(-\zeta\omega_n + \omega_n\sqrt{\zeta^2-1}\right)t} + A_2 e^{\left(-\zeta\omega_n - \omega_n\sqrt{\zeta^2-1}\right)t}$
- If it is zero ($\zeta = 1$): $x_{1h}(t) = e^{-\zeta\omega_n t}\left(A_1 + A_2 t\right)$
- If it is negative ($\zeta < 1$): $x_{1h}(t) = e^{-\zeta\omega_n t}\left(A_1\cos\omega_d t + A_2\sin\omega_d t\right)$

Whilst the first expression shows an overdamped behaviour, the second one shows a critically damped behaviour and the third one shows an underdamped behaviour (being undamped if $\zeta = 0$). See the Figure 3.3 to get a more visual description.

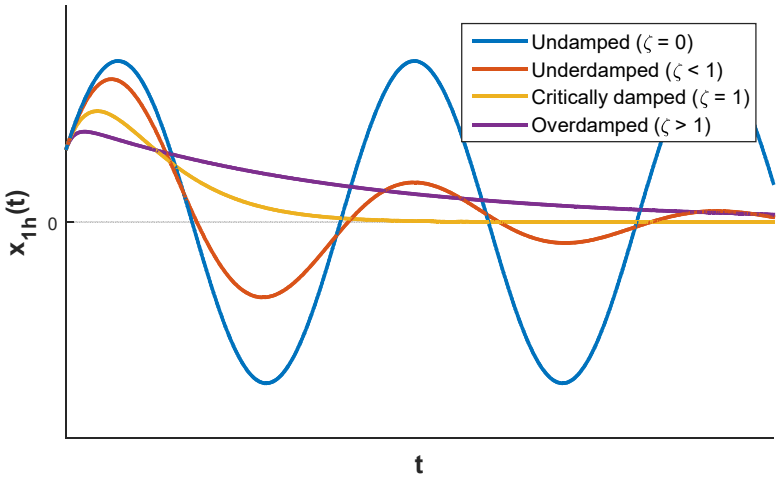

Figure 3.3 Types of solutions of the homogeneous ODE.

As it can be seen in the foregoing, the solution begins to oscillate at a damping ratio lower than $\zeta = 1$, i.e. $c = c_{cr}$. That solution ($\zeta < 1$) vibrates with the damped natural frequency, being the undamped natural frequency if $\zeta = 0$, that is, if there is not any damper. Just those oscillating solutions ($\zeta < 1$) are of interest.

Typical technical values of the damping ratio are well below 0.2 (20%) according to [30 p. 54], therefore $\omega_d \simeq \omega_n$ would be a good hypothesis if necessary.

On the other hand, as pointed out in the expression of the solution for the underdamped case, the larger the product $\zeta\omega_n$ is, the sooner the response vanishes. This is because of the exponential envelope.

Regarding the values of the constants which appear in the solution expression, A_1 and A_2, they come from the

application of the initial conditions. This has a special meaning: if $F(t)=0$, then the vibration is induced by the initial conditions. This case is called free vibration. More details about the importance of initial conditions can be found in section 3.2.

The next step is to obtain the particular solution $x_{1p}(t)$ of Eq. (3.2), which will be found in sections 3.3 and 3.4. The general solution of the entire problem (3.3) will be obtained by summing both $x_{1h}(t)$ and $x_{1p}(t)$.

Needless to say, the appearance of the solution is exclusive of the here-used SDOF. A set of different solved examples can be found in [31]. In several cases, it will be indispensable to linearize the equation of motion obtained (e.g. in the example of the simple gravity pendulum) to be able to follow a handmade procedure like the here-presented one. It is enough with linearizing near the equilibrium point of the system.

Finally, a brief overview of the SDOF analysis that is covered throughout thi section is shown in Figure 3.4.

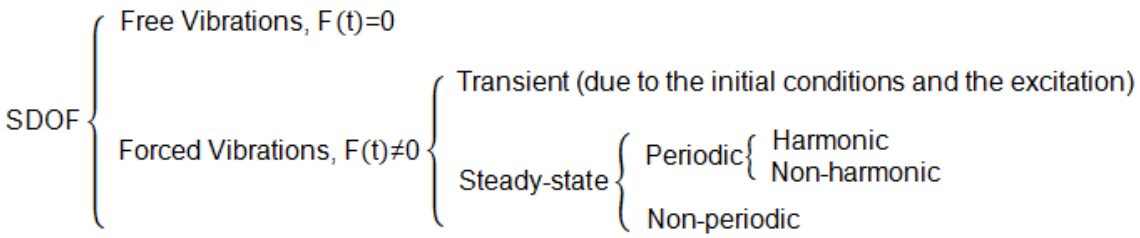

Figure 3.4 Classification of the vibration problem.

3.2 Forced Vibrations: Transient and Steady-State

In order to clarify the role of the initial conditions in the response of the system, it will be obtained the symbolic value of the constants A_1 and A_2 in the solution of Eq. (3.3).

Since $x_1(t)$ can be expressed as sum of $x_{1h}(t)$ and $x_{1p}(t)$:

$$x_1(t)=x_{1h}(t)+x_{1p}(t)=e^{-\zeta\omega_n t}\left(A_1\cos\omega_d t+A_2\sin\omega_d t\right)+x_{1p}(t) \tag{3.7}$$

Applying the initial conditions of Eq. (3.3), it turns out

$$x_1(t=0)=A_1+x_{1p}(0)=x_{10} \tag{3.8}$$

$$\dot{x}_1(t=0)=\left(-\zeta\omega_n A_1+A_2\omega_d\right)+\dot{x}_{1p}(0)=\dot{x}_{10} \tag{3.9}$$

and therefore

$$A_1=x_{10}-x_{1p}(0) \tag{3.10}$$

$$A_2=\frac{1}{\omega_d}\left[\dot{x}_{10}-\dot{x}_{1p}(0)+\zeta\omega_n\left(x_{10}-x_{1p}(0)\right)\right] \tag{3.11}$$

If the values obtained above are introduced into Eq. (3.7) and the resulting expression is properly recast, it is found that

$$\begin{aligned} x_1(t)=&e^{-\zeta\omega_n t}\left(x_{10}\cos\omega_d t+\frac{\dot{x}_{10}+\zeta\omega_n x_{10}}{\omega_d}\sin\omega_d t\right)\\ &+(-1)e^{-\zeta\omega_n t}\left(x_{1p}(0)\cos\omega_d t+\frac{\dot{x}_{1p}(0)+\zeta\omega_n x_{1p}(0)}{\omega_d}\sin\omega_d t\right)+x_p(t)\end{aligned} \tag{3.12}$$

The former result means that the response can be divided into two parts[12]:

- transient: it comprises the first two addends and ends up disappearing because of the exponential decay;
- steady-state: it comprises the last addend and is permanent as long as the excitation $F(t)$ is different from zero.

See Figure 3.5 to obtain a visual interpretation of the result.

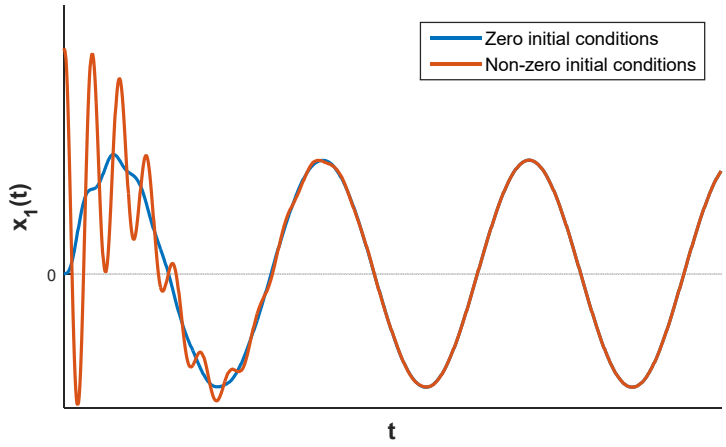

Figure 3.5 Response for the whole time range.

As it can be extracted from the Eq. (3.12) and Figure 3.5, the transient is due to both the initial conditions (x_{10} and $\dot{x}_{10}$) and the excitation ($x_{1p}(0)$ and $\dot{x}_{1p}(0)$). This transitory motion vibrates at the damped natural frequency. If $F(t)=0$, then it is clear that the motion would start due to the initial conditions, vanishing with time.

3.3 Forced Periodic Vibrations

This section is centred on the steady-state. Its aim is to obtain the response $x_{1p}(t)$. In order to clarify the problem, the nature of $F(t)$ is classified into two types: periodic and non-periodic. Whilst the first one is the objective of the current part, the second one will be the objective of the following section 3.4. Additionally, inside the periodic type, it is possible to distinguish harmonic excitation from non-harmonic excitation. Firstly, it is found the response for the harmonic case, and at the end it is mentioned the difference with respect to the non-harmonic case.

The harmonic excitation is modelled by a sinusoidal force $F(t)=F_0 \sin \omega t$ without loss of generality. According to that expression, the force has an amplitude F_0 and oscillates at the frequency ω. To obtain $x_{1p}(t)$, it is necessary to substitute the previous expression of $F(t)$ into (3.2), taking into consideration that the form of the response will be $X_0 \sin(\omega t-\varphi)$[13]. Nevertheless, the resulting algebraic expressions can be simplified by using a complex number approach[14], that is, by considering the force $F_0 e^{i\omega t}$ and the response $X_0 e^{i(\omega t-\varphi)}$ (or $X_0 e^{-i\varphi} e^{i\omega t}$, where the term $X_0 e^{-i\varphi}$ is generally a complex number, simply expressed as X). Finally, the response of the actual problem will be found by simply taking the imaginary part of the output of the system. The process is described below.

[12] This idea is key. The type of analysis reported in this document is a response spectrum analysis instead of a transient analysis due to the nature of the excitation of the problem. Since a response spectrum analysis does not calculate the dynamic response for the entire time range, where the dynamic forces have been acting, a conservative estimation for the maximum response of the desired output is obtained from this type of analysis [32].

[13] Using the so-called method of undetermined coefficients in mathematics.

[14] Euler's formula establishes that $e^{ix} = \cos x + i \sin x$.

Plug $F_0 e^{i\omega t}$ and $Xe^{i\omega t}$ into (3.2), resulting

$$X\left(-m\omega^2 + ic\omega + k\right)e^{i\omega t} = F_0 e^{i\omega t} \tag{3.13}$$

and therefore

$$X\left(-m\omega^2 + ic\omega + k\right) = F_0 \tag{3.14}$$

A more useful way to express the foregoing is

$$X = \frac{F_0}{k - m\omega^2 + ic\omega} = \frac{F_0 / k}{1 - \left(\frac{\omega}{\omega_n}\right)^2 + i2\zeta\frac{\omega}{\omega_n}} = \frac{F_0 / k}{1 - \tau^2 + i2\zeta\tau} \tag{3.15}$$

where the definitions of ω_n and ζ , as well as the frequency ratio $\tau = \omega/\omega_n$, have been used.

Now, to obtain the values of X_0 and φ, it is sufficient with obtaining the complex modulus and the complex argument, respectively.

$$X_0 = |X| = \frac{F_0 / k}{\sqrt{\left(1-\tau^2\right)^2 + \left(2\zeta\tau\right)^2}} \tag{3.16}$$

$$\varphi = \arg\left(X\right) = \arctan\frac{2\zeta\tau}{1-\tau^2} \tag{3.17}$$

On the other hand, it is interesting to express the solution as the product between a function $H(\tau)$ and the force $F(t)$:

$$x_{1p}(t) = H(\tau)F(t) \tag{3.18}$$

where $H(\tau)$ is the so-called Frequency Response Function (FRF) or simply transfer function, whose definition is

$$H(\tau) = \frac{1/k}{1 - \tau^2 + i2\zeta\tau} \tag{3.19}$$

Modelling the system in the way of (3.18), this can be associated with a Single Input Single Output (SISO) schematic. The response of the system oscillates at the same frequency as the excitation, being amplified/attenuated and delayed depending on the value of τ , i.e. of ω .

Now, the amplitude of the system and its phase are plotted in Figure 3.6. A more useful way to do the first thing is by means of the so-called Dynamic Amplification Factor (DAF). In this way, it can be plotted the ratio between the amplitude of the motion X_0 and the static amplitude (if $\omega = 0$), showing by which factor the motion is amplified or mitigated.

$$DAF = \frac{X_0}{X_{static}} = \frac{1}{\sqrt{\left(1-\tau^2\right)^2 + \left(2\zeta\tau\right)^2}} \tag{3.20}$$

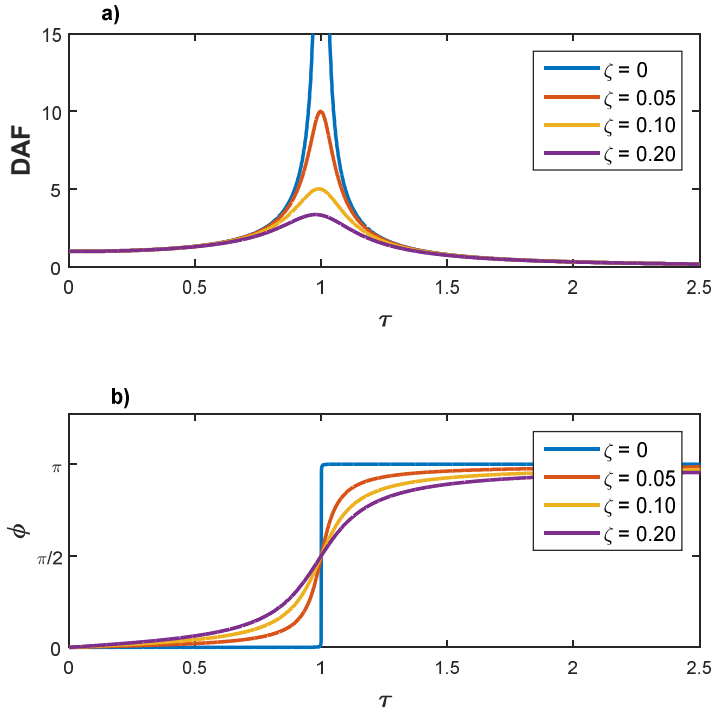

Figure 3.6 a) Graph of DAF against τ. **b)** Graph of φ against τ.

According to the graph plotted in Figure 3.6a, the DAF has a peak in $\tau = \sqrt{1-2\zeta^2}$ (really close to 1 because $\zeta \ll 1$) as long as $\zeta \leq 1/\sqrt{2}$ (i.e. for all the typical technical values). The lower ζ is, the higher the peak is, diverging for $\zeta = 0$. This peak is related to the phenomenon of resonance, where a small excitation can lead to large amplitude vibrations if the frequency of the excitation is close enough to the so-called resonant frequency (which is practically equal to the natural frequency and exactly equal to it if the damping ratio is zero). Addionally, it should be noted that the response of the system is the static deflection if the exciting frequency equals zero. In other words, if $\omega = 0$, the system is governed by the external loads, whereas if $\omega \simeq \omega_n$ it is governed by the inertial loads. Finally, if $\omega \to \infty$, the response of the system tends to disappear.

Before finishing this part, it is convenient to mention what to do if the force is periodic with period $T = 2\pi/\omega_0$, but non-harmonic. In this case, the main idea is to descompose the periodic excitation into the sum of many harmonics by using a Fourier series, and then to find the response as the sum of the individual responses to each harmonic excitation (applying the superposition principle), following the procedure viewed in this section. In this case, the excitation expression reads

$$F(t) = \frac{a_0}{2} + \sum_{k=1}^{\infty} \left(a_k \cos\left(k\omega_0 t\right) + b_k \sin\left(k\omega_0 t\right) \right) \tag{3.21}$$

where a_0, a_k and b_k are the Fourier coefficients defined by

$$a_k = \frac{2}{T}\int_0^T F(t)\cos k\omega_0 t dt, \quad k = 0,1,2,3,... \tag{3.22}$$

$$b_k = \frac{2}{T}\int_0^T F(t)\sin k\omega_0 t dt, \quad k = 1,2,3,... \tag{3.23}$$

Once Fourier coefficients are found, a useful manner to quantify the contribution of each harmonic to the periodic excitation is by way of a discrete frequency spectrum.

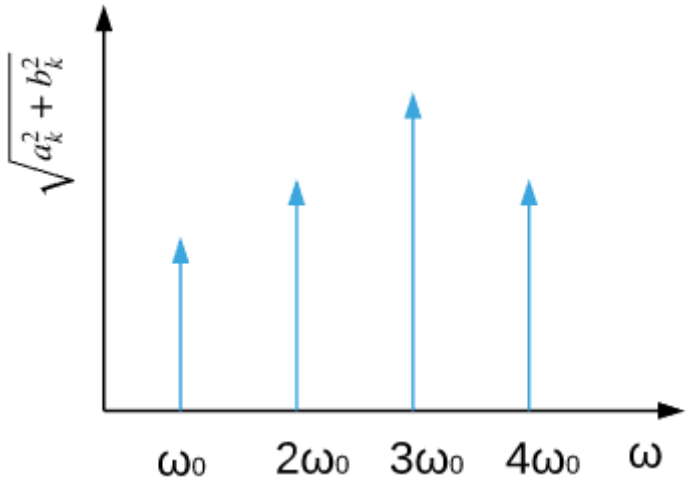

Figure 3.7 Discrete excitation frequency spectrum.

3.4 Forced Non-periodic Vibrations

It has just seen what happens when the excitation is harmonic (or a sum of harmonics) in 3.3. That study is useful if the aim is to determine the response of a linear system to harmonic loads (e.g. unbalance rotor), in order to verify the fulfillment of the design requirements in terms of resonance or fatigue. However, there are many phenomenons that are governed by non-periodic excitations. It is the case of wind loads, engine vibrations or seismic loads, where the loads can be applied suddenly for a really short time or for a finite time interval.

The non-periodic excitations are classified into two types: deterministic and non-deterministic.The first one refers to those that vary in some (known or unknown) way with time, whereas the second one refers to those that do not follow any relationship with time, that is, the time history of the load is unique every time. The deterministic loads are precisely within the scope of this work, since the focus is on the response of ITER FILD to seismic loads and inertial excitation from the VV, whose values have already been calculated (with certain uncertainty) for upper level support structure (ULSS). For the study of non-deterministic loads, a statistical approach is needed.

Below, the procedure to follow in the case of non-periodic force is described grosso modo to avoid the tricky mathematical demonstrations that are out of the scope of this work. Nevertheless, the content is properly referenced in favour of the readers.

Regarding the methodology to follow to cope with this problem, there are two approaches according to chapter 6 in [33]: the time-domain analysis and the frequency-domain analysis. As it will be mentioned later, there is a relationship between both approaches.

Firstly, the time-domain approach is described. The key to understand this alternative is that the force can be descomposed as sum of multiple short-duration impulsive loads. If the excitacion $f(t)$ is considered[15], a impulse occurring at $t = \tau$ during the time interval $d\tau$ is represented by $f(\tau)d\tau$. To this excitation, the system responds with $f(\tau)d\tau h(t-\tau)$, where $h(t-\tau)$ is the system response to the unit impulse[16] at $t = \tau$ [33 pp. 88-89]. For zero initial conditions, the expression of $h(t-\tau)$ is

[15] Instead of $F(t)$, it is used $f(t)$ by convention.
[16] Since the system is linear, the excitation multiplied by a scalar produces the response of such isolated excitation multiplied by the same scalar.

$$h(t)=\begin{cases} 0, & t<\tau \\ \dfrac{1}{m\omega_d}e^{-\zeta\omega_n t}\sin\omega_d t, & t\geq\tau \end{cases} \tag{3.24}$$

To take into consideration the entire loading history, it is enough with integrating each differential impulse, resulting the generally known as the Duhamel's integral, which usually has to be evaluated numerically.

$$x_{1p}(t)=\int_0^t f(\tau)h(t-\tau)d\tau, \quad t\geq 0 \tag{3.25}$$

Secondly, the frequency-domain approach is presented. As it is known, it does not exist any repeated pattern. To overcome this trouble, the main idea is to imagine that it does exist a pattern, which is repeated with a very large period ($T\to\infty$). In this way, it is possible to express the excitation as a sum of functions via the Forier transform, in a similar way to the non-harmonic force case. Nevertheless, in this case, the addends are complex exponential functions, the summation becomes integration and the Forier coefficients become the Fourier transform of the excitation multiplied by $d\omega/2\pi$ [33 pp. 98-99].

$$f(t)=\frac{1}{2\pi}\int_{-\infty}^{\infty}F(\omega)e^{i\omega t}d\omega \tag{3.26}$$

where

$$F(\omega)=\int_{-\infty}^{\infty}f(t)e^{-i\omega t}dt \tag{3.27}$$

In order to find the system response to the excitation already mentioned, it is required to work in the frequency domain, obtaining the response $X(\omega)$ as a product of $F(\omega)$ and $H(\omega)$, and then return to the time domain via the inverse transform. This FRF takes the expression (3.19) and it is proved that it is the Forier transform of $h(t)$.

$$x_{1p}(t)=\frac{1}{2\pi}\int_{-\infty}^{\infty}H(\omega)F(\omega)e^{i\omega t}d\omega \tag{3.28}$$

Similarly to the time-domain approach, the integrals that appear in the frequency-domain analysis usually have to be calculated by numerical methods, such as the Discrete Fourier Transforms (DFT) [33 pp. 100-102], which uses the Fast Fourier Transforms (FFT) algorithms [33 pp. 102-106].

3.5 Problem of interest: Base Motion

A very typical problem, extensively solved in vibration courses and which can be easily found in the literature, is the study of the vibration caused by the base motion (e.g. the displacement of a car on a roughness pavement or the ground motion during an earthquake).

In relation to Figure 3.8, the equation of motion for this problem can be easily found by a force balance similar to the one used to obtain the Eq. (3.1). This equation of motion can be express in absolute coordinates (refered to the static equilibrium position):

$$m\ddot{x}_1+c(\dot{x}_1-\dot{y})+k(x_1-y)=0 \tag{3.29}$$

or in relative coordinates, by the change of variable $z=x_1-y$:

$$m(\ddot{z}+\ddot{y})+c\dot{z}+kz=0 \tag{3.30}$$

Observe that the resulting acceleration in the Eq. (3.30) is in absolute coordinates.

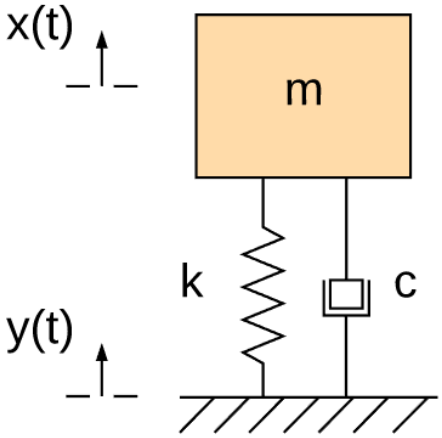

Figure 3.8 Vibration $x_1(t)$ caused by the base motion $y(t)$.

The problem of base motion helps to understand the concept of transmissibility, that is, the ratio of output to input, which also depends on the frequency ratio and on the damping ratio. If the focus is on the receiver, the transmissibility can be defined by the ratio of (absolute or relative) displacement of the receiver to displacement of the base (supporting structure). However, sometimes it can be necessary to bring the source of the vibrations into focus. In this case, the transmissibility can be defined by the ratio of transmitted force to supporting structure to excitating force.

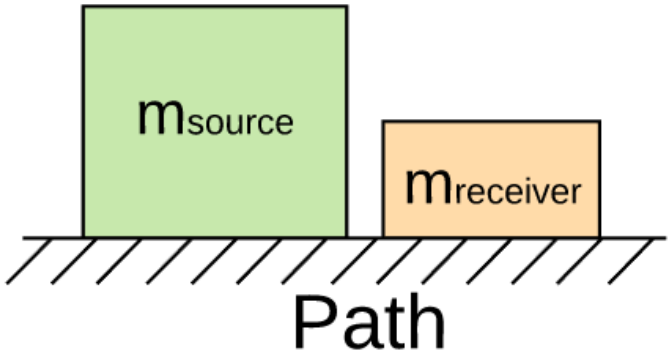

Figure 3.9 In the source-path-receiver model, the vibrations are propagated through the path from the source to the receiver.

If an harmonic excitation is considered, $y(t) = Y_0 \sin \omega t$, the response can be obtained by using the same approach as in Eq. (3.13) – Eq. (3.16). In this case, it turns out that the transmissibility has the form:

$$\frac{X_0}{Y_0} = \frac{\sqrt{1+(2\zeta\tau)^2}}{\sqrt{(1-\tau^2)^2+(2\zeta\tau)^2}} \tag{3.31}$$

In relation to the analyses that are inside the scope of the present work, it is interesting to see what happens when the natural frequency is high enough, that is, when $\tau \to 0$. In this case, $X_0/Y_0 \to 1$, meaning that the response follows the excitation as a rigid solid.

Regarding the particular cases of seismic loads and inertial excitation from VV, both of interest in this work, it is possible to interpret their effects on ITER FILD as base motion problems. In effect, the VV may excite ULSS during seismic events and fast EM transient, and, in turn, massive ULSS may develop additional inertial effects on on-board components such as ITER FILD, attached to the DSM.

The concept of transmissibility, in turn, leads to the study of vibration isolation, either by isolating the source or the receiver by means of springs and dampers [30 pp. 89-92]. In general, others techniques that might be useful consist in fixing the origin of the vibration if possible (or worthwihle), or using devices like the dynamic vibration absorber [30 pp. 112-133], based on a two degree-of-freedom system.

3.6 Introduction to Multi Degree-of-Freedom (MDOF) Systems

The objective of this section is to generalize the concepts associated with SDOF systems for MDOF systems. In particular, the form of the equations of motion will be found, the concept of natural frequency will be extended, the concept of natural mode will be introduced and the influence of the initial conditions will be discussed.

In order to address the purposes above-mentioned, a representative two degree-of-freedom example is proposed in Figure 3.10.

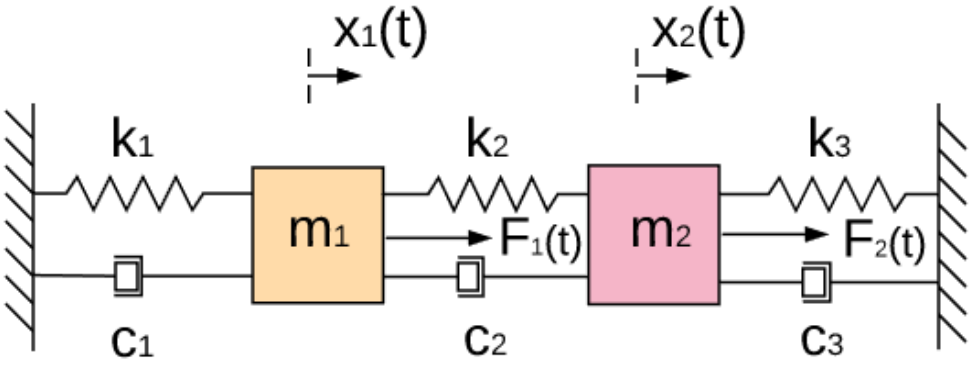

Figure 3.10 Description of a two degree-of-freedom model.

As a two degree-of-freedom system, the motion is entirely determined by two coordinates, $x_1(t)$ and $x_2(t)$. After a force balance on each mass, m_1 and m_2, the two following equations are obtained:

$$\begin{cases} m_1\ddot{x}_1 + c_1\dot{x}_1 + c_2\left(\dot{x}_1 - \dot{x}_2\right) + k_1x_1 + k_2\left(x_1 - x_2\right) = F_1(t) \\ m_2\ddot{x}_2 + c_2\left(\dot{x}_2 - \dot{x}_1\right) + c_3\dot{x}_2 + k_2\left(x_2 - x_1\right) + k_3x_2 = F_2(t) \end{cases} \tag{3.32}$$

The equations found in (3.32) are two coupled linear ODEs. It is interesting to express them in matrix notation:

$$\begin{bmatrix} m_1 & 0 \\ 0 & m_2 \end{bmatrix}\begin{Bmatrix} \ddot{x}_1 \\ \ddot{x}_2 \end{Bmatrix} + \begin{bmatrix} c_1 + c_2 & -c_2 \\ -c_2 & c_2 + c_3 \end{bmatrix}\begin{Bmatrix} \dot{x}_1 \\ \dot{x}_2 \end{Bmatrix} + \begin{bmatrix} k_1 + k_2 & -k_2 \\ -k_2 & k_2 + k_3 \end{bmatrix}\begin{Bmatrix} x_1 \\ x_2 \end{Bmatrix} = \begin{Bmatrix} F_1(t) \\ F_2(t) \end{Bmatrix} \tag{3.33}$$

or simply

$$[M]\{\ddot{x}\} + [C]\{\dot{x}\} + [K]\{x\} = \{F(t)\} \tag{3.34}$$

where $[M]$ is the mass matrix, $[C]$ is the damping matrix, $[K]$ is the stiffness matrix and $\{F(t)\}$ is the (generalized and/or physical) excitation force vector.

Together with the intial conditions, the system of ODEs forms the initial value problem:

$$\begin{cases} [M]\{\ddot{x}\} + [C]\{\dot{x}\} + [K]\{x\} = \{F(t)\} \\ \{x(0)\} = \{x_0\} \\ \{\dot{x}(0)\} = \{\dot{x}_0\} \end{cases} \tag{3.35}$$

Analogously to the SDOF system, the solution is found by dividing the problem into homogeneous equation

system and non-homogeneous equation system. At least for now, the free vibration problem ($\{F(t)\}=\{0\}$) is brought into focus. The analysis derived from this assumption is called modal analysis. In this case, it is sought a solution like

$$\{x(t)\}=A\{\phi\}e^{pt} \tag{3.36}$$

where $\{\phi\}$ generalizes the solution when there are more than one degree-of-freedom.

After substituting the solution (3.36) into the homogeneous equation system, it results that

$$A\left(p^2[M]+p[C]+[K]\right)\{\phi\}e^{pt}=\{0\} \tag{3.37}$$

and, therefore, for $A\neq 0$,

$$\left(p^2[M]+p[C]+[K]\right)\{\phi\}=\{0\} \tag{3.38}$$

Now, assume zero damping, i.e. set all the elements of the damping matrix to zero (the non-zero case will be discussed in subsection 3.7) and, since p has to be complex to produce an oscillating motion according to section 3.1, renaming the parameter like $p^2=-\lambda$. In this way, Eq. (3.38) becomes

$$\left(-\lambda[M]+[K]\right)\{\phi\}=\{0\} \tag{3.39}$$

or equivalently

$$[K]\{\phi\}=\lambda[M]\{\phi\} \tag{3.40}$$

The preceding Eq.(3.40) corresponds to a generalized eigenproblem[17], where the eigenvalues are the natural frequencies squared of the system and the eigenvectors are generally known as natural modes (or mode shapes).

The solution can be expressed like:

$$\{x(t)\}=\sum_{r=1}^{2}\{\phi_r\}\left(A_{1r}\cos\omega_{nr}t+A_{2r}\sin\omega_{nr}t\right) \tag{3.41}$$

How to obtain the eigenvalues and the eigenvectors is an algebra problem. Since the trivial solution of (3.40) is not of interest, the determinant of the matrix $[K]-\lambda[M]$ has to be zero. This condition leads to the characteristic equation

$$\left|[K]-\lambda[M]\right|=0 \tag{3.42}$$

which yields the eigenvalues. Then, to find the eigenvectors, it is enough with substituting the eigenvalues one by one into (3.40) and solving the resulting linearly dependent homogeneous equation system. For the example proposed, assuming $m_1=m_2$ and $k_1=k_2=k_3$ in the interest of time, the following results are obtained:

$$\begin{cases}\omega_{n1}=\sqrt{\dfrac{k}{m}}\Rightarrow\phi_{11}=\phi_{12}\\ \omega_{n2}=\sqrt{\dfrac{3k}{m}}\Rightarrow\phi_{21}=-\phi_{22}\end{cases} \tag{3.43}$$

where ϕ_{11} and ϕ_{12} are the components of the first natural mode $\{\phi_1\}$, and ϕ_{21} and ϕ_{22} are the components of the second one $\{\phi_2\}$.

As deduced from Eq. (3.43), absolute magnitudes are not obtained, but ratios. What is usually done is to

[17] This generalized form can be transformed into a standard formulation by multiple methods. This is a really tricky problem from an algebraic and numerical point of view, being completely out of the scope of this document. However, some light details will be presented in section 4.3 when the numerical approach of the problem is addressed.

normalize the natural modes. There are different ways to do it, some of them are: giving the value one to the largest component; or imposing

$$\{\phi_r\}^T [M] \{\phi\}_r = 1 \tag{3.44}$$

The advantages of this last approach will be shown in section 3.7.

In summary, two pairs natural frequency-natural mode are obtained. Each one is associated with one pattern of sinusoidal motion (depending on the form of the natural mode) in which the system moves at one frequency (natural frequency). The amplitude of each pattern of motion is still unknown, but to solve this problem, it is sufficient with applying the initial conditions. This has an important meaning: the initial conditions excite the different patterns of motion depending on their values, being possible to excite just one of them, excite both but with different amplitudes and so on. In Figure 3.11, there is a qualitative illustration of the two patterns of motion, and the influence of the initial conditions on the final solution.

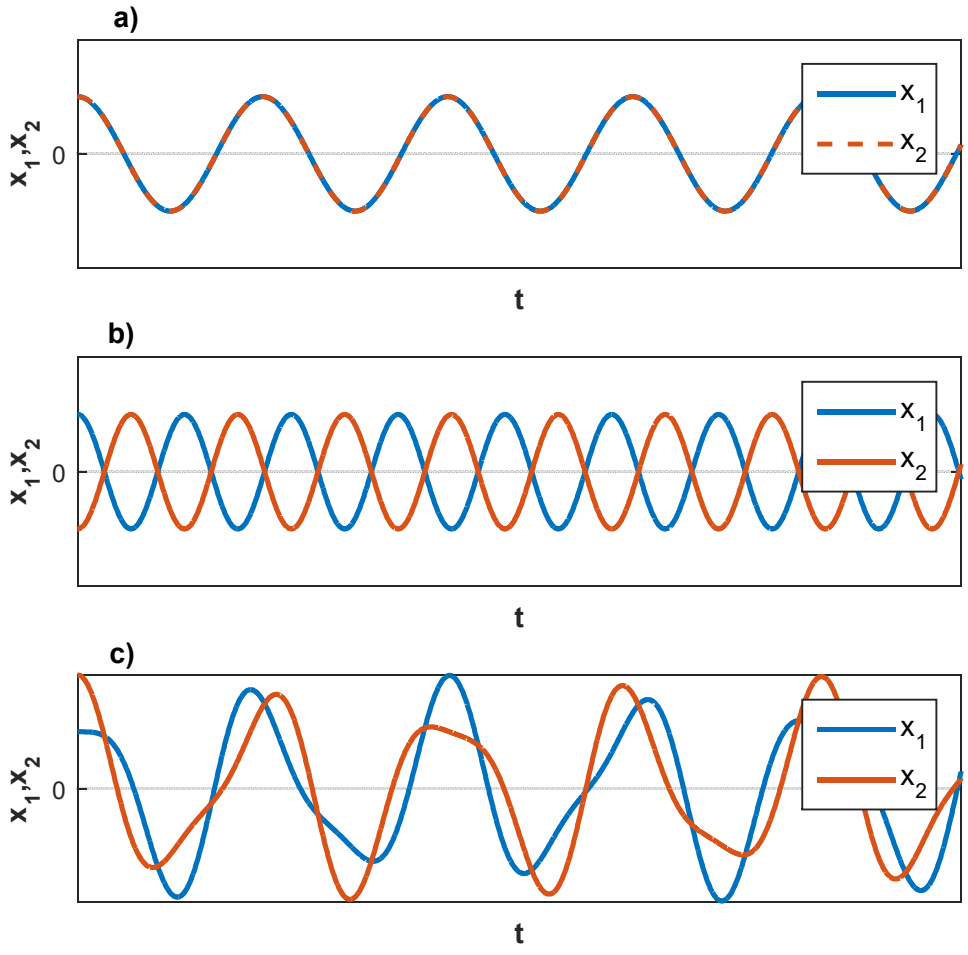

Figure 3.11 Resulting oscillating motion of the two rigid masses from the application of the initial conditions: zero initial velocities and **a)** both initial displacements are identical **b)** both initial displacements are inverse **c)** both initial displacements are arbitrary.

As illustrated in the previous figure, the shape of the solutions is really dependent on the initial conditions. For the sake of clarity, just the initial displacements have been modified, but needless to say that the role of the initial velocities is also determinant. First, the initial displacements are indentical (non-trivial solution), producing just the excitation of the first mode. In this case, both masses, m_1 and m_2, are in phase, and, due to the symmetry of the problem, the amplitude is the same for both (this would be different if k_1 and k_2 had

taken different values, e.g. $k_1 \neq 0$ and $k_3 = 0$, which means that the right extreme would be free). Secondly, the initial displacements are inverse, yielding just the excitation of the second mode. In this case, both masses are out of phase. In fact, the phase difference is π because the masses start on the opposite side. Finally, the third case excites both modes in a messy way.

Regarding the frequency of the modes, the natural frequency of the second mode is higher than the one of the first mode. In real life, with a non-zero damping ratio, this fact would lead to the faster damping of the second mode, resulting that the first mode remains visible for longer.

Lots of systems can be modelled satisfactorily with two degree-of-freedom. Several examples are the models of buildings which consider just the lateral displacement and the torsion to study the response to ground motion and to wind excitation [34]; or the models to conduct flutter research using a rigid wing such that just pitch and plunge oscillations are permitted [35]. Nevertheless, this reasoning can be generalized for multiple degree-of-freedom systems. Here is a brief summary:

- The equation system of motion is a set of N ODEs. In matrix notation, this means that the mass matrix, the damping matrix and the stiffness matrix are $N \times N$ matrices.
- $[M]$ and $[K]$ are symmetric[18]. Moreover, $[M]$ is definite positive, while $[K]$ is either positive definite or positive semi-definite[19], what ensures the existence of N real eigenvalues, either positive or zero.
- There are N natural frequencies and N linearly independent natural modes.
- The initial conditions are responsible for exciting the modes of the system. In general, for arbitrary initial conditions, the N modes of motion are excited, although, depending on the value of the natural frequencies, most of them (higher natural frequencies) vanish quickly.

3.7 Modal Superposition

Once the (undamped) natural frequencies and the natural modes have been obtained, there are some issues to address: non-zero damping and forced vibrations. In order to discuss those issues, a technique called modal superposition is introduced.

The main idea of the modal superposition technique is to express the dynamic response of the system under study by a linear combination of its N undamped natural modes, which is supported by the linear independence of the modes. This linear combination reads:

$$\{x(t)\} = \sum_{i=1}^{N} \{\phi_i\}\, \tilde{x}_i(t) = [\Phi]\{\tilde{x}(t)\} \tag{3.45}$$

Each column of the matrix $[\Phi]$ is comprised of a natural mode, whereas each row of the vector $\{\tilde{x}(t)\}$ is comprised of the so-called modal coordinate or modal amplitude. In other words, the Eq. (3.45) represents a change of basis, from the generalized coordinates $\{x(t)\}$ to the modal coordinates in the modal subspace. The Eq. (3.45) expresses the known modal expansion theorem.

Applying the change of basis in the equation system of motion, it results that

$$[M][\Phi]\{\ddot{\tilde{x}}\} + [C][\Phi]\{\dot{\tilde{x}}\} + [K][\Phi]\{\tilde{x}\} = \{F(t)\} \tag{3.46}$$

The former equations are generally a set of coupled ODEs as before the change of basis. In particular, if the mass matrix is non-diagonal, it is said that there is mass or dynamical coupling, and if the stiffness matrix is non-diagonal, it is said that there is stiffness or static coupling. Either of the couplings supposes a big obstacle in terms of understanding the oscillating phenomenon, especially when a large number of modes are

[18] The symmetry of the stiffness matrix is based on the Maxwell reciprocal work theorem.
[19] It occurs when there are rigid body modes, associated with zero eigenvalues, due to either inadequate constraints or inherent behaviour of structures such as aircrafts in flight.

considered. In order to overcome this problem, it is crucial to attempt a diagonalization of the matrices, which can be accomplished by way of the orthogonality of the modes with respect to the mass matrix and the stiffness matrix[20]. This is

$$\begin{cases} \{\phi_i\}^T [M] \{\phi_j\} = 0, & i \neq j \\ \{\phi_i\}^T [K] \{\phi_j\} = 0, & i \neq j \end{cases} \tag{3.47}$$

Therefore, it is enough with left multiplying the Eq. (3.46) by the transposed matrix of $[\Phi]$.

$$[\Phi]^T [M][\Phi]\{\ddot{\tilde{x}}\} + [\Phi]^T [C][\Phi]\{\dot{\tilde{x}}\} + [\Phi]^T [K][\Phi]\{\tilde{x}\} = [\Phi]^T \{F(t)\} \tag{3.48}$$

Since $[\Phi]$ is an orthogonal matrix with respect to $[M]$, and taking into account the normalization shown in Eq. (3.44), it is obtained that

$$[\Phi]^T [M][\Phi] = [I] \tag{3.49}$$

where $[I]$ is the identity matrix. Aditionally, since $[\Phi]$ is also an orthogonal matrix with respect to $[K]$, Eq. (3.48) can be expressed like

$$[I]\{\ddot{\tilde{x}}\} + [C_n]\{\dot{\tilde{x}}\} + [K_n]\{\tilde{x}\} = \{\tilde{F}(t)\} \tag{3.50}$$

where $[K_n]$ is

$$[K_n] = \begin{bmatrix} {\omega_{n1}}^2 & 0 & 0 \\ 0 & \ddots & 0 \\ 0 & 0 & {\omega_{nN}}^2 \end{bmatrix} \tag{3.51}$$

and $\{\tilde{F}(t)\}$ is called modal force and includes the modal participation.

Supposing that $[C_n]$ is also diagonal, it is obtained a set of N uncoupled ODEs:

$$\begin{cases} \ddot{\tilde{x}}_1 + 2\zeta_1\omega_{n1}\dot{\tilde{x}}_1 + {\omega_{n1}}^2\tilde{x}_1 = \tilde{F}_1(t) \\ \vdots \\ \ddot{\tilde{x}}_i + 2\zeta_i\omega_{ni}\dot{\tilde{x}}_i + {\omega_{ni}}^2\tilde{x}_i = \tilde{F}_i(t) \\ \vdots \\ \ddot{\tilde{x}}_N + 2\zeta_N\omega_{nN}\ddot{\tilde{x}}_N + {\omega_{nN}}^2\tilde{x}_N = \tilde{F}_N(t) \end{cases} \tag{3.52}$$

where ζ_i is known as modal damping.

However, $[C_n]$ is not diagonal in general. For the undamped modes calculated above, the damping matrix becomes diagonal if $[C]$ is proportional to the mass matrix and the stiffness matrix by the well-known Rayleigh damping:

$$[C] = \alpha[M] + \beta[K] \tag{3.53}$$

where α is the so-called mass coefficient and β is the so-called stiffness coefficient.

The initial conditions expressed in modal coordinates are readily calculated like this:

[20] This property is easy to demonstrate just taking into consideration the symmetry of both matrices.

$$\begin{cases} \{x_0\} = [\Phi]\{\tilde{x}_0\} \Rightarrow \{\tilde{x}_0\} = [\Phi]^{-1}\{x_0\} \\ \{\dot{x}_0\} = [\Phi]\{\tilde{x}_0\} \Rightarrow \{\dot{\tilde{x}}_0\} = [\Phi]^{-1}\{\dot{x}_0\} \end{cases} \tag{3.54}$$

As it can be imagined, the modal superposition is a really powerful technique, not only in terms of understanding, since each mode is expressed independently in a SDOF way, but also in terms of required CPU-time during numerical simulations.

Finally, it has to be mentioned the generally known as effective modal mass, which can be understood as the part of the total mass of the system responding to the excitation in each mode. This concept will be key to choose the cut-off frequency in section 4.4.

3.8 Response Spectrum Analysis

According to [36], when a dynamic analysis is required, there are basically three different approaches:

- A **dynamic transient simulation** on the non-linear assembled system model, which produces the time history response.
- A **static analysis** equivalent to a dynamic one by using a DAF.
- A **Reponse Spectrum Analysis (RSA)**. Although this technique is going to be described in this part, it reduces the complex time-dependent information of a transient event using a single parameter: the maximum response.

As it can be deduced, in the ITER design process, a transient analysis is beyond the scope of the CD phase, because it requires an (generic) assembled PP where to insert the diagnostic system, which is too time-consuming as well as useless at this premature stage. On the other hand, an equivalent static analysis is not recommended when the main natural frequencies of the structure are unknown. Therefore, a RSA is viewed as the most appropriate approach to study the vibration problem of ITER FILD currently. Moreover, it is the most used to define the response to both seismic loads and inertial excitation from VV (which are inside the scope of this work). Even so, a static analysis will be used to verify the results obtained with the RSA, since it can be performed facing the CDR. Go to part 5.4.3.3 to see the results of that verification.

Before explaining the key concepts of the RSA, an important step to perform the dynamic analysis is to decouple ITER FILD from the points where it is attached. This decoupling is possible since the mass of ITER FILD is significantly small with respect to the mass of the ULSS (just a pack DFW + DSM has a mass of 10 t). In this way, ITER FILD, like many other equipment, is not included into the global finite-element model, but it is independtly analysed just by means of the excitation that exists at ITER FILD support points [37 p. 38].

In relation to the RSA, the input for the analysis is a Response Spectrum[21] (RS). The RS is not an excitation itself, but the responses of SDOF systems with different natural frequencies[22] to a given base excitation at a certain position. In fact, the peaks of their responses are which are stored in the spectrum. A SDOF system is also characterized by its own damping ratio, so a family of curves can be obtained by varying it. In Figure 3.12, it is given an overview of obtaining the envelope of peak response against modal frequency.

[21] It is specifically known as Point Response Spectra, In-Structure Spectra or Secondary Spectra.
[22] The hypothesis $\omega_d \simeq \omega_n$ is perfectly valid as it was mentioned in section 3.1.

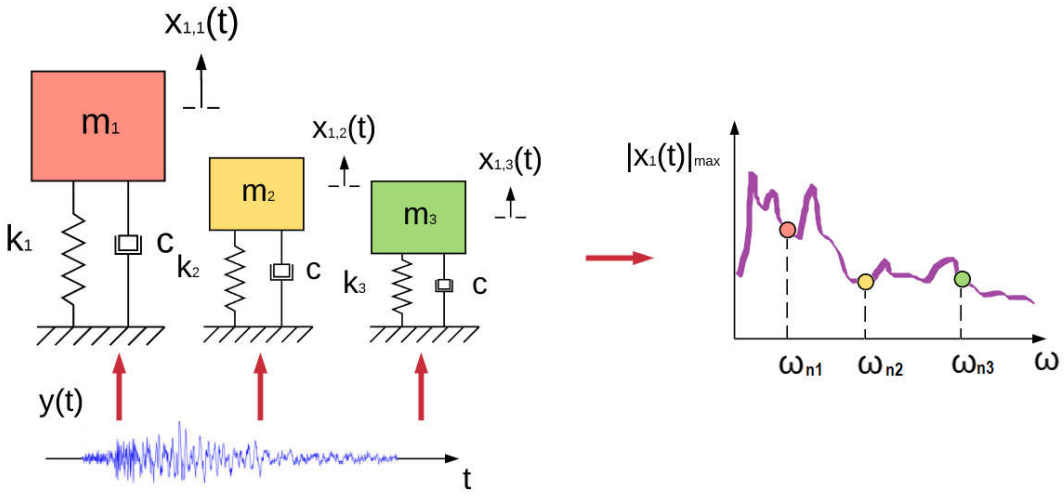

Figure 3.12 Schematic of the generation of a response spectrum based on time-history analysis, using the same notation as in section 3.5.

In Figure 3.12, to give the base excitation and the response of the SDOF systems, it has been used the base displacement and the absolute displacement of each mass, respectively. This is for a simple reason; in this way, it is easier to connect the problem with what was presented in section 3.5. However, it is common to express the response spectrum in terms of the maximum values of the relative displacement $z(t)$, the relative velocity $\dot{z}(t)$ and the absolute acceleration $\ddot{x}_1(t)$. In particular, those values are called spectral relative displacement, spectral relative velocity and spectral absolute acceleration, respectively, and the following notation is used:

$$\begin{cases} S_d(\zeta,\omega) \equiv |z(t)|_{\max} \\ S_v(\zeta,\omega) \equiv |\dot{z}(t)|_{\max} \\ S_a(\zeta,\omega) \equiv |\ddot{x}_1(t)|_{\max} \end{cases} \tag{3.55}$$

In addition, in practice, it is assumed a relation among them by means of the natural frequency. In [33 pp. 576-578], it can be found the justification and the numerical error. In this case, the spectral values of the velocity and the acceleration are called pseudo-velocity spectral response $S_{pv}(\zeta,\omega)$ and pseudo-acceleration spectral response $S_{pa}(\zeta,\omega)$.

$$S_{pa}(\zeta,\omega) = \omega S_{pv}(\zeta,\omega) = \omega^2 S_d(\zeta,\omega) \tag{3.56}$$

Therefore, it is unimportant which plot is chosen as the input for the RSA.

On the other hand, the time response of each SDOF oscillator is calculated by the concepts presented in section 3.4, based on the time-history analysis at the position where the system under study is attached. Nevertheless, the accelerogram is not available at the support points in general. Therefore, an alternative approach is usually used, which consists in a spectrum-to-spectrum method [38]. In fact, this approach has been used in the design at port stub level and at lower levels as shown in Figure 3.13.

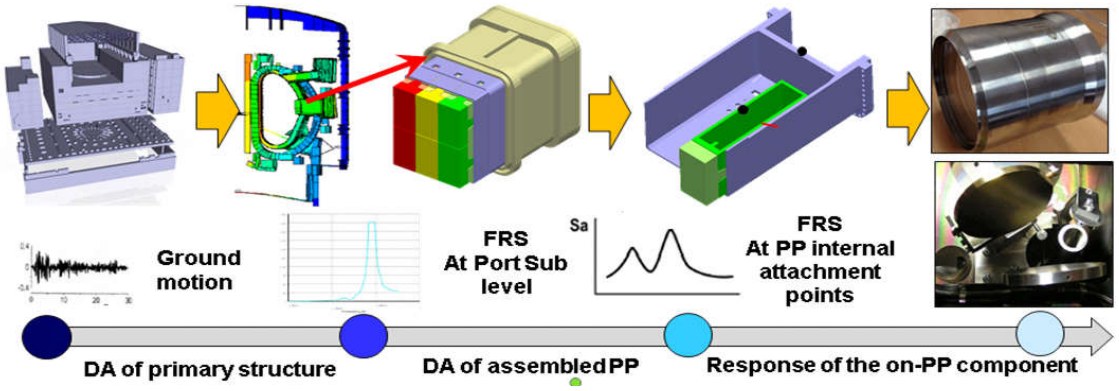

Figure 3.13 Sequence of the derivation of the seismic action in ITER [36].

Once the response spectra are at analyst's disposal, the RSA can be carried out by using a software package. The details about the numerical implementation of the RSA will be described in section 4. However, the main ideas to understand the internal procedure are covered herein based on [39 pp. 7-10].

In order to address the explanation above-mentioned, it is helpful to recover Eq. (3.30), to use the definitions of ω_n and ζ and to rearrange it like this

$$\ddot{z} + 2\zeta\omega_n\dot{z} + \omega_n{}^2 z = -\ddot{y} \tag{3.57}$$

Now, if the base motion equation (3.30) is extended to a MDOF system, it is obtained that

$$\{F(t)\} = -[M]\{D\}\ddot{y} \tag{3.58}$$

where $[M]$ is the mass matrix and $\{D\}$ is a vector which describes the excitation direction. Therefore, the modal force vector becomes

$$\left\{\tilde{F}(t)\right\} = -[\Phi]^T[M]\{D\}\ddot{y} = -\{\gamma\}\ddot{y} \tag{3.59}$$

where each element of the vector $\{\gamma\}$ represents the modal participation factor for the i^{th} mode. Thus, the set of uncoupled ODEs from (3.52) looks like

$$\begin{cases} \ddot{\tilde{x}}_1 + 2\zeta_1\omega_{n1}\dot{\tilde{x}}_1 + \omega_{n1}{}^2\tilde{x}_1 = -\gamma_1\ddot{y} \\ \vdots \\ \ddot{\tilde{x}}_i + 2\zeta_i\omega_{ni}\dot{\tilde{x}}_i + \omega_{ni}{}^2\tilde{x}_i = -\gamma_i\ddot{y} \\ \vdots \\ \ddot{\tilde{x}}_N + 2\zeta_N\omega_{nN}\dot{\tilde{x}}_N + \omega_{nN}{}^2\tilde{x}_N = -\gamma_N\ddot{y} \end{cases} \tag{3.60}$$

Each of the previous differential equations represents the equation of a SDOF oscillator excited by a base motion. Compairing Eq. (3.57) to each one of (3.60), it can be deduced that $\tilde{x}_i(t) = \gamma_i z(t)$. Hence, $\left|\tilde{x}_i(t)\right|_{\max} = \gamma_i \left|z(t)\right|_{\max}$, where $\left|z(t)\right|_{\max}$ is a known value. In fact, it is the before called spectral relative displacement $S_d(\zeta,\omega)$, so it is sufficient with selecting the proper value in the RS (see Figure 3.12).

After calculating each modal coordinate, it is necessary to combine adequately the maximum response values. As it can be deduced, the maximum values do not happen at the same time in general, so it is an incorrect approach to use the linear combination of Eq. (3.45). Instead, various modal combination methods have been developed and can be found in the literature [39 pp. 30-38].

Many sources as well as software package manuals point out that the kwnon as the Square Root of the Sum of

Squares (SRSS) rule[23] is used quite widely. Its formula is

$$R_a = \left(\sum_{i=1}^{N} \left(R_i \right)^2 \right)^{1/2} \tag{3.61}$$

where R_r represents the modal response in the i^{th} mode and R_a the total modal response.

One of the problems related to the use of the SRSS rule arises when the responses to be combined are from modes with closely spaced frequencies. In this case, those responses are in-phase, so their maximum values need to be summed algebraically. A generalized combination has the form:

$$R_a = \left(\sum_{i=1}^{N} \sum_{j=1}^{N} \varepsilon_{ij} R_i R_j \right)^{1/2} \tag{3.62}$$

where ε_{ij} is called the coupling coefficient or modal correlation coefficient. For the purpose of this work, the Combination Quadratic Combination (CQC) method will be used as recommended by [30]. Although the entire formula can be found in the literature, here is the form of its expression:

$$R_a = \left(\left| \sum_{i=1}^{N} \sum_{j}^{N} k \varepsilon_{ij} R_i R_j \right| \right)^{1/2} \tag{3.63}$$

where $k = 1$ if $i = j$ or $k = 2$ if $i \neq j$, and $\varepsilon_{ij} = \varepsilon_{ij} \left(\omega_j, \omega_i, \xi_i', \xi_j' \right)$. The term ζ_i' is the so-called effective damping ratio for mode i^{th} and takes into consideration the Rayleigh damping, a constant modal damping ratio, the dependency on the different material properties and the corresponding modal damping ratio.

After completing the combination, it results a conservative estimation of the peak response to the original transient loading. Although it is meaningless from a physical point of view, because the maximum values do not really happen simultaneously, its value lies in its simplicity and rapidity to obtain a conservative response, either displacement or other output of interest.

[23] It can be used not only for the degree-of-freedom response, but also to combine reactions or stresses.

4 Numerical Modelling

In section 3, an overview of the theoretical background which permits to understand the key concepts of a RSA has been presented. Nevertheless, there are still a few issues to highlight from a practical point of view. Firstly, the set of examples which have been used consists in SDOF/MDOF rigid models, whereas in reality, systems, e.g. the ITER FILD, are continuous. Secondly, as it can be deduced, the difficulty of obtaining the solution of the vibration problem basically depends on how to extract the eigenvalues and eigenvectors of Eq. (3.40). Other minor issues are related to the number of eigenvalues that are necessary to extract to properly represent the response of the system; the way in which a real system, with its inherent nonlinearities, is analysed by a RSA, which is intrinsically a linear method; how to model the damping, because, even by a Rayleigh damping, it exists the problem to assign values to the mass and stiffness coefficients; or how a pre-stress status can affect the eventual response of the system under study.

The answer to the aspects previously mentioned will be addressed throughout the following sections. In addition, the settings of the numerical analyses will be briefly described at the end.

4.1 Formulation of the Equations of Motion

As it can be extracted from the section 3.6, the ultimate objective of deducing the equations of motion is to obtain the mass matrix and the stiffness matrix (the damping matrix can be obtained by them if proportional damping is assumed). In the examples followed, a direct approach has been used, based on the use of the d'Alembert's principle. However, this approach becomes unpractical when the complexity of the system grows, involving the use of vectors. For this reason, an alternative formulation of the equations of motion is sought.

Assuming N degrees of freedom, a more convenient approach, based on energy concepts, involves Lagrange's equations, whose particular form is

$$\frac{d}{dt}\left(\frac{\partial T}{\partial \dot{q}_i}\right)+\frac{\partial D}{\partial \dot{q}_i}+\frac{\partial U}{\partial q_i}=Q_i\,,\quad \left(i=1,2,\ldots,N\right) \tag{3.64}$$

where T represents the kinetic energy, D is the dissipation function, U represents the elastic strain energy, $\left\{q_1,q_2,\ldots,q_N\right\}$ is the set of generalized coordinates and Q_i is the generalized force corresponding to the coordinate q_i.

The expressions of kinetic and strain energies are

$$\begin{cases} T=\dfrac{1}{2}\displaystyle\sum_{i=1}^{N}\sum_{j=1}^{N}m_{ij}\dot{q}_i\dot{q}_j=\dfrac{1}{2}\left\{\dot{q}\right\}^T\left[M\right]\left\{\dot{q}\right\} \\ U=\dfrac{1}{2}\displaystyle\sum_{i=1}^{N}\sum_{j=1}^{N}k_{ij}q_iq_j=\dfrac{1}{2}\left\{q\right\}^T\left[K\right]\left\{q\right\} \end{cases} \tag{3.65}$$

where $\left\{\dot{q}\right\}$ and $\left\{q\right\}$ are column vectors formed by the transposes of $\left\{\dot{q}_1,\dot{q}_2,\ldots,\dot{q}_N\right\}$ and $\left\{q_1,q_2,\ldots,q_N\right\}$,

respectively, and m_{ij} and k_{ij} are each component of the mass and stiffness matrices, respectively.

In order to calculate them, it is enough with using the adequate expression of the kinetic energy and the elastic strain energy:

$$\begin{cases} T = \frac{1}{2}\int_V \rho\left(\dot{u}^2 + \dot{v}^2 + \dot{w}^2\right) dV \\ U = \frac{1}{2}\int_V \{\sigma\}^T \{\varepsilon\} dV \end{cases} \tag{3.66}$$

The value $\dot{u}^2 + \dot{v}^2 + \dot{w}^2$ is the squared norm of the absolute velocity of a point P with Cartesian coordinates (x, y, z), belonging to the solid of volume V. It is readily understandable that the components u, v and w can be expressed in terms of the generalized coordinates, which correspond to the degrees of freedom of the structural system.

On the other hand, the stress vector $\{\sigma\}$ is formed by the transpose of the vector $\{\sigma_x, \sigma_y, \sigma_z, \tau_x, \tau_y, \tau_z\}$, while the strain vector $\{\varepsilon\}$ is formed by the transpose of the vector $\{\varepsilon_x, \varepsilon_y, \varepsilon_z, \gamma_{xy}, \gamma_{xz}, \gamma_{yz}\}$. The stress vector can be expressed in terms of the strain vector by means of the stress-strain relationships, generally known as constitutive equations or material laws. In the case of an isotropic material, they are

$$\begin{Bmatrix} \sigma_x \\ \sigma_y \\ \sigma_x \\ \tau_x \\ \tau_y \\ \tau_z \end{Bmatrix} = \frac{E}{(1+\nu)(1-2\nu)} \begin{bmatrix} 1-\nu & \nu & \nu & 0 & 0 & 0 \\ \nu & 1-\nu & \nu & 0 & 0 & 0 \\ \nu & \nu & 1-\nu & 0 & 0 & 0 \\ 0 & 0 & 0 & (1-2\nu)/2 & 0 & 0 \\ 0 & 0 & 0 & 0 & (1-2\nu)/2 & 0 \\ 0 & 0 & 0 & 0 & 0 & (1-2\nu)/2 \end{bmatrix} \begin{Bmatrix} \varepsilon_x \\ \varepsilon_y \\ \varepsilon_x \\ \gamma_{xy} \\ \gamma_{xz} \\ \gamma_{yz} \end{Bmatrix} \tag{3.67}$$

where E is the Young's modulus and ν is the Poisson's ratio.

Additionally, the strain vector can be expressed in terms of the displacements by using the strain-displacement relationships:

$$\begin{Bmatrix} \varepsilon_x \\ \varepsilon_y \\ \varepsilon_x \\ \gamma_{xy} \\ \gamma_{xz} \\ \gamma_{yz} \end{Bmatrix} = \begin{Bmatrix} \partial u/\partial x \\ \partial v/\partial y \\ \partial w/\partial z \\ \partial u/\partial y + \partial v/\partial x \\ \partial u/\partial z + \partial w/\partial x \\ \partial v/\partial z + \partial w/\partial y \end{Bmatrix} \tag{3.68}$$

Once again, the potential energy can be defined by the generalized coordinates.

4.2 Finite Element Method

A major issue to overcome is the discretization of the solid, since it is impossible to analyse infinite degrees of freedom. In other words, N has to be a finite number. This discretization can be addressed from different points of view, being three of them [33 pp. 4-8]:

- **Lumped-Mass procedure.** This approach consists in assuming that the mass of the system is concentrated at discrete points of the structure. Therefore, it is just required to define the displacements and accelerations at these mass points. Generally, each mass will have 6 DOF in 3D. The greater the number of mass points is, the better the model will represent a continuous mass distribution, with its infinite degrees of freedoms.

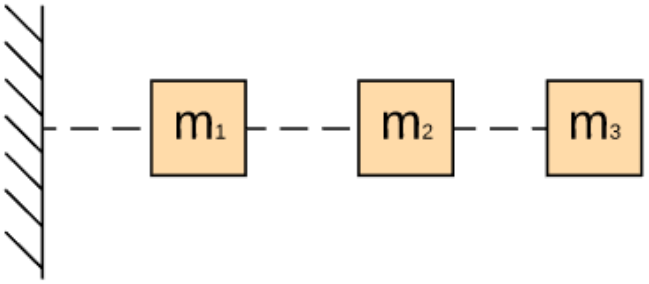

Figure 4.1 Lumped-mass idealization for a cantilever beam.

- **Rayleigh-Ritz method.** This alternative approach rests on the idea that the deflection of the structure can be modelled by way of a linear combination of N prescribed functions of the position, which are linearly independent, and which represent the different displacement patterns. For instance, the expression for the displacements of a beam with length L can be written

$$v(x,t) = \sum_{i=1}^{N} \varphi_i(x) q_i(t), \ 0 \le x \le L \tag{3.69}$$

  where each φ_i is a permisible shape function, which is compatible with the geometric boundary conditions and ensures the continuity required by the internal displacements; and each q_i corresponds to an unknown generalized coordinate. As it can be deduced, the function φ_i represents the i^{th} vibration mode of a continuous system. With this approach, the number of degrees of freedom can be reduced for a given certain accuracy, as long as the shape functions are properly chosen.

- **Finite element method.** This third approach might be understood as a mixture of the two previous methods. It combines a discrete idealization similar to the lumped-mass' one, with the use of one prescribed function associated with each degree of freedom. However, here the idealization involves elements instead of mass points, making more feasible the discretization of continuous mass distributions. These elements are divisions of the structure which are assembled in points called nodal points. The displacements of the nodal points, or simply nodes, correspond to the generalized coordinates of the structural system. As it can be deduced, this method leads to a larger number of degrees of freedom in comparaison to the Rayleigh-Ritz method, and therefore, to a larger number of prescribed functions. Nevertheless, this approach overcomes the difficulty to find shape functions compatible with the existing geometric-support conditions for complex systems. In fact, it proposes the recipe to build them up. Basically, these functions are such that take a unit value in the point of their corresponding nodes, and assign zero values for the rest of points. Due to the simplicity of this method, widely used in all kinds of industries, it is chosen to analyse the vibration of the ITER FILD, since it is implemented in the finite element (FE) software package that will be used (ANSYS).

Now, the FE method will be discussed in more detail. For simplicity, a cantilever beam, subjected to either bending or axial loading, is choosen to explain the key ideas related to the form of the so-called interpolation functions, the evaluation of the mass and stiffness matrices and other aspects of interest.

Given the uniformity of a cantilever beam, it may be divided into a small set of elements. As a criterion to establish the divisions of the beam, it is recommended to locate the nodes not arbitrarily, but making them coincide with singular features of the beam, such as supports or punctual loads, and properly distributing them along the beam to better represent the deflected shape. In this case, it is possible to assume the following discretization:

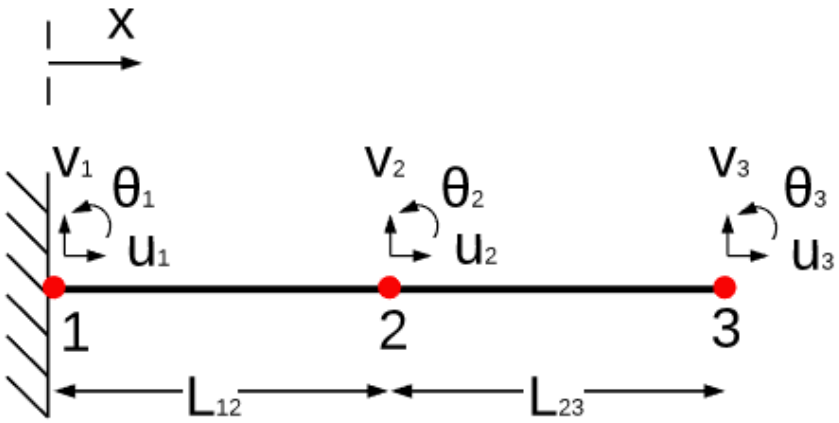

Figure 4.2 Discretization of a cantilever beam into two elements and three nodes.

Based on the discretization illustrated in Figure 4.2, the displacements can be approximated like in Eq. (3.70) taking into account that u_1, v_1 and θ_1 are fixed by the support.

$$\begin{cases} u(x,t) = \psi_2^u(x)u_2(t) + \psi_3^u(x)u_3(t) = \{\psi^u(x)\}^T \{q^u(t)\} \\ v(x,t) = \psi_3^v(x)v_2(t) + \psi_4^v(x)\theta_2(t) + \psi_5^v(x)v_3(t) \\ \qquad + \psi_6^v(x)\theta_3(t) = \{\psi^v(x)\}^T \{q^v(t)\} \end{cases} \tag{3.70}$$

As mentioned early, the interpolation functions are constructed by giving a unit value to their corresponding nodes and zero to the others, taking into account that they are associated with either translation or rotation. In fact, they are piecewise polynomial functions, not being defined in the entire domain and, consequently, being independent of the complexity of the domain. The order of the polynomials is given by the number of degrees of freedom that affect the displacement of each element in a direction. In other words, the order of the polynomials is given by the number of degrees of freedom that take part in the interpolation procedure inside each element. See Figure 4.3 for a visualization of these ideas.

In relation to the requirements for the interpolation functions, as well as satisfying the geometric boundary conditions, it is indispensable that they, and their derivatives, are sufficiently continuous and complete to permit to use them in the integrals of Eq. (3.66).

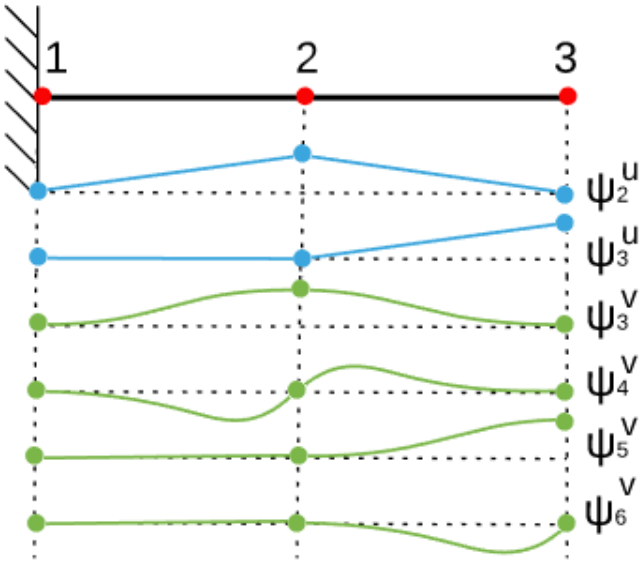

Figure 4.3 Interpolation functions for a beam with two elements and three nodes. In particular, for the interpolation functions associated with rotation, they have a unit slope at their corresponding nodal points.

Once the interpolation functions are defined, the following step is to construct the so-called consistent-mass and consistent-stiffness matrices. First, the consistent-mass matrix is constructed by using the expression of the kinetic energy of Eq. (3.66).

$$T = \frac{1}{2}\int_L \rho_x \left[\left(\{\psi^u(x)\}^T \{\dot{q}^u(t)\} \right)^2 + \left(\{\psi^v(x)\}^T \{\dot{q}^v(t)\} \right)^2 \right] dx \tag{3.71}$$

Using the commutative property of the dot product, it is possible to rearrange the expressions

$$\begin{cases} \left(\{\psi^u(x)\}^T \{\dot{q}^u(t)\} \right)^2 = \{\dot{q}^u(t)\}^T \{\psi^u(x)\}\{\psi^u(x)\}^T \{\dot{q}^u(t)\} \\ \left(\{\psi^v(x)\}^T \{\dot{q}^v(t)\} \right)^2 = \{\dot{q}^v(t)\}^T \{\psi^v(x)\}\{\psi^v(x)\}^T \{\dot{q}^v(t)\} \end{cases} \tag{3.72}$$

The resulting expression of Eq. (3.71) also permits to be reexpressed in a more interesting way

$$T = \frac{1}{2}\int_L \rho_x \left(\{\dot{q}^u(t), \dot{q}^v(t)\}^T \begin{bmatrix} \{\psi^u(x)\}\{\psi^u(x)\}^T & [0]_{2\times 4} \\ [0]_{4\times 2} & \{\psi^v(x)\}\{\psi^v(x)\}^T \end{bmatrix} \begin{Bmatrix} \dot{q}^u(t) \\ \dot{q}^v(t) \end{Bmatrix} \right) dx \tag{3.73}$$

or simply

$$T = \frac{1}{2}\int_L \rho_x \left(\{\dot{q}(t)\}^T \{\psi(x)\}\{\psi(x)\}^T \{\dot{q}(t)\} \right) dx \tag{3.74}$$

Hence, according to Eq. (3.65), the consistent-mass matrix is defined like this

$$[M] = \int_L \rho_x \left(\{\psi(x)\}\{\psi(x)\}^T \right) dx \tag{3.75}$$

Each component m_{ij}, which reprensents the force corresponding to the coordinate i due to a unit acceleration of the coordinate j, can be calculated by the following expression

$$m_{ij} = \int_L \rho_x \psi_i(x) \psi_j(x) dx \tag{3.76}$$

Analogously to the reasoning described above, the consistent-stiffness matrix can be constructed. Separately, each component k_{ij}, which represent the force corresponding to coordinate i due to a unit displacement of coordinate j, is defined for axial loading like this

$$k_{ij} = \int_L EA\psi_i'(x)\psi_j'(x)\,dx \tag{3.77}$$

or for bending like this

$$k_{ij} = \int_L EI\psi_i''(x)\psi_j''(x)\,dx \tag{3.78}$$

where A and I are the cross-sectional area and the second moment of area about the z axis, respectively. Also, primes denote differentiation with respect to x.

In order to evaluate the integrals that appear in the definition of m_{ij} and k_{ij}, they can be divided by elements, being easy to understand that the integrals will be non-zero just in those elements where both of the interpolation functions are defined. In general, although mass coupling exists, there will be a lot of zeros in off-diagonal terms.

Moreover, it is common to use natural coordinates instead of global coordinates as far as the definition of the interpolation functions and the calculation of the integrals is concerned. In this way, dimensionless coordinates are used and a generalization of the elements results, being feasible to use the same interpolation functions for more than one element.

On the other hand, it is interesting to mention the types of error involved in the FE method:

- **Error due to the discretization of the geometry** by means of elements. In the case above-presented, there is no problem because of the simplicity of the geometry (beam), but in more complex geometries the selection of adequate elements, and its size, becomes an authentic issue. To avoid having an excessive error, FE softwares often come with shape checking tools that check if the FE mesh repects some shape criteria, such as Jacobian ratio.
- **Error due to the polynomial approximation.** There are two ways of reducing this error: increasing the mesh density by a larger number of elements; and/or increasing the order of the interpolation polynomials by using more nodes per element. It has to be pointed out that the results of the FE method are exact for nodal displacements, but generally inexact for magnitudes such as stresses and strains derived from them.
- **Error due to other sources** such as the calculation of the integrals, truncation, rounding, material properties chosen, etc.

Finally, it has to be noted that this section includes just those ideas indispensable to understand the numerical analysis that will be performed in subsequent sections of this document. Therefore, there are lots of contents about the FE method which have not been mentioned here, because they are considered to be beyond the scope of the work. Nevertheless, it is interesting to outline several sources that have helped to develop the present section. Several general ideas have been taken from [40], while some more specific ones have been taken from [33 pp. 7-9, 179-182, 185-189, 351-353] and [41].

4.3 Mode-extraction methods

Once the discretization procedure has been overcome, it is time to address the way to solve the generalized eigenproblem of Eq. (3.40). Similarly to the approach of the previous section, the aim of this section is just to outline the main ideas involved in solving the eigenproblem, instead of attempting a deep discussion that is out of the scope of the work.

In the first place, one idea that results from Eq. (3.40), consists in transforming the generalized eigenproblem into a standard one, with the typical form $[A]\{v\} = \lambda\{v\}$. Left multiplying both sides of the equation by $[M]^{-1}$ could seem an option, or equivalently doing it with $[K]^{-1}$ if the stiffness matrix is positive definite. However, as well as removing the symmetric properties of the resulting matrix, the computational cost of the process becomes excessive.

Other alternatives for the same purpose, may attempt a descomposition of the mass or stiffness matrices by the use of Cholesky factorization[24] , and then a rearrangement of the matrix expression [42]. Neverthelesss, this reasoning sets out problems related to eigenvalues badly separated, the back transformation required for the eigenvectors (with considerable numerical error involved due to an ill-conditioned matrix), a large number of eigenvalues, etc.

The foregoing reveals how tricky the resolution of the generalized eigenproblem can become. Without further delay, the version of the FE software (Ansys 16.0) that will be used, proposes a set of seven different methods to overcome those difficulties. Some of their main features are included in

Table **4.1**.

Table 4.1 Eigensolver types included in Ansys 16.0

Method	Damping	Mass and Stiffness matrices
(1) Block Lanczos, (2) PCG Lanczos, (3) Subspace, (4) Supernode	Undamped	Symmetric
(5) Unsymmetric	Undamped	Unsymmetric
(6) Damped, (7) QR damped	Damped	Symmetric or unsymmetric

Since a Rayleigh damping will be supposed in the analysis, the undamped mode shapes and the damped mode shapes will be coincident. Therefore, the choice of an undamped method is valid and all what was explained in section 3.6 is perfectly of value. The only thing that differs is the natural frequencies, but the small value of the damping ratio makes the results more than acceptable.

On the other hand, among the undamped methods, it has to be chosen those methods that dealwith symmetric mass and stiffness matrices. An unsymmetric stiffness matrix is considered to be a result of a pre-stressed state, frequently encountered in fluid-structure-interaction problems or when concentrated forces appear [32]. In the case of interest of pre-stress due to, for instance, gravity or thermal loads, the unsymmetry will be not a problem, so the selection among the first four methods presented in

Table **4.1** is justified.

Although letting the program select the optimal method according to the characteristics of the problem is permissible, it is interesting to know some of the main external differences between each of the four resulting methods. An overview is given in Table 4.2, whose content is extracted from [43].

Table 4.2 Comparing undamped-mode-extraction methods for symmetric mass and stiffness matrices.

Method	# of Modes	Sturm sequence check[25] (by default)	Features of the Model
Block Lanczos (Direct)	About 40+	Performed	Recommended when the model consists of shells or a combination of shells and solids, even if poorly shaped solid and shell elements exits.
PCG Lanczos (Iterative)	Up to about 100	Not performed	Recommended when the model is dominated by well-shaped 3D solid elements.
Subspace	About 40+	Not performed	Recommended when the mass matrix is partially zero.
Supernode	Up to 10,000	*Not found*	Recommended for 2D plane or shell/beam structures, and for 3D solid structures.

[24] $A = R^T R$, where R is an upper triangular matrix, which is unique. This descomposition is feasible if A is a symmetric positive definite matrix.

[25] It ensures no missing modes.

4.4 Number of modes needed

According to [28], the number of vibration modes needed to properly represent the dynamic description of the system has to accrue sufficient effective mass (calculated by γ_i^2), in particular, at least 90% of the total mass.

The recommendation mentioned above serves as a criterion to select the cut-off frequency. However, if the form of the response spectrum is deepdly examined, a couple of interesting points can be extracted. In Figure 4.4, a generic response spectrum is shown.

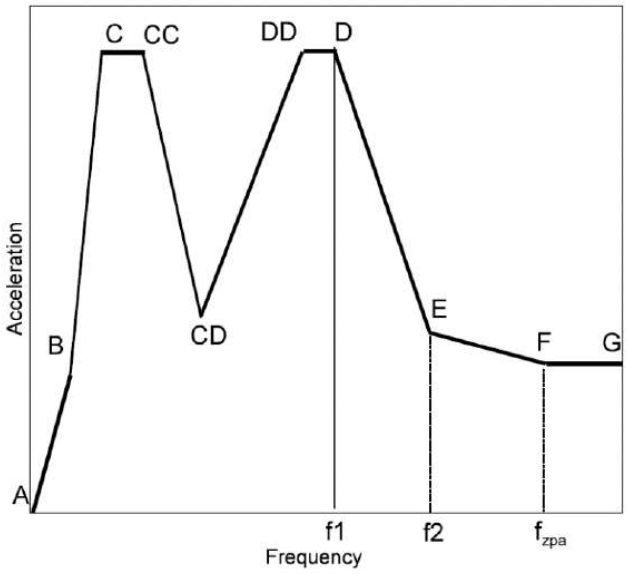

Figure 4.4 Generic multiple narrow-banded response spectrum [28].

The response spectrum consists of two parts, the "damped-periodic" (or simply "periodic") response and the "rigid" response. The periodic response is formed by the first frequency interval, where the spectrum presents amplification, whereas the rigid response takes a constant value at sufficiently higher frequencies. In fact, this constant value corresponds to the maximum ground motion (as mentioned in 3.5 when the transmissibility was introduced). Ideally, if the frequency is high enough, the period becomes zero, that is why the second interval's value is often called zero period acceleration (ZPA). This value is reached early because the influence of the periodic response vanishes quickly.

Additionally, if the periodic response is analysed, it is corroborated that it comprises two parts: the periodic part and the rigid part (the part between f_1 and f_2). This is due to the transition between the periodic response (transient) and the rigid response (steady-state). To take into consideration this transition, multiple methods have been developed. A method which is particularly interesting because of its accuracy is the so-called Gupta method, which is, by the way, included in Ansys. A detailed description of this method and more information about the periodic and rigid responses can be found in chapter 3 of [39].

In summary, a dynamic analysis is only required for the periodic response, so just those modes with natural frequencies below f_{ZPA} need to be calculated. In practice, just those below f_2 are necessary. On the other hand, the main contribution to the response of the system is usually supported by the lowest modes. However, it is possible that the cumulative effective mass is lower than 90% of the total mass if just those modes below f_2 are taken into account. In order to overcome this error, a practical way to add the rest of the significant contribution (commonly called residual response) consists in performing a static analysis that equals the missing mass multiplied by ZPA. All this reasoning helps to reduce the CPU-time required to accurately solve the problem.

4.5 Damping

The damping model that will be used in the analyses of interest is the Rayleigh damping. This model needs the definition of two parameters as it was mentioned in 3.7, α and β. Nevertheless, from the expressions (3.52) and (3.53), it is obtained that

$$\alpha\begin{bmatrix}1 & 0 & 0\\ 0 & \ddots & 0\\ 0 & 0 & 1\end{bmatrix}+\beta\begin{bmatrix}\omega_{n1}{}^2 & 0 & 0\\ 0 & \ddots & 0\\ 0 & 0 & \omega_{nN}{}^2\end{bmatrix}=\begin{bmatrix}2\zeta_1\omega_{n1} & 0 & 0\\ 0 & \ddots & 0\\ 0 & 0 & 2\zeta_N\omega_{nN}\end{bmatrix} \tag{3.79}$$

meaning that there are N equations and just two unknown parameters. In practice, a common procedure to calculate the two parameters consists in selecting just two modes: the corresponding equations to the lowest frequency and the highest frequency that contributes significantly to the dynamic response [33 p. 236]. Since the modal damping ratio takes a constant value, which is the one used to determine the response spectrum, the expressions that permit to estimate the mass and stiffness coefficients are:

$$\begin{cases}\alpha=\dfrac{2\zeta}{\omega_{n1}+\omega_{n,cut-off}}\omega_{n1}\omega_{n,cut-off}\\ \beta=\dfrac{2\zeta}{\omega_{n1}+\omega_{n,cut-off}}\end{cases} \tag{3.80}$$

4.6 Linearization of the problem

The types of analyses that will be performed are totally linear, so any nonlinearity specified by the user is ignored. The materials selected for the ITER FILD design present a linear behaviour, so the potential sources of nonlinearity come from the conceptual model, specifically from the existing/possible contacts between different parts of the model, the damping model and the pre-stress effect.

First, the contacts used to model the system will be addressed in each subsection related to the conceptual model used. However, it is interesting to notice that just bonded[26] and no separation[27] contacts are linear.

Second, the damping model used to model the system is the Rayleigh damping, so there is no problem. In addition, according to part 7.1.1.4 of [37], damping is generally assumed to be viscous, so there is no problem related to, for example, friction.

Third, the pre-stress effect can be taken into consideration by performing a previous static analysis. The resulting state will be the state used by the modal analysis to determine the eigenvalues. If, for instance, there is a contact which is nonlinear, different static analysis can be carried out, all of those associated with different states of the contact of interest. This is understood as a linearization of the nonlinear contact around different equilibrium points.Moreover, if the static analysis considers a small deflexion solution, then the analysis is linear, but if the deflexion is large, then the analysis becomes nonlinear. The effect of the self-weight, which is of interest, generally produces small deflexions, so a nonlinear static analysis is not required. In fact, the effect of the gravity on the natural frequencies and natural modes is considered to be negligible, since the stresses are not significantly high.

4.7 Finite Element Modelling

The software package that will be used is ANSYS Release 16.

[26] As welded or glued.

[27] Similar to bonded but it can exist frictionless sliding.

4.7.1 General descriptions

Unless otherwise specifically indicated all magnitudes referenced hereafter are expressed using units of the International System (SI).If necessary, decimal multiples and submultiples of SI units could be used. Models are developed in SI units.

For each conceptual model, the coordinate system used has been defined like this:

- Origin point: on the further side from the vacuum.
- X direction: coinciding with the main axis of the movable part, from the origin to the probe head heat shielding.
- Z direction: parallel to the Z direction of the global coordinate system of the tokamak.
- Y direction: forming a right-handed trihedron.

On the other hand, there are three analysis methods that have been used for each conceptual model:

- Static Structural: it serves to calculate the effect of the gravity.
- Modal: it serves to calculate the natural frequencies and modes.
- Response Spectrum: it serves to calculate the effect of the VDE III and SMHV, based on the response spectrum provided by ITER. The results of the previous modal analysis are used.

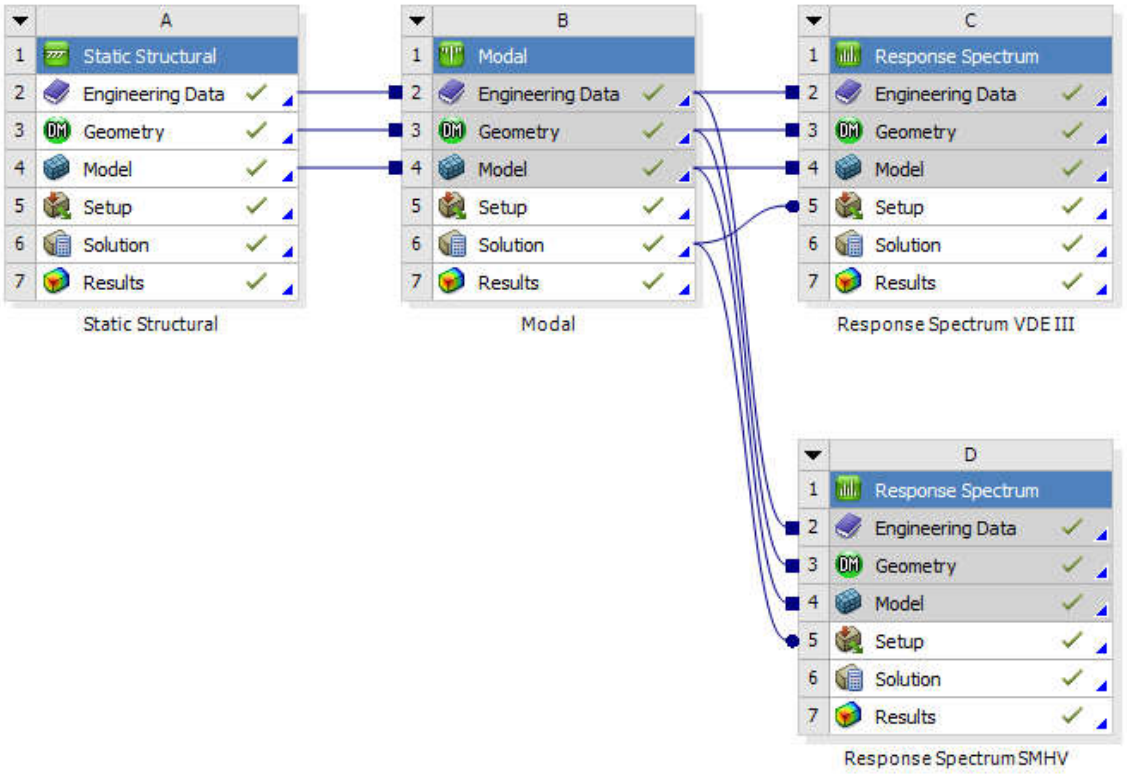

Figure 4.5 Project schematic required to solve the problem.

4.7.1.1 Material properties

Table 4.3 Physical-mechanical properties of the materials used.

#	Material	Density (kg/m^3)	Young's modulus (GPa)	Poisson's ratio	Allowable stress (MPa)
1	Stainless steel	7850	200	0.3	270
2	Molybdenum	10200	200	0.3	270
3	Boron carbide	2520	450	0.2	270

Unless otherwise specifically indicated:

#2 is used for the probe head heat shielding, #3 is used for the inner and outer shielding cylinders and #1 for the rest of parts.

All the values are taken from [44]. It should be noted that the values associated with molybdenum have been chosen from the intervals so that the the only difference between molybdenum and stainless steel is the density.

On ther other hand, it is considered, at least for this academic work, the elastic limit as the allowable stress. The elastic limits of the three materials have been taken equally for simplicity.

The impact of the material properties on the results is evident, and this will be one of the uncertainties included in the section 6.2.

4.7.1.2 Load application

The response spectra are provided by the Common Port Plug Engineering Sub-Section (CPPE), within ITER. To be accurate, the RS should be derived in the location of interest, where the system under study is attached. However, for the conceptual phase, taking into account that the RS are not available on the vertical blades of the DSMs, it is allowed to take the RS calculated at the point illustrated in Figure 4.6:

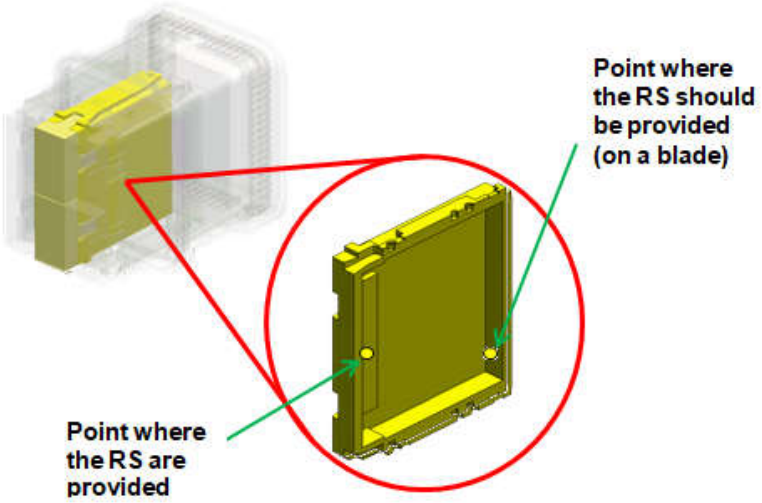

Figure 4.6 Location of the RS provided by ITER.

The RS are ahown in Figure 4.7 - Figure 4.12. They are calculated with $\zeta = 3\%$. The broadened curves will be used, since at least a 10% of uncertainty should be assumed in the calculation of the natural frequencies, according to the Nuclear Regulation.

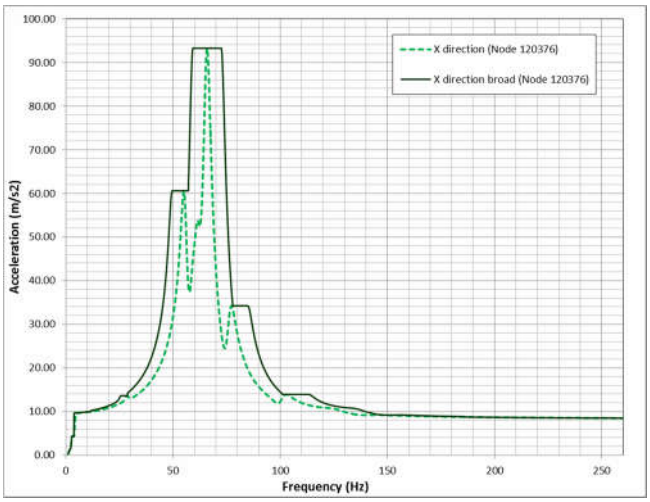

Figure 4.7 Response spectrum for VDE III in the X direction.

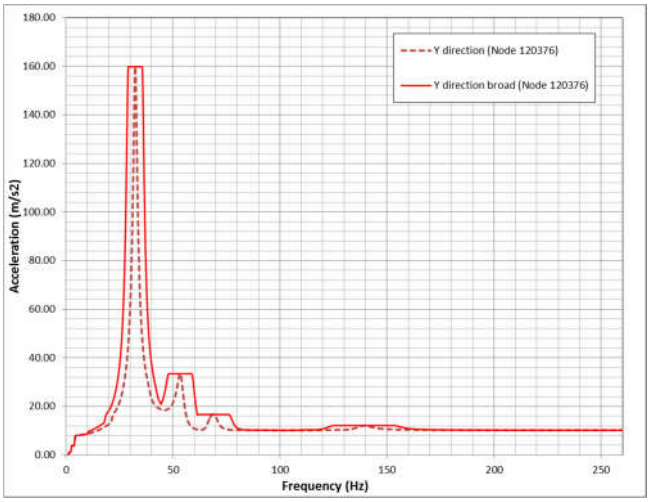

Figure 4.8 Response spectrum for VDE III in the Y direction.

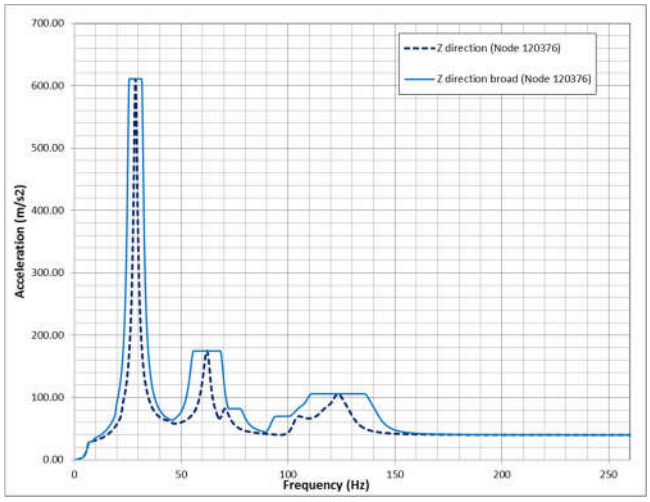

Figure 4.9 Response spectrum for VDE III in the Z direction.

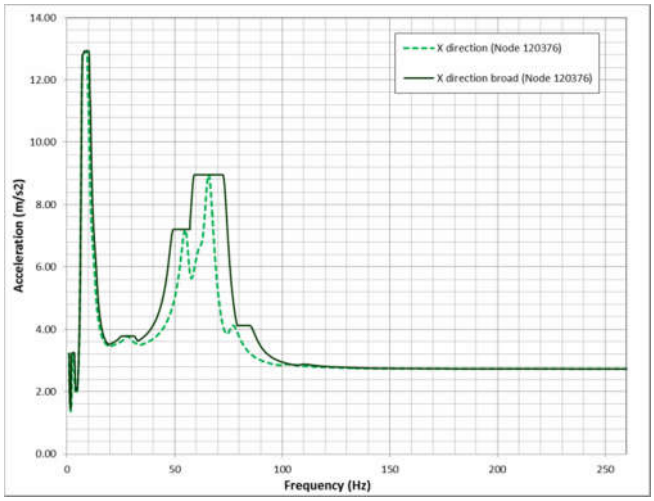

Figure 4.10 Response spectrum for SMHV in the X direction.

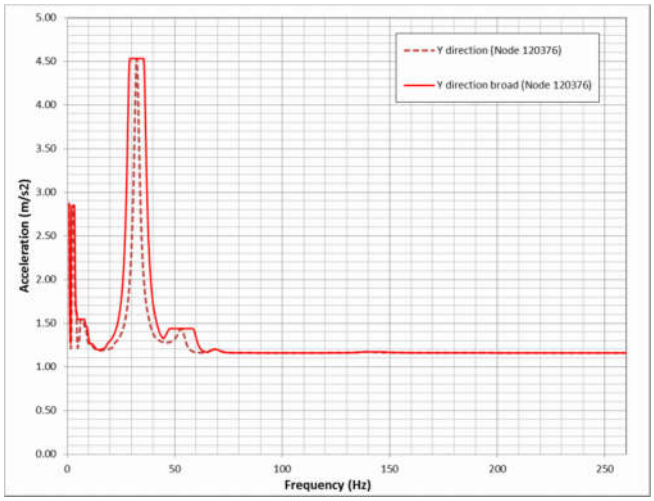

Figure 4.11 Response spectrum for SMHV in Y direction.

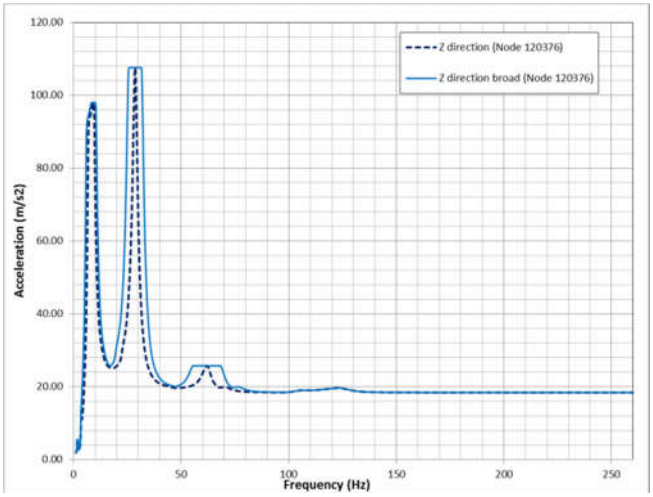

Figure 4.12 Response spectrum for SMHV in Z direction.

4.7.1.3 Solution settings

The steps that have been followed to perform the numerical analyses (modal analyses and RSA) are enumerated now.

Modal Analysis

1. Create Analysis System
2. Define Engineering Data: density (ρ), Young's modulus (E) and Poisson's ratio (ν) are required.
3. Attach Geometry
4. Define Part Behavior: a point mass is allowed if necessary.
5. Define Connections
6. Apply Mesh Controls/Preview Mesh
7. Establish Analysis Settings. In the Tree Outline window, select "Analysis Settings" inside Modal. Now, adjust the following settings:
   7.1. Options: specify the number of frequencies of interest.

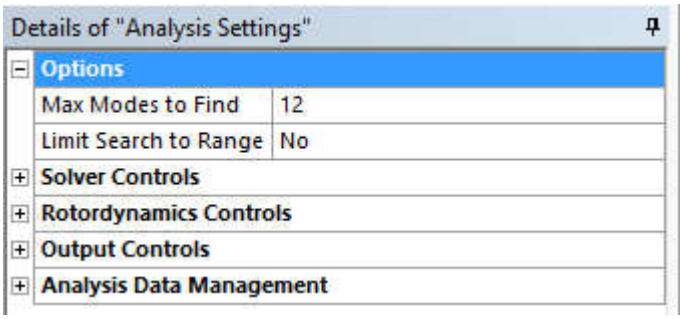

Figure 4.13 Adjustement of Options.

   7.2. Solver Controls: Select "No" to specify that undamped modes will be considered. It is not necessary to change the solver type.

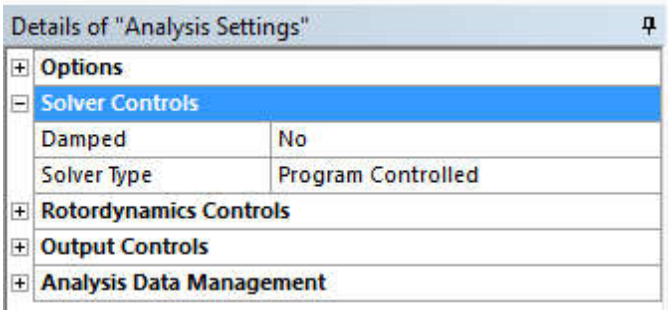

Figure 4.14 Adjustement of Solver Controls.

7.3. Output Controls: As well as the mode shapes, select the outputs of interest. Do not forget to say that the modal results need to be stored to use them in the RSA.

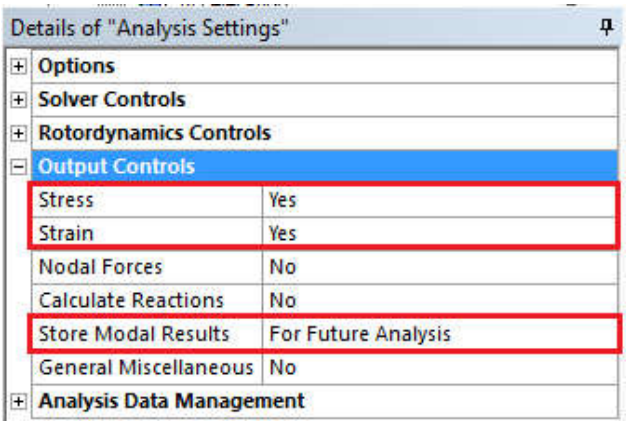

Figure 4.15 Adjustement of Output Controls.

8. Apply Supports

<u>Response Spectrum Analysis</u>

1. Create Analysis System
2. Establish Analysis Settings. In the Tree Outline window, select "Analysis Settings" inside Response Spectrum. Now, adjust the following settings:

2.1. Options: Specify the number of modes to use according to what was mentioned in 4.4. Select "Single Point" in Spectrum Type to say that just one response spectrum curve will be defined at the fixed supports. Specify the modes combination type, in our case, the CQC method.

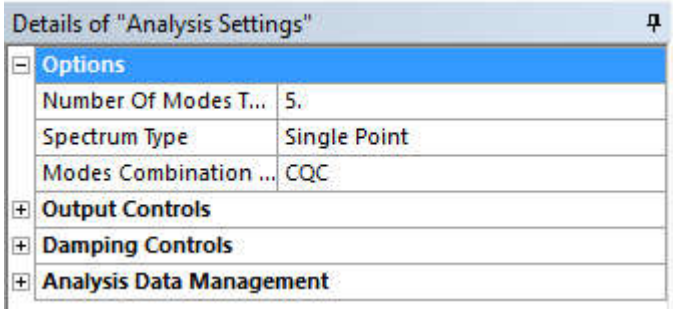

Figure 4.16 Adjustement of Options.

2.2. Damping Controls: specify the stiffness coefficient and the mass coefficient.

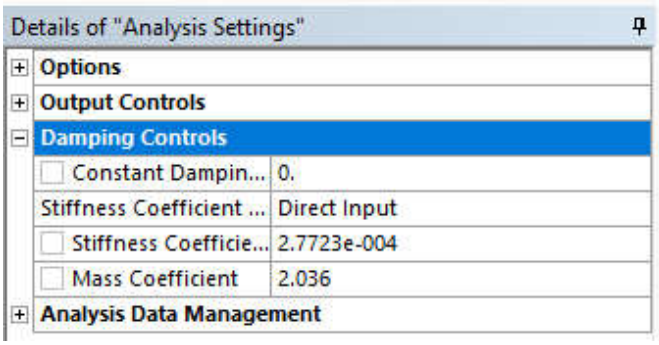

Figure 4.17 Adjustement of Damping Controls.

3. Apply Loads and Supports. Insert an acceleration input excitation (RS Acceleration) for each direction at all BC supports previously specified during the modal analysis configuration. Activate the missing mass effect to calculate the residual response. Also, active the rigid response effect to take into account the rigid part inside the periodic response.

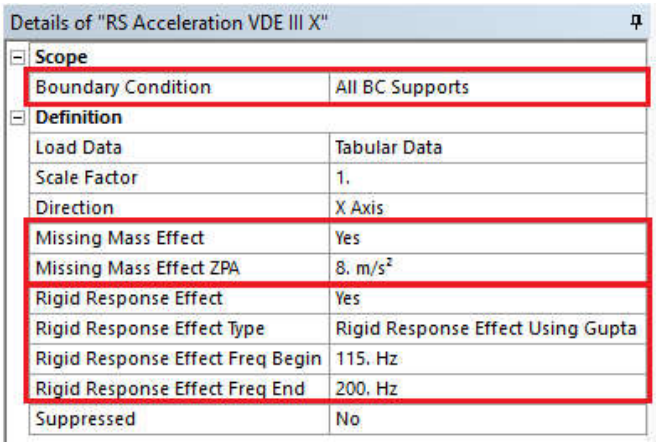

Figure 4.18 Adjustement of RS Acceleration.

4.7.2 Conceptual model #1

In order to represent the physical reality sufficiently accurately, a sequencial strategy has been adopted. This strategy consists in increasing the complexity of the model little by little. In this way, the starting point is a simplified version of the movable part. Since the slenderness ratio of the bar of the rolling guide and the probe head support is high enough (over 20) a beam formulation is justified.

The inner shielding cylinder is modelled by adding its mass to the volume of the bar of the rolling guide. On the other hand, since the probe head heat shielding has a different material assigned and it is not slender enough, it is decided to model the couple probe head support + probe head heat shielding with a unique beam made of stainless steel, and the difference of mass between stainless steel and molybdenum is included as a mass point in the center of gravity of the probe head heat shielding. The model is shown in the following Figure 4.19:

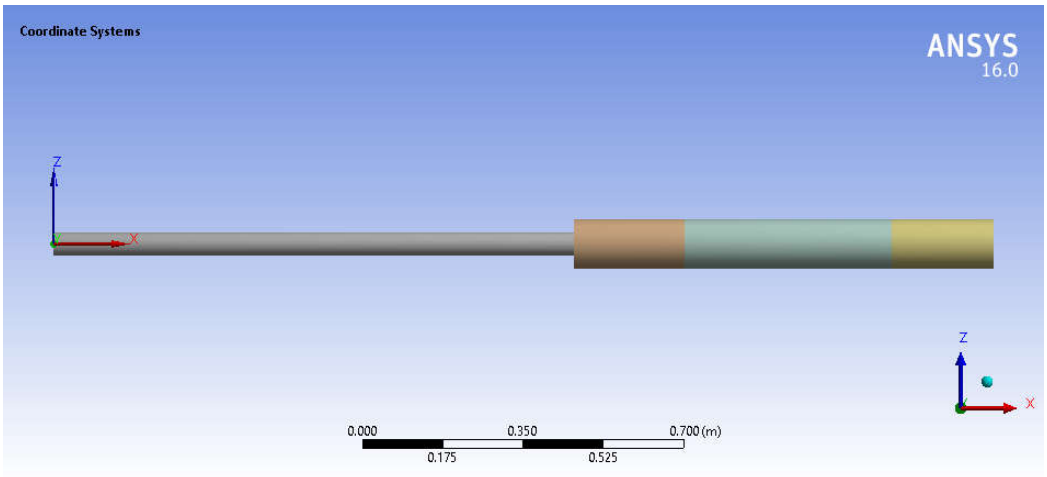

Figure 4.19 Model formed by two beams with different cross-sections.

4.7.2.1 Contacts

Not applicable.

4.7.2.2 Element types

BEAM188 elements are used.

4.7.2.3 Boundary conditions

A fixed support is used at the leftest point, as shown in Figure 4.20.

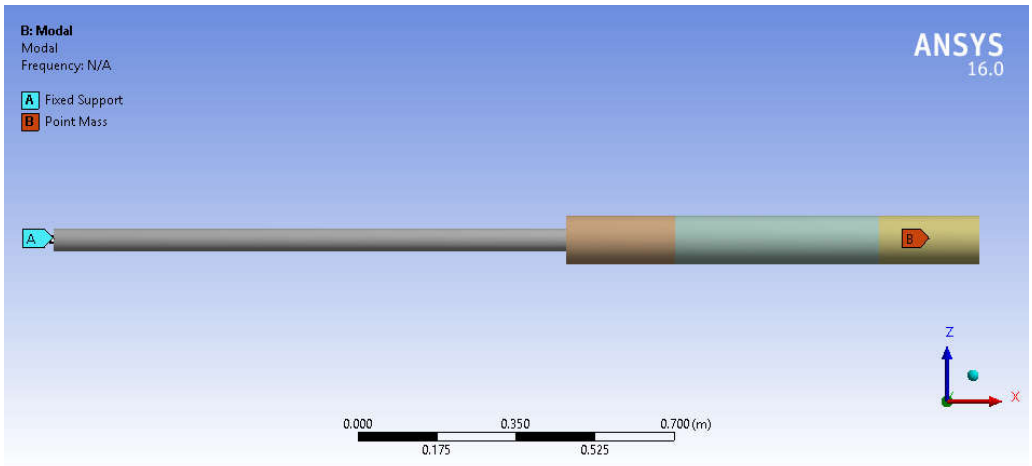

Figure 4.20 Boundary conditions used.

4.7.3 Conceptual model #2

The same conceptual model as #1 is used for this second step. There is an essential difference: a support is considered at some point along the probe head support. As it will be explained in the results section, contacts between the probe head support and the outer pipe are expected. Therefore, in order to avoid undesirable contacts, it is preferred to impose the contact area by means of a part that stands out. See Figure 4.25. Since the analyses performed must be totally linear, the eventual contact is transformed into a permanent contact. This is justified by the fact that the radial gap between the probe head support and the outer pipe is in the order of 1 mm.

4.7.3.1 Contacts

Not applicable.

4.7.3.2 Element types

BEAM188 elements are used.

4.7.3.3 Boundary conditions

As well as the fixed support, the Y and Z displacements are restricted at B to model the support. See Figure 4.21.

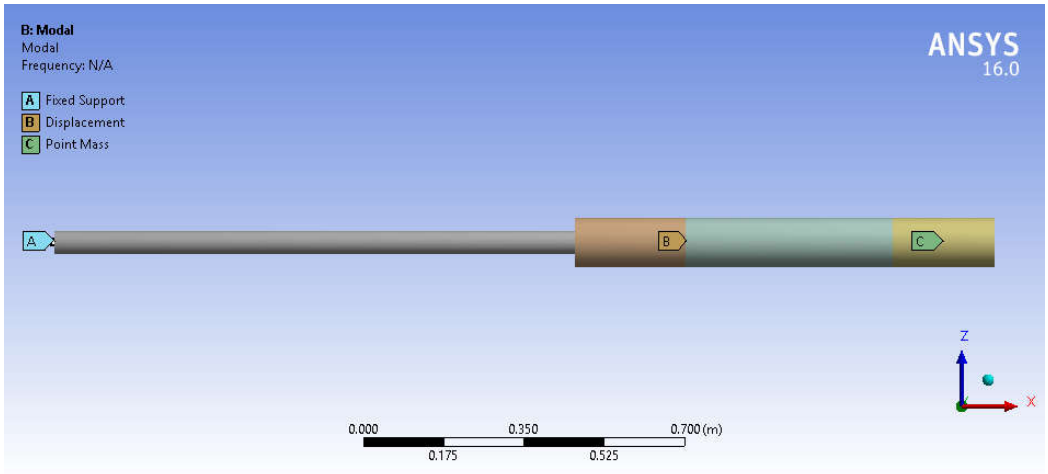

Figure 4.21 Boundary conditions used.

4.7.4 Conceptual model #3

The next step consists in representing the movable part by a 3D formulation, as shown in Figure 4.22.

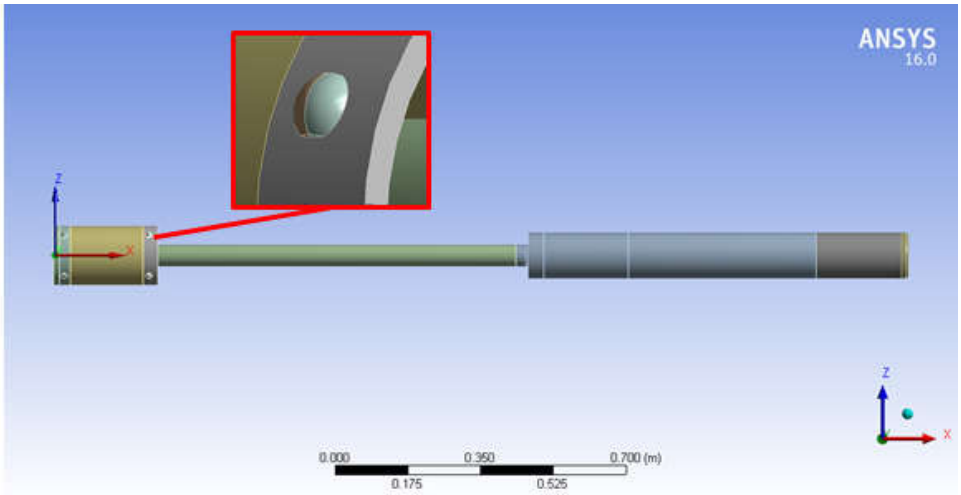

Figure 4.22 Simplified model of the movable part.

There are three main simplifications that have been used: the probe head heat shielding shape is considered to be uniform; the hole used by the optical system is not considered; and the rollers are represented but just in a way that permits to model the boundary conditions.

The inner shielding cylinder is modelled by using two approaches: with a solid cylinder and with a mass

distributed along the bar of the rolling guide.

4.7.4.1 Contacts

Bonded contacts are used between: rollers and rolling guide; inner shielding cylinder and the rolling guide; probe head support and probe head heat shielding.

4.7.4.2 Element types

SOLID186 and SOLID187 elements are used. See Figure 4.23.

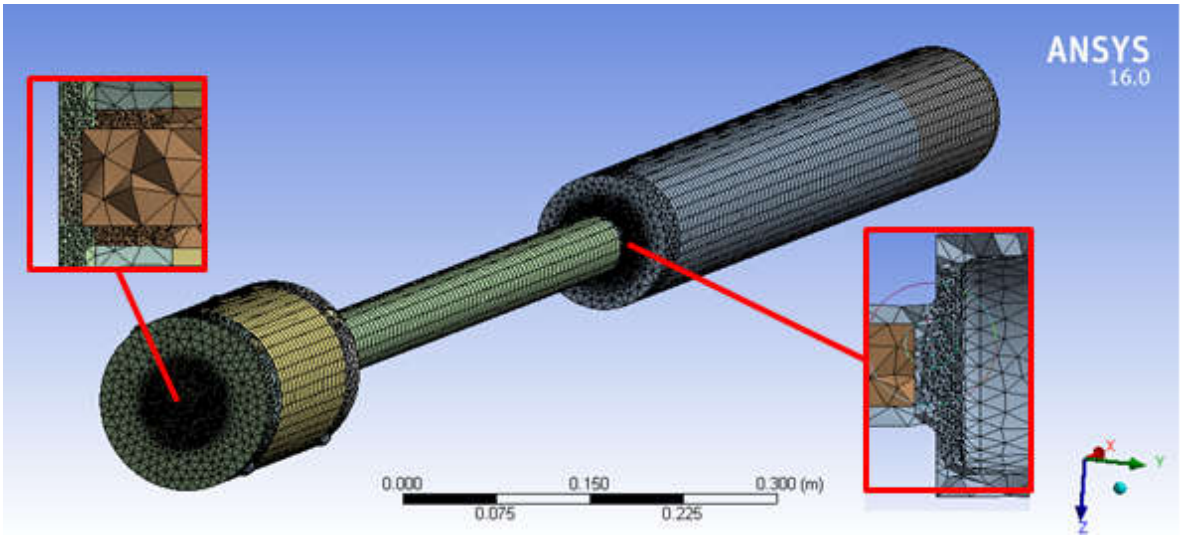

Figure 4.23 Meshing solution after refining in two areas: at the root of the rolling guide; and where the rolling guide finishes and the probe head support starts.

4.7.4.3 Boundary conditions

The first four rollers are fixed, whereas the second four ones have their Y and Z displacements restricted. The support (C) is modelled in the same way as B. See Figure 4.24.

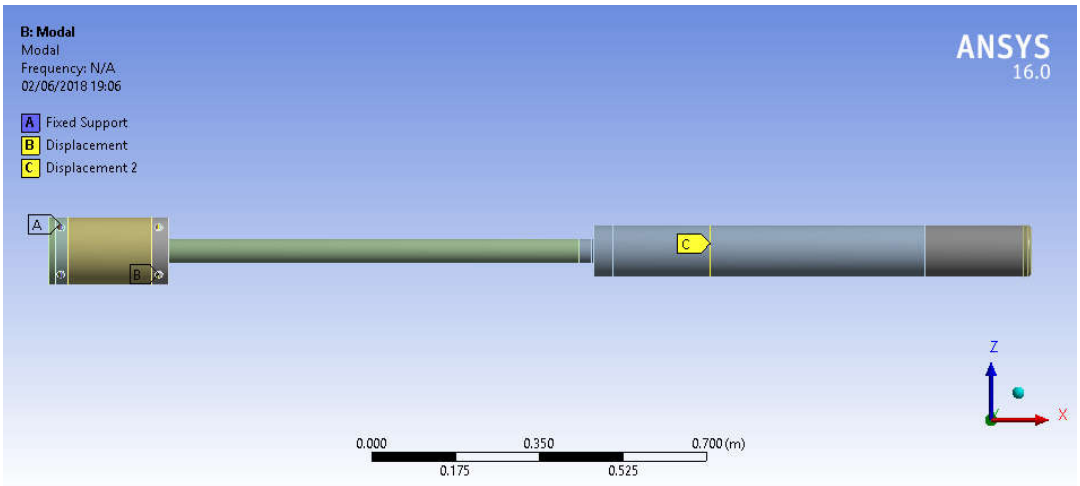

Figure 4.24 Boundary conditions used.

4.7.5 Conceptual model #4

This conceptual model is the final one. It is considered to be the most accurate representation of ITER FILD.

The entire linear manipulator is modelled.The part that stands out on the probe head support is easily modelled. In addition, the pusher of the linear actuator is modelled in a simplified way. See Figure 4.25.

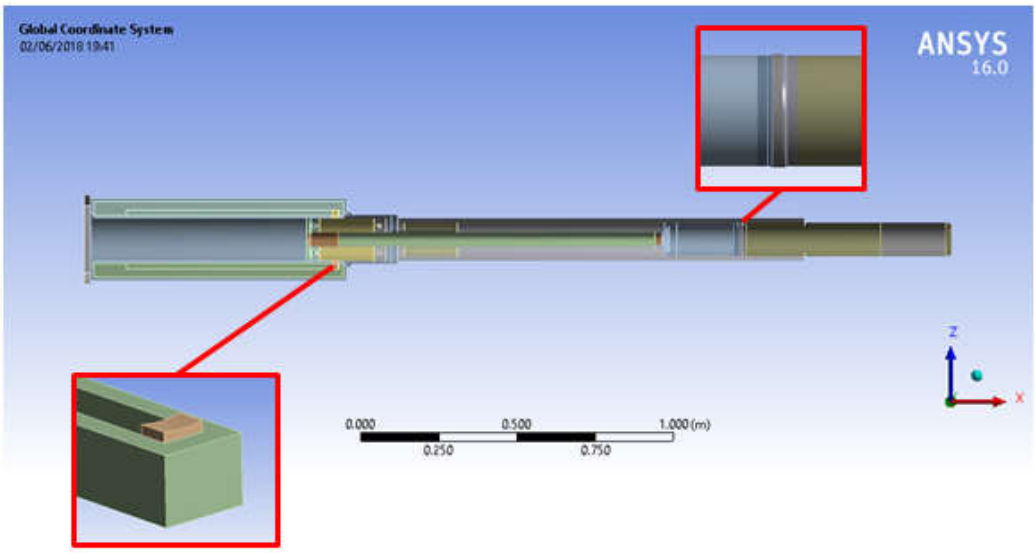

Figure 4.25 Final model used to represent ITER FILD.

4.7.5.1 Contacts

As well as the bonded contacts used in #3, there are bonded contacts between: the outer pipe and the fixed support; the outer pipe and the outer shielding cylinder; the fixed support and the two linear actuators; each pusher and the rolling guide. Additionally, no separation contacts are used between: all the rollers and the fixed support; the outer pipe and the part that stands out on the probe head support.

4.7.5.2 Element types

SOLID186 and SOLID187 elements are used. See Figure 4.26.

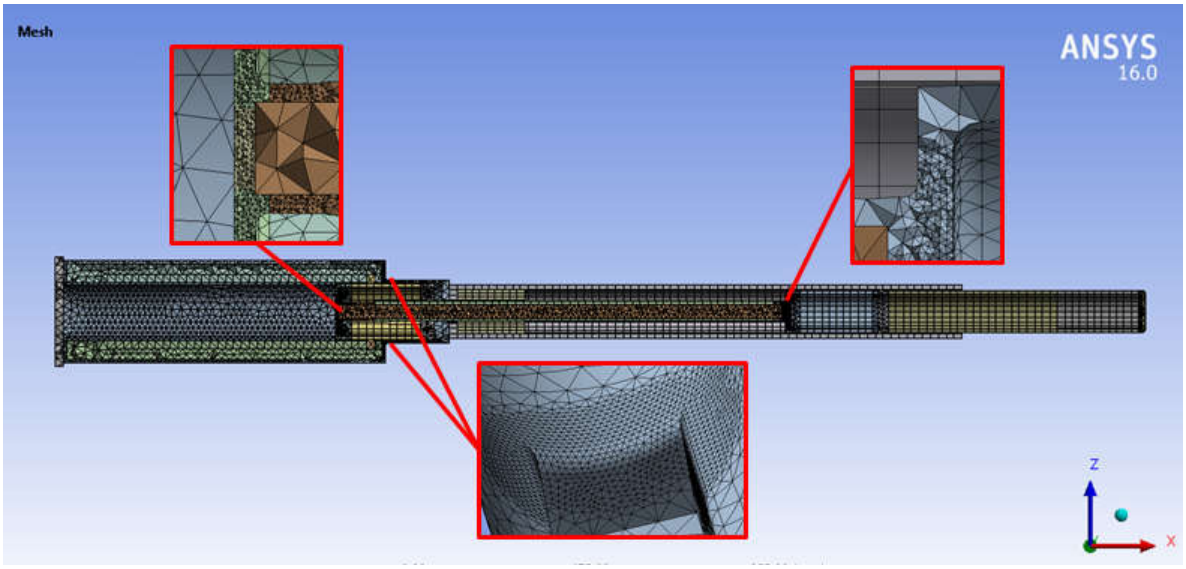

Figure 4.26 Meshing solution after refining in three areas: at the root of the rolling guide; where the rolling guide finishes and the probe head support starts; and on the corners of the rectangular parts and the cylindrical part of the fixed support.

4.7.5.3 Boundary conditions

A fixed support is applied on the inner side of the leftest part of the fixed support.

5 Results

5.1 Conceptual model #1

5.1.1 Static Structural Analysis

The displacements and stresses produced by the gravity effect are 9.2 mm and 42.3 MPa, respectively. The maximum displacement is produced at the tip of the probe head heat shielding, whereas the maximum equivalent stress is obtained at the root of the rolling guide.

5.2 Conceptual model #2

The position of the part that stands out is measured from the end of the probe head support. Three cases have been calculated: 0.4 m, 0.45 m and 0.5 m.

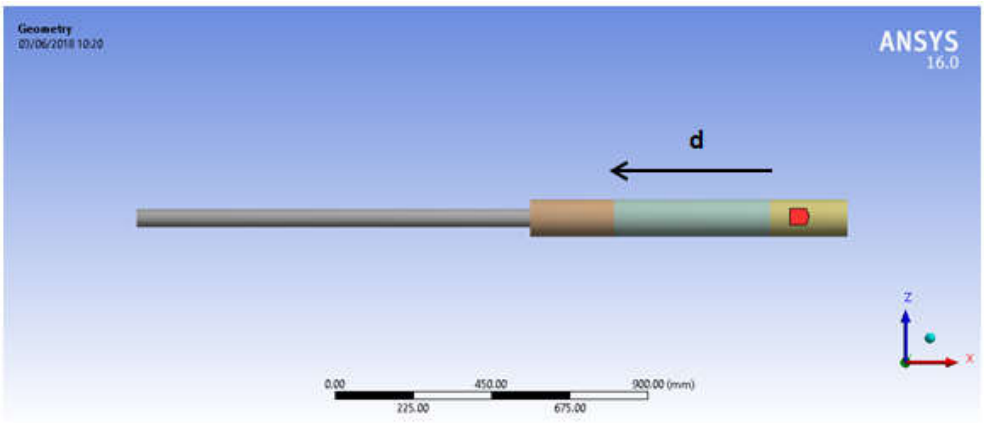

Figure 5.1 Location of the support.

5.2.1 Static Structural Analysis

The displacements and stresses produced by the gravity effect are listed below in Table 5.1. The maximum displacement takes place at the tip of the probe head heat shielding, whereas the maximum equivalent stress is produced where the cross-section changes, from the rolling guide to the probe head support.

Table 5.1 Maximum values obtained for the different values of *d*.

d (m)	Maximum displacement (mm)	Maximum stress (MPa)
0.4	0.037	2
0.45	0.076	3.1
0.5	0.12	4.3

5.2.2 Modal Analysis

The natural frequencies obtained are listed below in Table 5.2.

Table 5.2 Natural frequencies obtained for the different values of *d*.

d (m)	$f_n = \omega_n / 2\pi$ (Hz)				
	n=1	n=2	n=3	n=4	n=5
0.4	48.12	48.12	125.9	176.4	176.4
0.45	43.9	43.9	125.9	174.5	174.5
0.5	39.5	39.5	125.9	174.3	174.3

The mode shapes are illustrated for the case d=0.45 m in Figure 5.2, the other two cases are analogous.

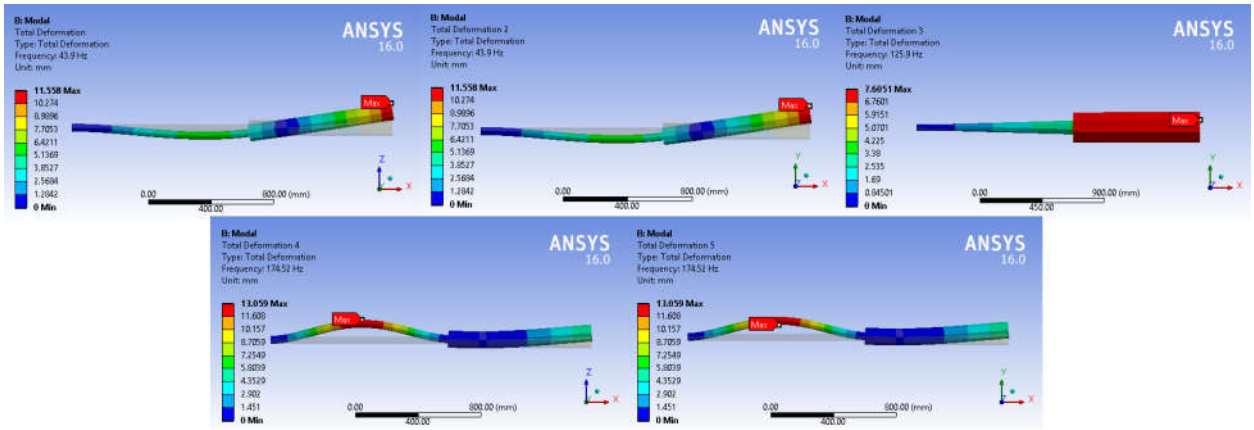

Figure 5.2 Mode shapes obtained for d=0.45 m. From left to right, from top to bottom, the natural frequencies associated are: 43.9 Hz, 43.9 Hz, 125.9 Hz, 174.5 Hz and 174.5 Hz.

5.2.3 Response Spectrum Analysis

5.2.3.1 VDE III

Five natural modes are necessary to calculate the solution. The displacements and stresses obtained are listed below in Table 5.3.

Table 5.3 Maximum values obtained for the different values of *d*.

d (m)	Maximum radial displacement (mm)	Maximum stress (MPa)
0.4	0.25	8.14
0.45	0.48	13.3
0.5	1.25	27.9

The solution for d=0.45 m is shown in Figure 5.3 and Figure 5.4. The maximum values are obtained at the same points where the maximum values due to the gravity were obtained.

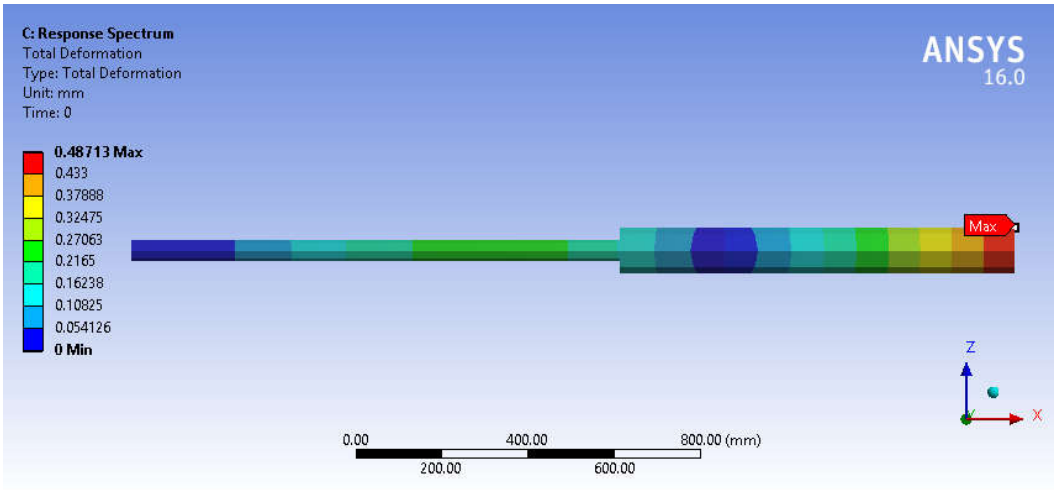

Figure 5.3 Displacements obtained for d=0.45 m.

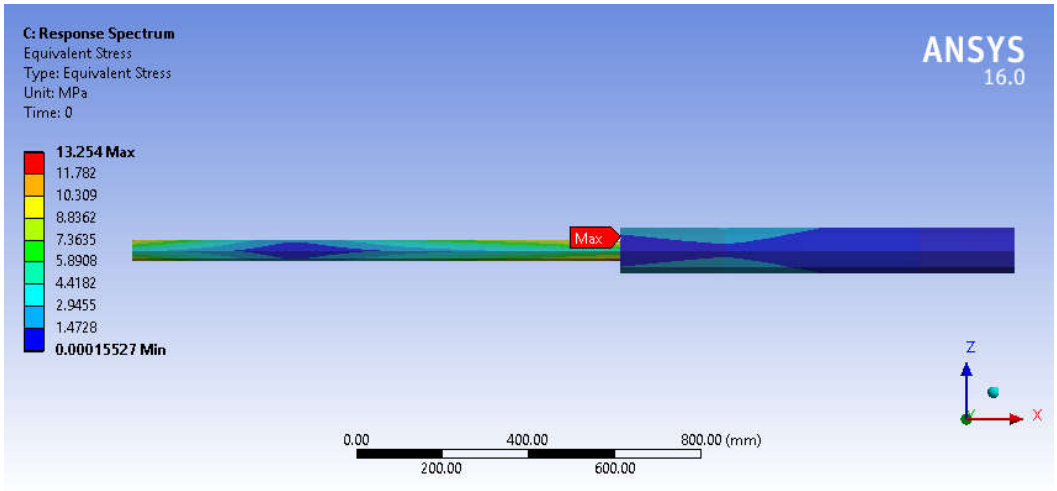

Figure 5.4 Equivalent (Von Mises) stresses obtained for d=0.45 m.

5.2.3.2 SMHV

Three natural modes are necessary to calculate the solution. The displacements and stresses obtained are listed below in Table 5.4.

Table 5.4 Maximum values obtained for the three cases.

d (m)	Maximum radial displacement (mm)	Maximum stress (MPa)
0.4	0.06	2.9
0.45	0.15	4.5
0.5	0.28	7.3

The solution for d=0.45 m is shown in Figure 5.5 and Figure 5.6. The maximum values are obtained at the same points where the maximum values due to the gravity were obtained.

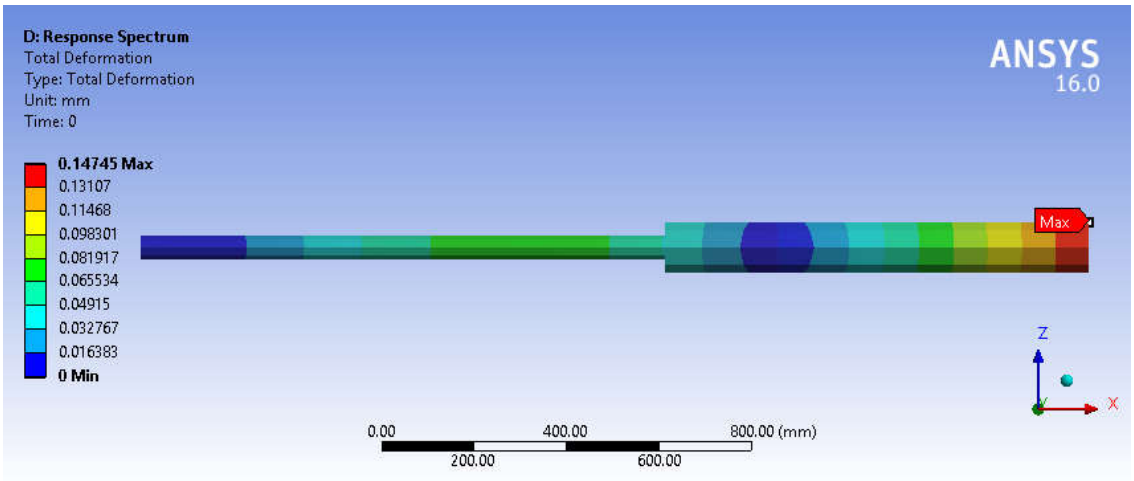

Figure 5.5 Displacements obtained for d=0.45 m.

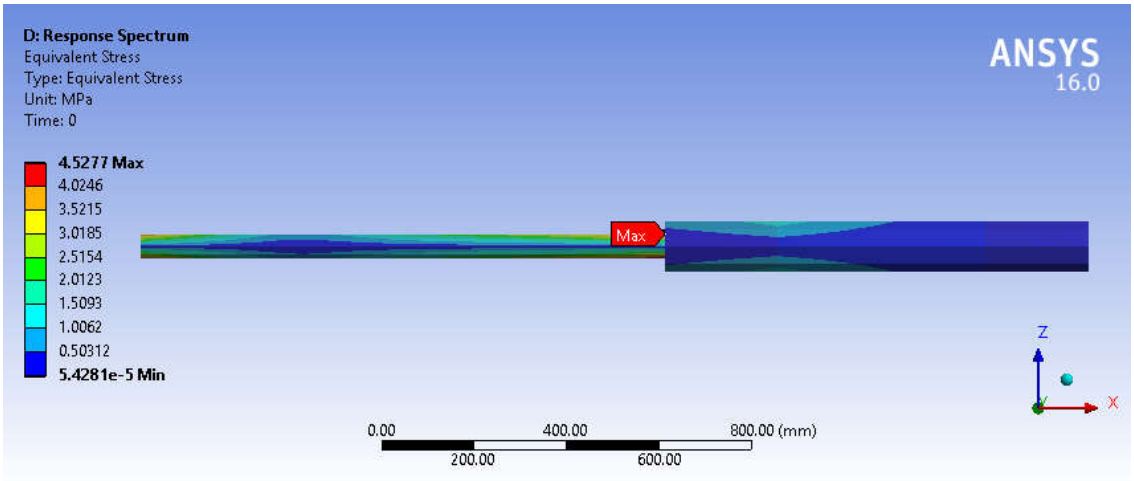

Figure 5.6 Equivalent (Von Mises) stresses obtained for d=0.45 m.

It is interesting to summarize the total values (gravity + VDE III and gravity + SMHV):

Table 5.5 Summary of maximum values.

d (m)	Load combination #1 (gravity + VDE III)		Load combination #2 (gravity + SMHV)	
	Maximum displacement in Z direction (mm)	Maximum stress (MPa)	Maximum displacement in Z direction (mm)	Maximum stress (MPa)
0.4	0.242	10.14	0.086	4.9
0.45	0.483	16.4	0.208	7.6
0.5	1.24	32.2	0.32	11.6

5.3 Conceptual model #3

The value of d=0.45 m has been assumed because it is the higher value that produces a total maximum displacement lower than 1 mm, which is the radial gap between the probe head support and the outer pipe.

The mass of the inner shielding cylinder is 2.57 kg.

5.3.1 Static Structural Analysis

The displacements and stresses produced by the gravity effect are listed below in Table 5.6. The maximum displacement is produced at the tip of the probe head heat shielding, whereas the maximum equivalent stress is produced where the cross-section changes, from the rolling guide to the probe head support. The similarity between the displacements obtained here in comparison to those obtained with the conceptual model #2, is acceptable. However, the comparison between stresses lead to an unacceptable similarity.

Table 5.6 Maximum values obtained for the two approaches.

d (m)	Inner shielding cylinder modelled as a solid		Inner shielding cylinder modelled as a distributed mass	
	Maximum displacement (mm)	Maximum stress (MPa)	Maximum displacement (mm)	Maximum stress (MPa)
0.45	0.07	8.11	0.09	8.12

5.3.2 Modal Analysis

The natural frequencies obtained are listed below in Table 5.7. It is noticeable that the first natural frequency obtained here is similar to the first natural frequency obtained with the conceptual model #2, 43.9Hz (1.4% with respect to the approach of solid cylinder and -16.1% with respect to the approach of mass distributed).

Table 5.7 Natural frequencies obtained for the two approaches.

Approach	$f_n = \omega_n / 2\pi$ (Hz)			
	n=1	n=2	n=3	n=4
Solid cylinder	44.51	44.51	167.9	167.9
Mass distributed	37.82	37.82	146.2	146.2
Relative error (%)	15.04	15.04	12.93	12.93

The mode shapes for the approach of solid sylinder are shown in Figure 5.7, the other case is analogous.

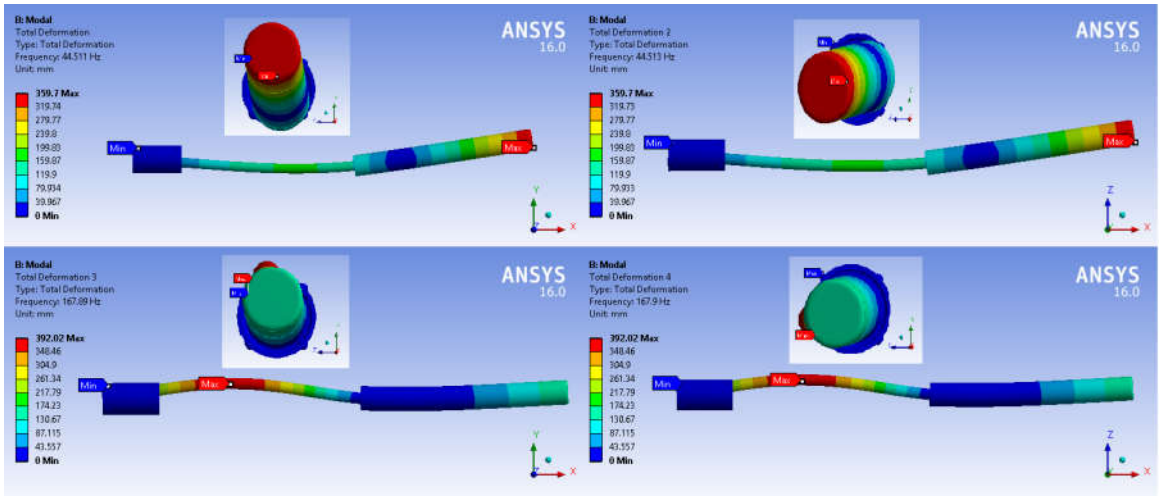

Figure 5.7 Mode shapes obtained for the solid approach. From left to right, from top to bottom, the natural frequencies associated are: 44.51 Hz, 44.51 Hz, 167.9 Hz and 167.9 Hz.

5.3.3 Response Spectrum Analysis

Since the relative error found is higher than the 10% assumed with the broadened curves, hereafter just the first approach (solid cylinder) will be used.

5.3.3.1 VDE III

Four natural modes are necessary to calculate the solution. The displacements and stresses obtained are shown below in Figure 5.8 and Figure 5.9. The maximum values are 8.44 mm (radial displacement) and 34.3 MPa, respectively. There are no similarities between these values and those that were obtained for conceptual model #2 because the natural frequencies are unacceptably different.

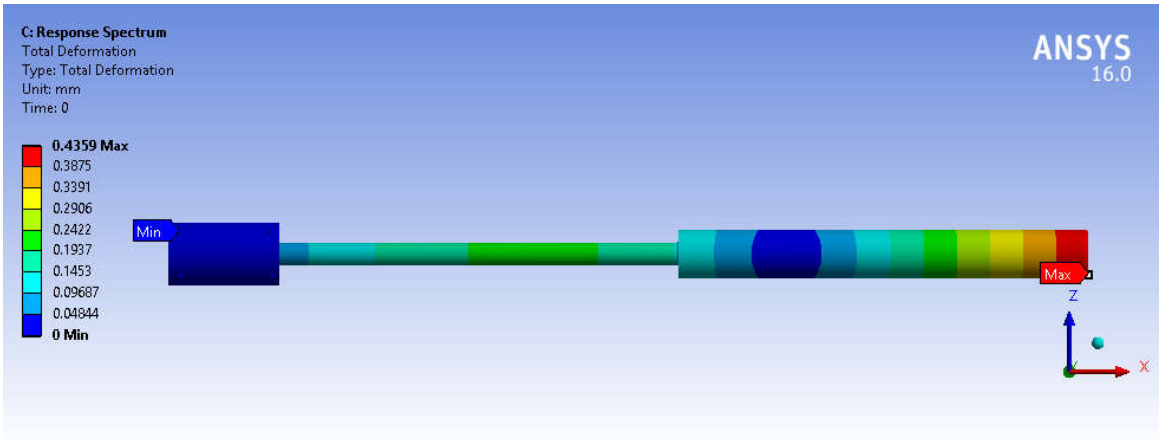

Figure 5.8 Displacements obtained with the approach of solid cylinder.

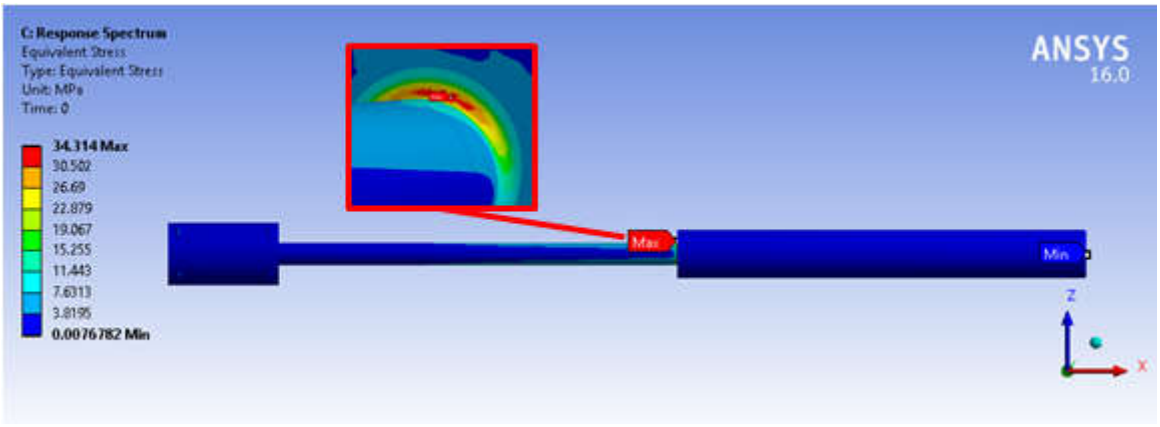

Figure 5.9 Equivalent (Von Mises) stresses obtained with the approach of solid cylinder.

5.3.3.2 SMHV

Two natural modes are necessary to calculate the solution. The displacements and stresses obtained are shown below in Figure 5.10 and Figure 5.11. The maximum values are 0.14 mm and 12 MPa. There are no similarities between these values and those that were obtained for conceptual model #2 because the natural frequencies are unacceptably different.

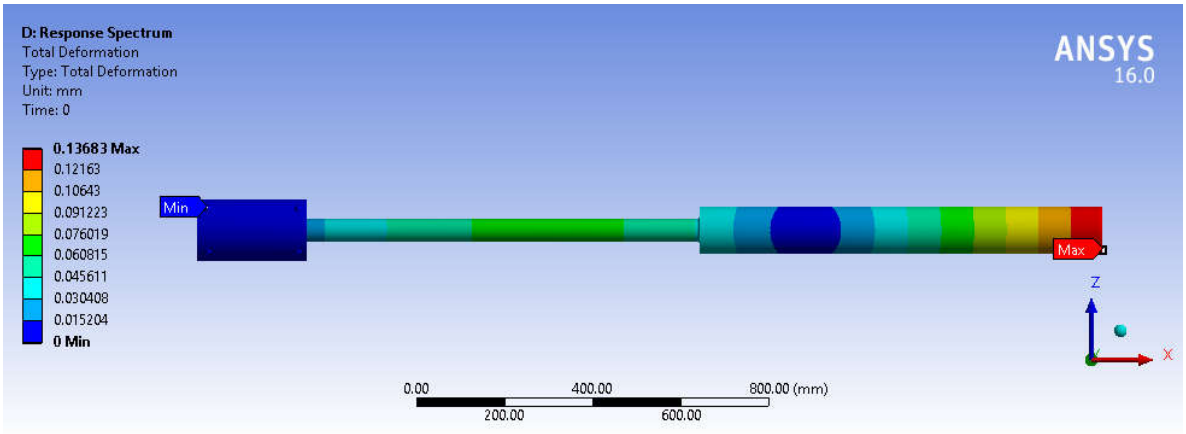

Figure 5.10 Displacements obtained with the approach of solid cylinder.

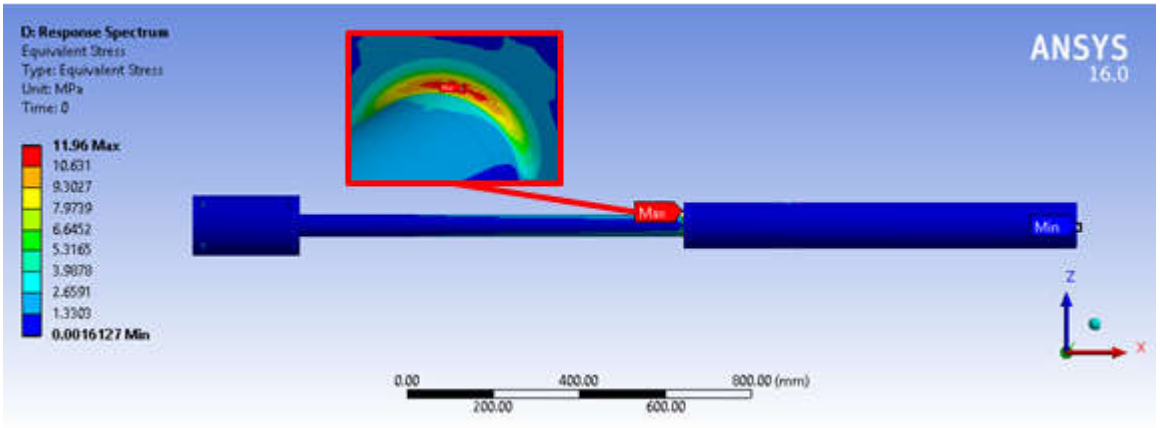

Figure 5.11 Equivalent (Von Mises) stresses obtained with the approach of solid cylinder.

It is interesting to summarize the total values (gravity + VDE III and gravity + SMHV):

Table 5.8 Summary of maximum values.

Approach	Load combination #1 (gravity + VDE III)		Load combination #2 (gravity + SMHV)	
	Maximum displacement in Z direction (mm)	Maximum stress (MPa)	Maximum displacement in Z direction (mm)	Maximum stress (MPa)
Solid cylinder	8.23	42.41	0.18	20.11

5.4 Conceptual model #4

As it will be justified below, it will be necessary to redesign the conceptual model before presented. Therefore, the results of the static analysis are postponed.

5.4.1 Modal Analysis

The natural frequencies obtained are listed below in Table 5.9. It is noticeable that the first natural frequency obtained here is different from the first natural frequency obtained with the conceptual model #3, since the boundary condition in the probe head support is slightly different. Now, the system is less rigid.

Table 5.9 Natural frequencies obtained for the starting design point.

Design Point	$f_n = \omega_n / 2\pi$ (Hz)								
	n=1	n=2	n=3	n=4	n=5	n=6	n=7	n=8	n=9
Starting Point	17.05	27.72	63.13	70.11	128.7	150.6	179.3	184.3	185.8

On the other hand, it is interesting to see the fraction of effective mass associated with mode and each direction. See Figure 5.12.

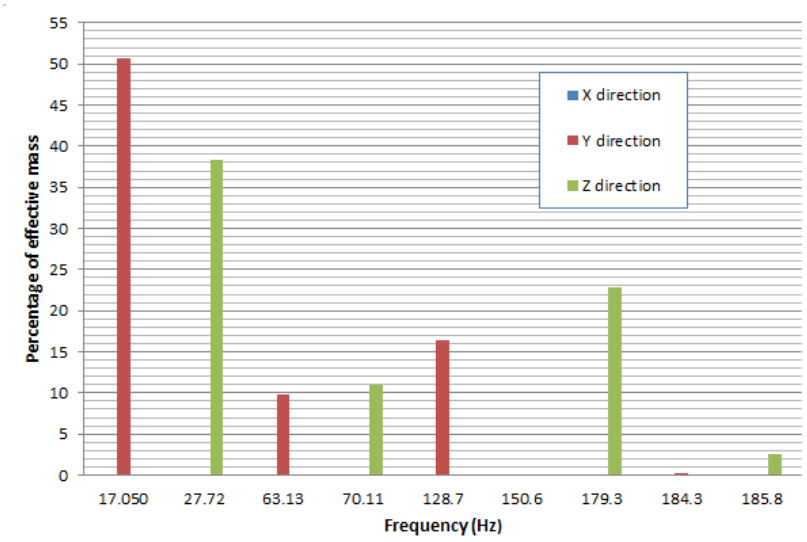

Figure 5.12 Percentages calculated with respect to the mass of the present model of ITER FILD (165.43 kg).

5.4.2 Response Spectrum Analysis: VDE III

For the moment, it is interesting to observe what happens just with the stresses produced by VDE III. As illustrated in Figure 5.13, excessive stresses are found, with 875 MPa.

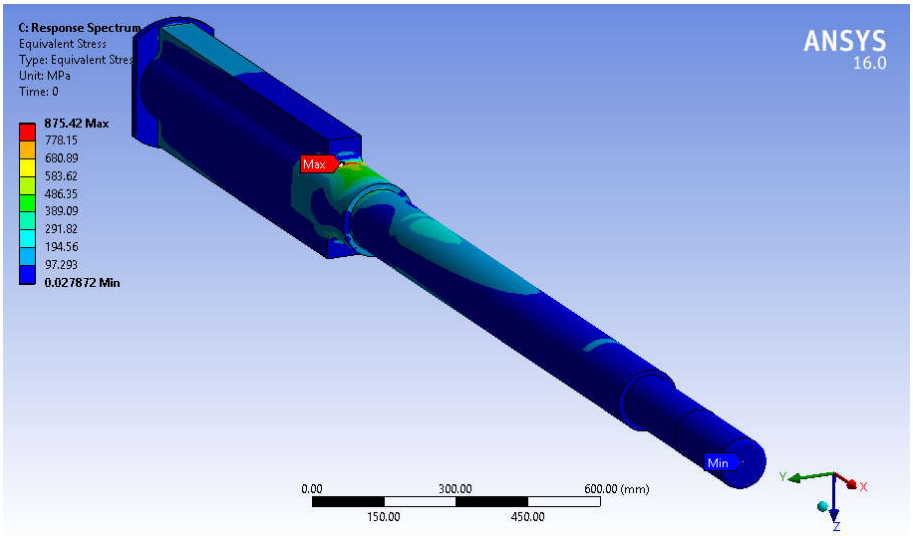

Figure 5.13 Equivalent (Von Mises) stresses obtained with the starting design point.

This result is found because one of the natural modes falls inside an interval with an excessively high acceleration value, in particular the acceleration in Z direction. Additionally, this natural frequency is associated with a 38.3% of effective mass in the Z direction. See Figure 5.14.

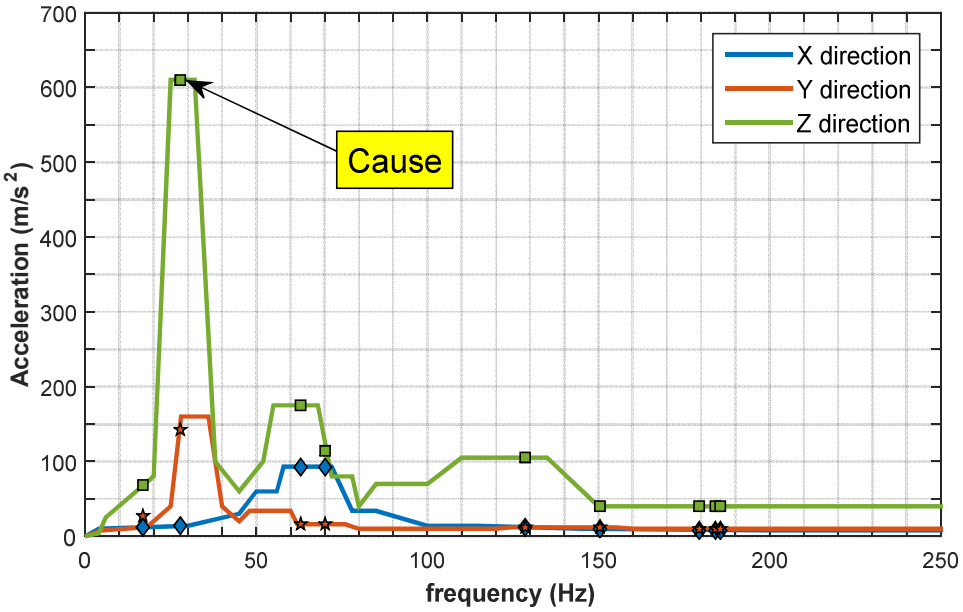

Figure 5.14 Spectral value associated with each natural frequency for the three directions.

5.4.3 Redesign

This subsection includes the results found for different design points. The aim of the redesign process has been to make the second natural frequency drop below 25 Hz (the maximum peak interval is 25-32 Hz), since 27.72 Hz is closer to 25 Hz than 32 Hz. The part that has been redesigned is the outer pipe.

5.4.3.1 Modal Analysis

The second natural frequency found for all the design points considered are listed in Table 5.10.

Table 5.10 Second natural frequency for different design points of the outer pipe.

#	Design Point	$f_2 = \omega_2 / 2\pi$ (Hz)
1	Starting Point	27.72
2	Reduce thickness of the outer pipe from 12 mm to 8 mm	26.75
3	#2 + reduce Young's modulus of the material used for the outer pipe to 190 GPa	26.51
4	Topology optimization[28]	16.73

The redesign result is shown in Figure 5.15. After redesigning, the mass of the outer pipe has been reduced from 47.97 kg to 26.31 kg.

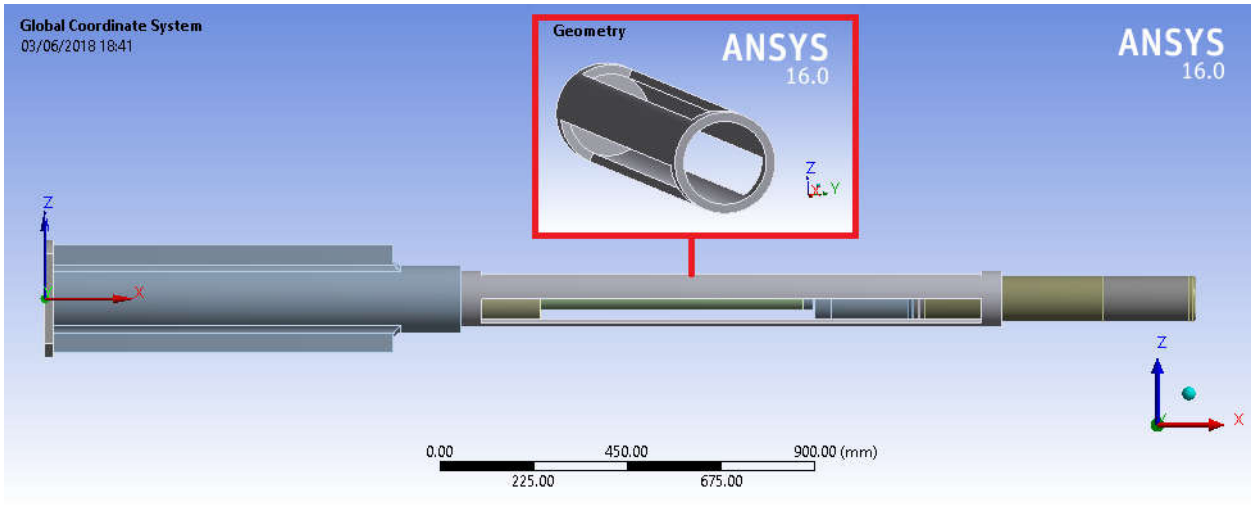

Figure 5.15 Topology optimization result.

The natural frequencies are listed below in Table 5.11.

Table 5.11 Natural frequencies obtanied for the redesigned model.

Design Point	$f_n = \omega_n / 2\pi$ (Hz)												
	1	2	3	4	5	6	7	8	9	10	11	12	13
Topology optimization	13.87	16.73	50.33	55.43	86.62	86.86	89.03	96.57	97.24	150.7	160.0	184	185.1

[28] It is not a real optimization, but an improvement that shows how interesting this strategy could be.

The mode shapes are illustrated Figure 5.16.

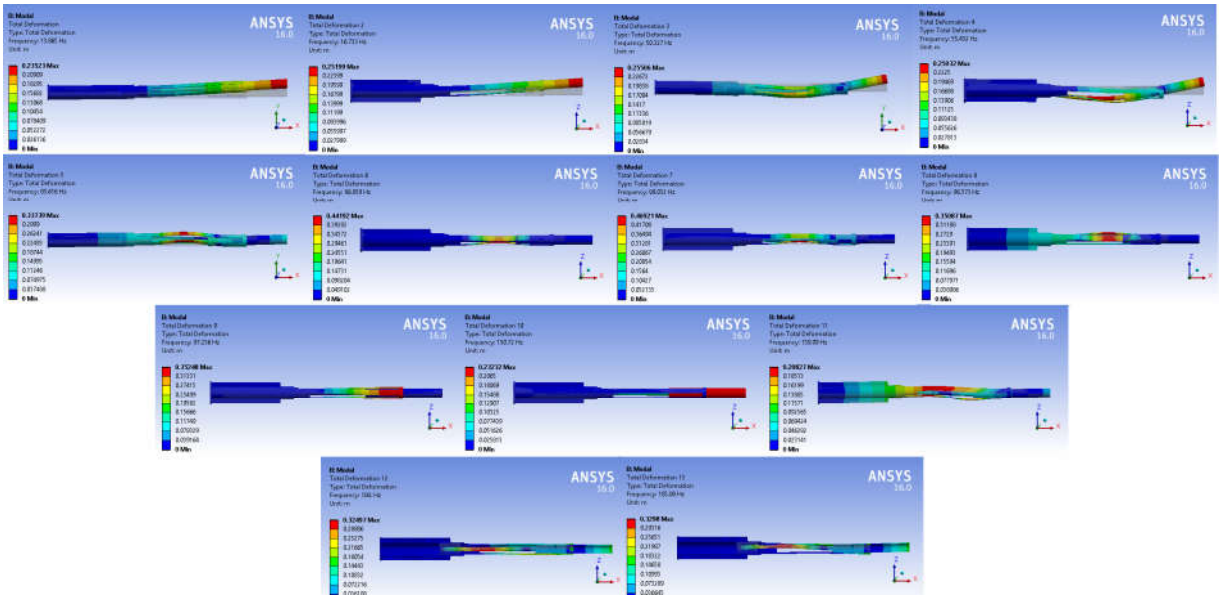

Figure 5.16 Mode shapes obtained for the solid approach. From left to right, from top to bottom, the natural frequencies associated are: 13.87 Hz, 16.73 Hz, 50.43 Hz, 55.43 Hz, 86.62 Hz, 86.86 Hz, 89.03 Hz, 96.57 Hz, 97.24 Hz, 150.7 Hz, 160.0 Hz, 184 Hz and 185.1 Hz.

It is also interesting to see the fraction of effective mass associated with each mode and each direction. See Figure 5.17.

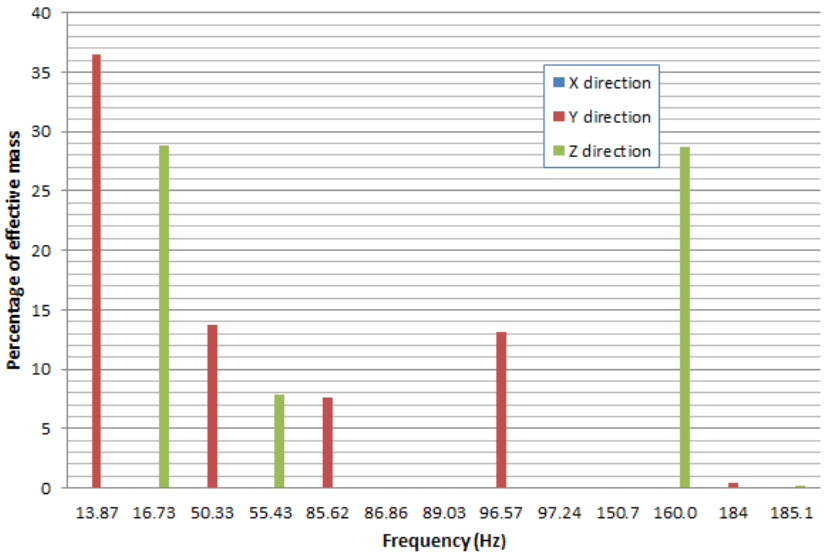

Figure 5.17 Percentages calculated with respect to the mass of the redesigned model of ITER FILD (143.76 kg).

5.4.3.2 Response Spectrum Analysis

5.4.3.2.1 VDE III

Thirteen natural modes are necessary to calculate the solution. The displacements and stresses obtained are shown below in Figure 5.18 and Figure 5.19. The maximum values are 11 mm and 185.2 MPa.

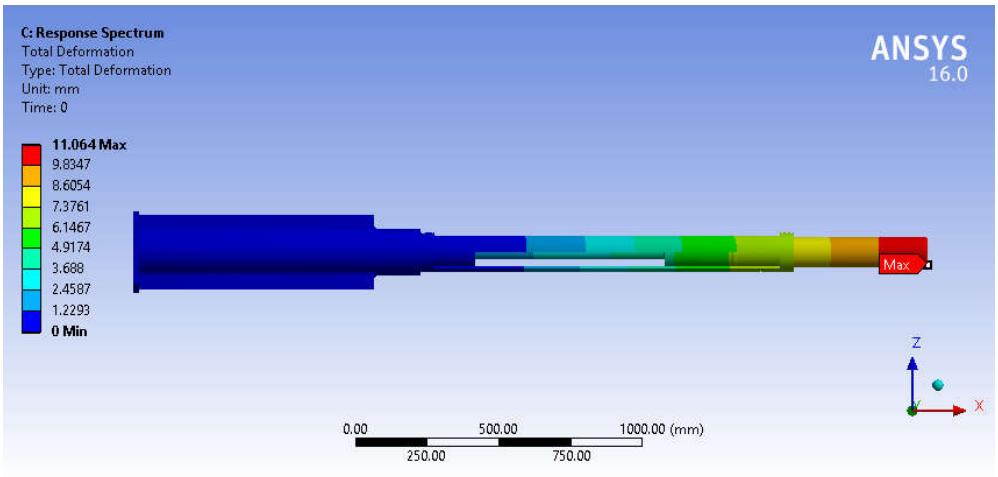

Figure 5.18 Displacements obtained for the redesigned model.

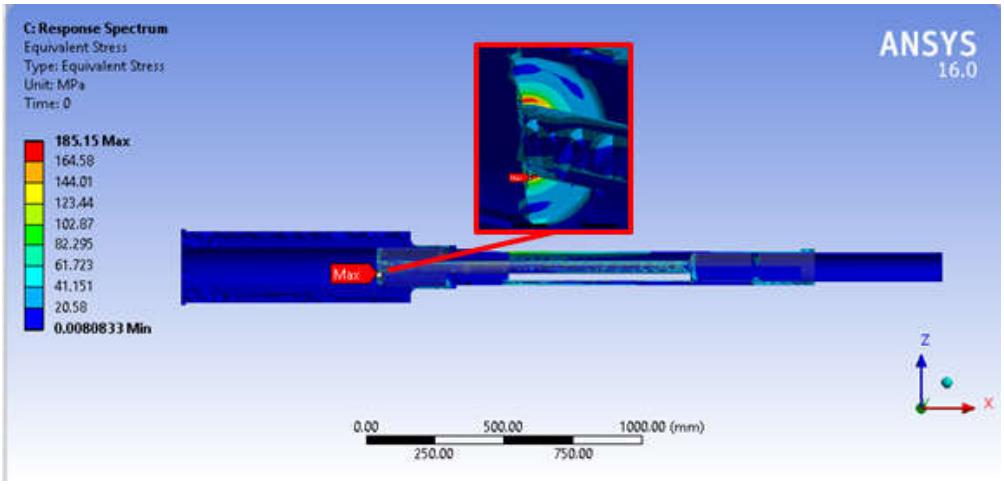

Figure 5.19 Equivalent (Von Mises) stresses obtained with the redesigned model.

5.4.3.2.2 SMHV

Nine natural modes are necessary to calculate the solution. The displacements and stresses obtained are shown below in Figure 5.20 and Figure 5.21. The maximum values are 3.9 mm and 51.9 MPa.

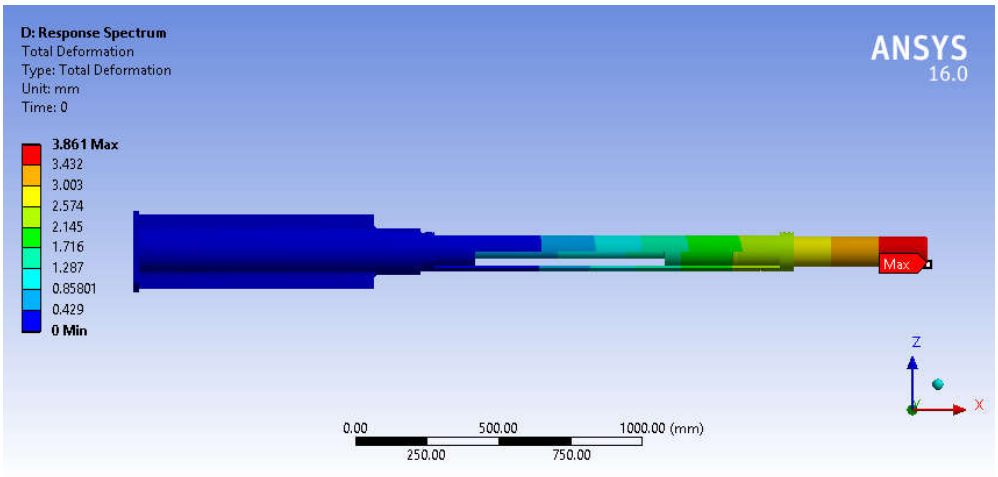

Figure 5.20 Displacements obtained for the redesigned model.

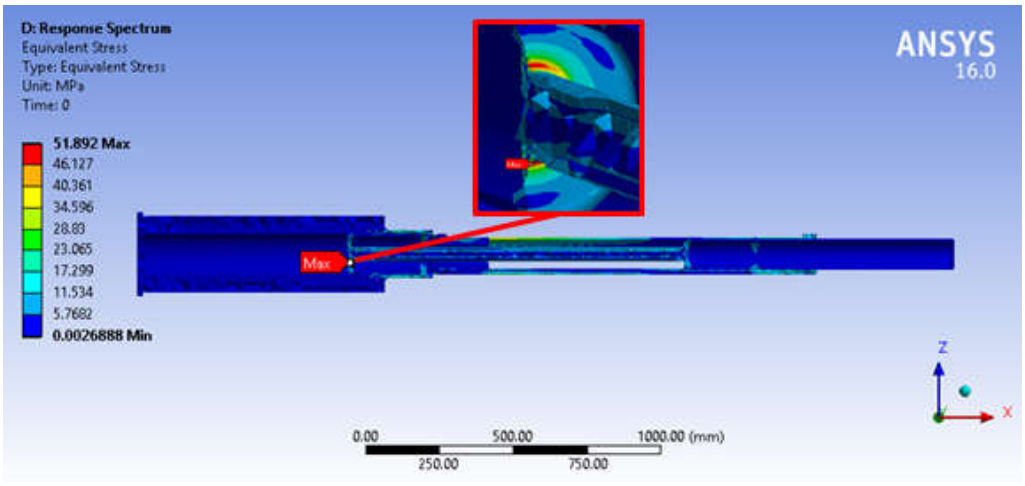

Figure 5.21 Equivalent (Von Mises) stresses obtained with the redesigned model.

5.4.3.3 Verification with an Alternative Method: Equivalent Static Analysis

As mentioned in section 3.8, in order to verify the results obtained for VDE III and SMHV, an equivalent static analysis is performed for each case. They consist in exciting the system with a certain acceleration multiplied by the DAF of 1.5. The values of the accelerations are extracted from the RS. For each direction, it is picked the maximum value that is situated on the right of the first natural frequency. This is repeated with each load case.

For VDE III:

Table 5.12 Comparison between RSA and equivalent static analysis for VDE III.

Method	Maximum displacement (mm)	Maximum stress (MPa)
RSA	11	185.2
Equivalent static analysis (139.5 m/s^2 in X, 240 m/s^2 in Y, 915 m/s^2 in Z)	138.2	2417

For SMHV:

Table 5.13 Comparison between RSA and equivalent static analysis for SMHV.

Method	Maximum displacement (mm)	Maximum stress (MPa)
RSA	3.9	51.9
Equivalent static analysis (13.5 m/s^2 in X, 6.795 m/s^2 in Y, 162 m/s^2 in Z)	22.7	416

In both cases, the alternative method (equivalent static analysis) is not useful, since it lead to over-conservative estimations.

5.4.3.4 Static Structural Analysis

The maximum displacement obtained is 1.37 mm, at the tip of the probe head heat shielding, whereas the

maximum equivalent stress is 24.9 MPa, produced at the root of the rolling guide (like the maximum of VDE III and SMHV). The reason why now these maximum stresses are obtained at the root of the rolling guide is because the system is less rigid in the part of the probe head supported.

It is interesting to summarize the total values (gravity + VDE III and gravity + SMHV):

Table 5.14 Summary of máximum values.

Load combination #1 (gravity + VDE III)		Load combination #2 (gravity + SMHV)	
Maximum displacement in Z direction (mm)	Maximum stress (MPa)	Maximum displacement in Z direction (mm)	Maximum stress (MPa)
12.1	210.1	5.03	76.8

Both load combinations are below the elastic limit (270 MPa).

5.5 Checklist

The accuracy of the results obtained with each FE model used has been verified and the checks used are briefly reported here:

- **Numerical Code Verification:** the solution algorithms are correctly implemented in the FE software used.
- **Mass Check:** the total mass, centre of gravity and second moments of inertia have been compared before and after the discretization.
- **Unit Acceleration Load Check:** the units involved in the calculation of the desired magnitudes have been checked.
- **VDE and Seismic Load Check:** the RS are applied correctly (magnitude, direction, etc.).
- **Contact Check:** the behavior of the contacts has been checked.
- **Damping Check:** it has not been performed, since the damping value is already provided by the CPPE (3%) and the use of the mass and stiffness coefficients is devoted to the calculation of the coupling coefficient.
- **FE Mesh Discretization:** the mesh density is justified by a mesh-sensitivity study. An error in the stresses calculated below 3% has been assumed, because it has generally led to an acceptable balance between accuracy in the results and CPU-time during numerical simulations. The parts that have needed to be refined are shown in Figure 4.23 and Figure 4.26.
- **Comparison with Alternative Results:** the results of each conceptual model have been compared to the ones obtained with the former conceptual model. Additionally, the results calculated with the conceptual model #4 have been compared to the ones obtained with an alternative method (linear equivalent static analysis).

6 Discussion

6.1 Summary

Throughout this document, the understanding of the RSA bases has been built up. This knowledge has made the dynamic study of ITER FILD possible. Thus, the elaboration of the report arranged by the document production plan is practicable.

In addition, the ANSYS package has been studied and its advantages to perform the RSA have been brought to light.

In order to understand and resolve the problem in sufficiently accurate way, it has been necessary to divide the analysis into four steps. In each step, a different conceptual model has been used, being its complexity from lowest to highest.

The conceptual model #1 has permited to justify the need of including in the ITER FILD design a part that stands out on the probe head support surface. Otherwise, the eventual deflexion will lead to undesirable and unexpected contacts or impacts during the EM or seismic transients. This additional part is just to get the project off the ground, since a permanent contact between moving parts is not allowed in vacuum, according to one of the functional requirements arranged for the ITER FILD. In the future, some kind of optimization will be indispensable before performing the dynamic analysis so that there will not be contact between the probe head support and the outer pipe.

The conceptual model #2 helps to decide where to locate the eventual contact. Since the nature of the RSA is linear, a linearization of the contact area has been crutial. A permantent contact is considered. This hypothesis is justified by the fact that the play between the probe head support and the outer pipe is 1 mm at present, which is assumed to be negligible. The location of the part that stands out is found by imposing a total maximum displacement at the tip of the probe head heat shielding of 1 mm.

The conceptual model #3 uses the previous conclusions, and permits to verify if the hypothesis of modelling the inner shielding cylinder as a mass distributed is feasible or not. The answer is no, because the stiffness of the inner shielding cylinder also contributes significantly.

All the previous knowledge is collected in the final model, the conceptual model #4. The ITER FILD is modelled entirely, with the exception of the bellow. It is assumed that its role is negligible for now, because it provides mass, as well as longitudinal and radial stiffness, in an area which is well fixed. On the other hand, the part that stands out is modelled in the easiest way since it is considered to be impracticable in reality.

The starting conceptual model #4 leads to excessively high stresses on the fixed support surface. The cause is a natural frequency that falls inside a forbidden interval. In order to reduce that natural frequency, it is necessary to redesign ITER FILD in some way. It is decided to redesign the outer pipe, which is considered to be the guilty part. The aim is to reduce its bending stiffness, proportional to the Young's modulus and the moment of inertia in the cross direction. It is found that the best way to achieve that goal is by using a strategy of topology optimization. What is obtained is not an optimization, but an improvement showing how interesting this strategy can be.

In summary, the elastic limit is not exceeded and the hypothesis of a unique contact area between the probe head support and the outer pipe is verified. Additionally, it is found that the RSA is the only feasible method to study the dynamic behaviour of ITER FILD, because the equivalent static analysis, also proposed by ITER at the conceptual stage, leads to over-conservative estimations.

6.2 Future Work

This study lays the foundation for the progressive refinement of the future vibrational analyses. Therefore, it permits to perform future response spectrum analyses in a quicker and more efficient way if necessary.

Throughout the developement of the refinement process, it will be indispensable to detect the sources of uncertainties and reduce them. This document highlights three main sources:

- **Geometry**. The current geometry is subject to eventual changes because of the design prematurity. Consequently, an update of the geometry could be necessary. Some kind of optimization is assumed to be indispensable before carrying out the future dynamic analysis. On the other hand, it would be interesting to investigate the possible use of other types of elements when meshing if higher analysis efficiency were needed; in particular, the elements SHELL181 and SOLSH190.
- **Materials**. On the one hand, the selection of the materials in the ITER FILD design has to be taken into consideration in future dynamic analyses. Here, just generic stainless steel and molybdenum have been used. On the other hand, the physical and mechanical properties, as well as the maximum allowable stress, of those materials have to be properly chosen, according to the corresponding standard (in particular, RCC-MRx 2012).
- **RS inputs**. It is necessary to ask CPPE for the values of the broadened curves. If possible, the adequate location also has to be asked.

In addition, the conclusions obtained with the final conceptual model show how interesting it is to further investigate about topology optimization. The application to other parts of the design could be studied.

Finally, and according to a general recommendation, the amplification frequencies should be avoided as much as possible. In this way, there is one natural frequency in the redesigned system that has a spectral acceleration of 175 m/s^2. Thus, it would be necessary to seek solutions like the ones presented in subsection 5.4.3.

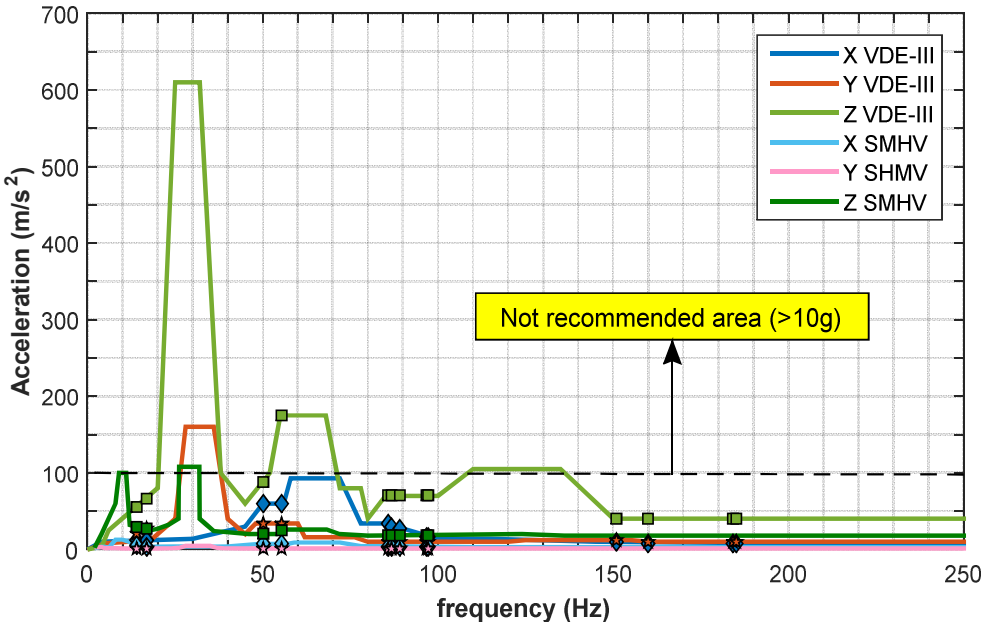

Figure 6.1 Safe frequency ranges for ITER FILD.

References

[1] **VISWANATHAN, B.** Chapter 6 – Nuclear Fusion in *Energy Sources: Fundamental of Chemical Conversion Processes and Applications*. Amsterdam: Elsevier, 2017, pp.133-134.

[2] **BILATO, R. and KLEIBER R. et al.** *IPP Summer University for Plasma Physics*. Greifswald: IPP, 2016.

[3] **CASCI, F. and LANZINGER, D.** *ITER, "the way" to the Future*. Garching: EFDA, 2006.

[4] **CIEMAT.** Laboratorio Nacional de Fusión. *Glosario de Términos de Fusión y ITER* [Online] 2003. [Cited: 11 March 2018] http://www-fusion.ciemat.es/New_fusion/en/Fusion/glosario_es.pdf.

[5] **EUROFUSION**. JET. [Online] 2014. [Cited: 11 March 2018] https://www.euro-fusion.org/jet/.

[6] **IPP.** ASDEX Upgrade. [Online] 2014. [Cited: 11 March 2018] http://www.ipp.mpg.de/16195/asdex.

[7] **GENERAL ATOMICS.** DIII-D. [Online] 2017. [Cited: 11 March 2018] https://fusion.gat.com/global/diii-d/home.

[8] **JT-60SA RESEARCH UNIT**. JT-60SA. [Online] 2018. [Cited: 11 March 2018] http://www.jt60sa.org.

[9] **ITER ORGANIZATION**. ITER. [Online] 2015. [Cited: 11 March 2018] https://www.iter.org/.

[10] **RODRÍGUEZ RAMOS, M.** *Calibración absoluta y aplicación de los detectores de pérdidas de iones rápidos basados en materiales centelleadores para dispositivos de fusión nuclear.* Seville: University of Seville, 2017. pp. 33-177, Dissertation.

[11] **RIVERO RODRÍGUEZ, J.F.** *Implementation of a Fast-Ion Loss Detector in the MAST Upgrade Spherical Tokamak.* Seville : University of Seville, 2017. pp. 27-45, Thesis.

[12] **GARCÍA MUÑOZ, M.** *Fast Response Scintillator Based Detector for MHD Induced Energetic Ion Losses in ASDEX Upgrade*. Munich : IPP, 2006. Dissertation.

[13] **GARCÍA MUÑOZ, M. et al.** Scintillator based detector for fast-ion losses induced by magnetohydrodynamic instabilities in the ASDEX upgrade tokamak, s.l.: AIP Publishing, 2009, *Rev. Sci. Instrum*, Vol. 80(5), 053503. doi: 10.1063/1.3121543.

[14] **AYLLÓN GUEROLA, J. et al.** A fast feedback controlled magnetic drive for the ASDEX Upgrade fast-ion loss detectors. s.l.: AIP Publishing, 2016, *Rev. Sci. Instrum*, Vol. 87(11), 11E705. doi: 10.1063/1.4959913.

[15] **BAEUMEL, S. et al.** Scintillator probe for lost alpha measurements in JET. s.l.: AIP Publishing, 2004, *Rev. Sci. Instrum.,* Vol. 75(10), 103563. doi: 10.1063/1.1787916.

[16] **GARCÍA MUÑOZ, M.** Conceptual design of the ITER fast-ion loss detector. s.l. : AIP Publishing, 2016, *Rev. Sci. Instrum*., Vol. 87(11), 11D829.

[17] **GARCÍA MUÑOZ, M.** Conceptual design of the ITER fast-ion loss detector. s.l. : AIP Publishing, 2016, *Rev. Sci. Instrum*., Vol. 87(11), 11D829.

[18] **KOCAN, M.** Functional requirements forthe ITER fast ion loss detector. s.l.: ITER Organization, 2015. Design guideline. RWBXA2.

[19] **KOCAN, M.** The impact of the fast ion fluxes and thermal plasma loads on the design of the ITER fast ion loss detector. Bordeaux: IOP Publishing, 2017, *J. Instrum*, Vol. 12, C12027. doi: 10.1088/1748-0221/12/12/C12027.

[20] **AYLLÓN GUEROLA, J. et al.** Dynamic and thermal simulations of a fast-ion loss detector for ITER. Prague: Elsevier, 2017, *Fus. Eng. Des.*, Vol. 123, pp. 807-810.

[21] **GUIGON, A. and LEE, C.H.** ITER Systems Engineering Management Plan. s.l.: ITER Organization, 2009. MQP Top Level Plan. 2F68EX.

[22] **GUIGON, A.** ITER System Design Process (SDP) Definition. s.l: ITER Organization, 2012. MQP Processes and Workflow. 437LC7.

[23] —. Design Review Procedure. s.l.: ITER Organization, 2016. MQP Procedure. 2832CF.

[24] **LEE, C.H.** ITER Document Breakdown Structure Overview. s.l.: ITER Organization, 2011. Plan. 43327Q.

[25] **GUIGON, A.** ITER System Design Process (SDP) Working Instruction. s.l.: ITER Organization, 2011. MQP Working Instruction. 4CK4MT.

[26] **BACHMANN, C.** Guideline for Structural Integrity Report. s.l.: ITER Organization, 2010. Guideline, p. 9. 35QTKD.

[27] **AYLLÓN, J.M et al.** 55.B9 - Load Spec(s) (SLS) for in-vessel/in-port components. s.l.: ITER Organization, 2018. System Load Specifications. VHADDD.

[28] **ZHANG, X.** Instructions for Seismic Analyses. s.l.: ITER Organization, 2018. MQP Working Instruction. VT29D6.

[29] **ROCCELLA, R.** Instructions for EM Analyses. s.l.: ITER Organization, 2018. MQP Working Instruction. TSZ9KQ.

[30] **DEN HARTOG, J.P.** *Mechanical Vibrations.* New York and London: McGraw-Hill, 1947. 10 1114353868/13 9781114353862.

[31] **GARCÍA DURÁN, MERCEDES, DOMINGUEZ ABASCAL, J. and MAYO NÚÑEZ, J.** *Problemas resueltos de vibraciones mecánicas.* Seville : Escuela Técnica Superior de Ingenieros, 2004. 84-887-837-28.

[32] **WANG, E. and NELSON, T.** Structural Dynamic Capabilities of Ansys. Munich: CADFEM GmbH, 2002.

[33] **CLOUGH, R.W. and PENZIEN, J.** *Dynamics of structures.* Berkeley: McGraw-Hill, 2003. 0070113947 9780070113947.

[34] **RUTENBERG, A.** A consideration of the torsional response of building frames. New Zealand: *National Society for Earthquake Engineering*, March 1979, Vol. 12(1), pp. 11-21.

[35] **FARMER, M. G.** A two-degree-of-freedom flutter mount system with low damping for testing rigid wings at different angles of attack. Blackburg: NASA Langley Research Center; Hampton, VA, United States, 1982. NASA-TM-83302, NAS 1.15:83302.

[36] **GUIRAO, J.** Building good Load Specifications. s.l.: ITER Organization, 2017. Training course. UM4UG6.

[37] **ITER ORGANIZATION.** Load Specifications (SL). s.l.: ITER Organization, 2017. Guideline. 222QGL.

[38] **ASME.** ASME Boiler and Pressure Vessel Code, Section III, Div. 1. Rules for Construction of Nuclear Facility Components, NMA Appendix N. Dynamic Analysis Methods, 2001, pp. 330-399.

[39] **KUMAR, A.** *Response Spectrum Method: In Seismic Analysis and Design of Structures*. North Carolina: Blackwell Scientific Publications, 1990.

[40] **PARÍS, F.** *Teoría de la Elasticidad.* Seville: GERM, 2000, pp. 424-453. 84-88783-32-9.

[41] **PETYT, M.** *Introduction to Finite Element Vibration Analysis.* Southampton: Cambridge University Press, 2010, pp. 45-77.

[42] **GRIMES, R. et al.** A shifted Block Lanczos algorithm for solving sparse symmetric generalized eigenproblems. s.l.: SIAM, 1994, *J. Matrix Anal. & Appl.*, Vol. 15(1), pp. 228-272.

[43] **ANSYS** 14.14 Eigenvalue and Eigenvector Extraction in *Ansys Documentation*, Ansys Release 16.0.

[44] **AZO.** Azo materials. [Online] 2001. [Cited: 15 May 2018] https://www.azom.com/.